Evaluation of small-molecule compounds and immunomodulatory agents as potential host-directed therapy for tuberculosis in *in vitro* models of *Mycobacterium tuberculosis* infection

by

Tamia Kelly Jasmyn Lawrence (223152645)

Supervisor: Associate Professor Mohlopheni Jackson Marakalala

Co-supervisor: Dr Thabo Rantanta Victor Mpotje

Submitted in the fulfillment of the requirements for the degree of

Master of Medical Science

In the department of Medical Microbiology

In the School of Laboratory Medicine and Medical Science

College of Health Sciences

University of KwaZulu-Natal

2025

Declaration

I, **Tamia Kelly Jasmyn Lawrence**, declare that:

1. The research reported in this thesis, except where otherwise indicated, is my original research.

2. This thesis has not been submitted for any degree or examination at any other university.

3. This thesis does not contain other persons' data, pictures, graphs or other information, unless specifically acknowledged as being sourced from other persons.

4. This thesis does not contain other persons' writing, unless specifically acknowledged as being sourced from other researchers. Where other written sources have been quoted, then:

a. Their words have been re-written but the general information attributed to them has been referenced

b. Where their exact words have been used, then their writing has been placed in italics and inside quotation marks, and referenced.

5. This thesis does not contain text, graphics or tables copied and pasted from the Internet, unless specifically acknowledged, and the source being detailed in the thesis and in the References sections.

Signed ____  _____ Date 17 April 2024

Dedication

To my grandparents, **Palmer** Alfred Lawrence and **Elizabeth** Maria Lawrence.

Acknowledgements

I would like to acknowledge the funders **Wellcome Trust**, **Medical Research Council** and the **Gates Foundation**. Thank you for making this work to be possible.

I would like to express my sincerest gratitude to Assoc. Prof. **Mohlopheni Jackson Marakalala** for allowing me to be a part of your lab and for believing in me. Thank you for the constant encouragement and motivation, and for always telling me that "I am going to do great." I am so grateful for all the opportunities, experience and knowledge I have gained being a part of your research group. Thank you for all your time and efforts. Thank you for being a kind and inspiring role model. Thank you for the guidance and unwavering support. I am eternally grateful to have you as a supervisor and mentor like you- I truly could not have asked for better.

To my co-supervisor, Doctor **Thabo Rantanta Victor Mpotje**, thank you for your unwavering support throughout my Master's journey. I am deeply grateful for your guidance, patience, and understanding. Thank you for the encouragement, especially during difficult times. Thank you for all the time and effort, and for helping me through long experiments. Words cannot express my gratitude. I have learned so much from you.

To **Pumla Eve Majozi**, thank you for being a great friend and companion. Thank you for all the support and words of faith you have given me throughout our journey as lab mates. Thank you for all the unforgettable memories and laughter.

To, **Kerishka Rajkumar-Bhugeloo** and **Denelle Moodley**, thank you for all the training, knowledge and mentorship you have offered me throughout my studies. Your encouragement and leadership have been invaluable

I would like to thank Prof **Adrie Steyn** for allowing me access to his lab's resources, and to **Vanessa Naidoo** and **Wadzanai Manjeese** for their kindness and support in training me on optimising my 3D model. Thank you to **Barry Truebody** for BSL-3 training. I am also grateful to Prof **Al Leslie** for granting me access to his lab and to **Mark Chambers** for his generosity in training me on the 3D model. I would like to thank **Kapongo Lumamba** for the encouragement and all the laughs.

To my **grandparents**, **Ma** and **Da**, thank you for all the unconditional love and support. You taught me the value of reading and learning. Thank you both for teaching me to never limit myself and that I can achieve anything I believe is possible. Words cannot express how grateful I am.

To my **parents**, thank you for the endless love and support. To my siblings and cousins- thank you for being the reason I strive to be better than I was yesterday. Thank you to all my **aunts** and **uncles** for the support throughout my academic journey and for being my role models.

I would like to offer my gratitude to **Merton**. Your emotional and physical support carried me through this journey. Thank you for all the meals you cooked while I wrote my thesis, for your calm presence during stressful moments and for your love, patience and encouragement every step of the way.

And above all, I would like to thank **God** for giving me the wisdom, strength, guidance and opportunity to complete my masters.

List of Presentations

Oral Presentations:

- Evaluation of anti-inflammatory drugs as potential host-directed therapy for tuberculosis in in vitro models of tuberculosis infection.
  MJM Lab Meeting
  22 August 2023
- Evaluation of anti-inflammatory drugs as potential host-directed therapy for tuberculosis in *in vitro* models of tuberculosis infection.
  MJM Lab meeting
  30 May 2024

Poster Presentations:

- Screening and evaluation of immunomodulatory compounds as host-directed therapy to potentiate antimycobacterial immunity.
  8th SA TB Conference
  4-7 June 2024
  Durban, South Africa
- Screening and evaluation of immunomodulatory compounds as host-directed therapy to potentiate antimycobacterial immunity.
  Africa Health Research Institute Scientific Retreat
  5-8 August 2024
  Southbroom, South Africa
- Boosting Immunity: Screening Immunomodulators for Enhanced Antimicrobial Therapy in Tuberculosis.
  The Union World Conference on Lung Health, TBScience
  12-16 November 2024
  Bali, Indonesia

Table of Contents

List of Figures

List of Tables

List of Abbreviations

3D: Three-dimensional

AHRI: Africa Health Research Institute

AM: Alveolar macrophage

ART: Anti-retroviral Treatment

ATT: Anti-tuberculosis treatment

BREC: Biomedical Research Ethics Committee

BCG: Bacillus Calmette-Guérin

CD: Cluster of differentiation

CFU: Colony forming unit

CLR: C-type Lectin Receptor

CO_2: Carbon dioxide

CNS: Central nervous system

COPD: Chronic obstructive pulmonary disease

COVID-19: Coronavirus disease

DAPI: 4',6-diamidino-2-phenylindole

DC: Dendritic cell

dH_2O: Deionized water

DNA: Deoxyribonucleic acid

DMSO: Dimethyl sulfoxide

ECM: Extracellular matrix

EDTA: Ethylenediaminetetraacetic acid

ELISA: Enzyme-linked immunosorbent assay

EPTB: Extrapulmonary tuberculosis

FBS: Fetal bovine serum

FDA: Food and Drug Administration

GM-CSF: Granulocyte-macrophage colony-stimulating factor

H&E: Hematoxylin and Eosin

HBSS: Hanks' Balanced Salt Solution

HDT: Host-directed therapy

HIF: Hypoxia-inducible factor

HIV: Human immunodeficiency virus

HSP: Heat shock protein

IFN: Interferon

JAK: Janus kinase

IL: Interleukin

IRF: Interferon regulatory factor

IRIS: Immune reconstitution inflammatory syndrome

LAM: Lipoarabinomannan

LPS: Lipopolysaccharide

LTBI: Latent tuberculosis infection

MAPK: mitogen-activated protein kinase

MDR: Multi-drug resistant

MGC: Multi-nucleated giant cell

MHC: Major-histocompatibility complex

MMP: Matrix metalloproteinase

MOI: Multiplicity of infection

Mtb: *Mycobacterium tuberculosis*

MyD88: myeloid differentiation primary-response protein 88

NF-κB: nuclear factor kappa-light chain-enhancer of activated B-cell

NK: Natural killer

NOD: Nucleotide-binding oligomerization domain-containing protein

OD_{600}: Optical density at a wavelength of 600 nm

PAMPs: Pathogen-associated molecular patterns

PBMC: Peripheral blood mononuclear cells

PBS: Phosphate-buffered saline

PLWH: People living with HIV

PDIM: Phthiocerol dimycocerosate

PI3K: Phosphoinositide 3-kinase

PID: Participant identification number

PMA: Phorbal-12-myristate-13-acetate

PTB: Pulmonary tuberculosis

PTLD: Post-tuberculosis lung disease

PRR: Pathogen recognition receptors

RPMI: Roswell Park Memorial Institute

RNA: Ribonucleic acid

RNS: Reactive nitrogen species

ROS: Reactive oxygen species

RPM: Revolutions per minute

RT: Room temperature

Sav-HRP: Streptavidin-horseradish peroxidase

SDG: Sustainable development goal

STAT: Signal transducers and activators of transcription

TB: Tuberculosis

TCR: T-cell receptor

TGF: Transforming growth factor

Th: T-helper cell

TLR: Toll-like receptor

TMB: Tetramethylbenzidine

TNF: Tumour necrosis factor

WHO: World Health Organization

XDR: Extreme-drug-resistant tuberculosis

List of symbols:

°C: Degree Celsius

α: Alpha

β: Beta

γ: Gamma

K: Kappa

Abstract: Part A

Background: Tuberculosis (TB), caused by the bacterium *Mycobacterium tuberculosis* (*Mtb*), is a global health concern that currently affects millions of individuals and causes significant mortality annually. The problem is aggravated by the emergence of drug-resistant *Mtb* strains and TB-associated tissue pathology, which may result in post-TB lung disease and lung function challenges. New therapeutic strategies are required to treat TB-associated lung pathology. Host-directed therapies (HDTs) offer a novel approach to treating TB and improving outcomes by enhancing the host's immune response, alleviating tissue damage caused by extreme inflammation, and shortening treatment duration. This study aims to screen small-molecule compounds as potential HDTs to target inflammation, reduce tissue damage, and alleviate pulmonary impairment associated with TB.

Methods: High-throughput screening of small-molecule compounds was performed on PBMCs infected with *Mtb* H37Rv. ELISA was used to quantify the release of TNF-α, IL-1β, and IL-6 to assess the anti-inflammatory effects of the compounds. A promising candidate, Tam-X1, which inhibits IL-5 from binding to its receptor IL-5R, was identified for its capacity to reduce pro-inflammatory cytokine production. Tam-X1 was further evaluated in a 3D biomimetic collagen-alginate model mimicking TB granulomas, using PBMCs infected with luminescent *Mtb* H37Rv LUX strain. ELISA and luminometry were employed to measure the anti-inflammatory and antimycobacterial effects of Tam-X1 in the 3D model, respectively. H&E staining and immunofluorescence staining were performed on resected TB-diseased lung tissue to examine the spatial association of proteins in the Tam-X1 target pathway, including IL-5 and IL-5Ra, with TB-induced inflammation and granuloma development.

Results: Tam-X1 significantly reduced the production of pro-inflammatory cytokines, TNF-α, IL-1β, and IL-6, during *Mtb* infection and inhibited intracellular *Mtb* growth within the 3D biomimetic model. Histopathological assays revealed that TB-driven inflammation is mediated by immune cells expressing IL-5Ra, including eosinophils, and that Tam-X1 targets a pathway spatially associated with pathology in the TB-diseased lung.

Conclusion: This study highlights the potential of Tam-X1 as a promising HDT for TB. By targeting the IL-5/IL-5R signalling pathway, Tam-X1 reduced the production of TNF-α, IL-1β, and IL-6 during *Mtb* infection and inhibited *Mtb* growth. This suggests that treatment with Tam-X1 may mitigate TB-associated tissue pathology by modulating the host's immune response.

Abstract: Part B

Background: Tuberculosis (TB), caused by the pathogen *Mycobacterium tuberculosis* (*Mtb*), remains a global health threat due to drug resistance, poor treatment adherence, and high mortality rates. Host-directed therapies (HDTs) offer a novel approach to improve TB treatment outcomes by enhancing the host's immune defence, controlling inflammation and reducing post-TB complications and mortality. This study aimed to assess the potential of immunomodulatory compounds targeting Toll-like receptors (TLRs) 7 and 8, as adjunctive HDTs for TB.

Methods: Screening of the effects of immunomodulatory agents in THP-1 cells infected with the luminescent *Mtb* strain, H37Rv LUX, was performed. The effects on the production of the pro-inflammatory cytokines, TNF-α, IL-1β and IL-6 were quantified using ELISA. Luminometry was used to analyse the effects of TLR modulation on bacterial clearance. A promising compound, TLR M, a TLR7/8 agonist, was identified as an activator of macrophage pro-inflammatory responses and underwent further evaluation using an in vitro 3D biomimetic TB granuloma model, analysing the effects on inflammation using ELISA and antimycobacterial effects using luminometry. H&E-stained and immunofluorescent labelled slides were imaged using confocal microscopy to spatially analyse the association of TLR M's protein target, TLR7/8, with TB-induced inflammation and granuloma formation in resected TB-diseased lung tissue.

Results: This study identified TLR7/8 as potential targets for adjunctive HDTs, revealing their potential to enhance the inflammatory response during *Mtb* infection. TLR7/8 activation with TLR M improved antimycobacterial properties. Using immunofluorescence staining on lung tissue from TB diseased participants, we observed that alveolar macrophages contribute to TLR7/8 mediated signalling, potentially amplifying effector functions and aiding in *Mtb* clearance.

Conclusion: Taken together, TLR M represents a potential adjuvant HDT for TB treatment. The ability of this TLR7/8 agonist to modulate the inflammatory immune response and enhance antimycobacterial activity suggests that it can improve treatment outcomes and mitigate TB-related morbidity and mortality. Further research into TLR7/8-targeted therapies may therefore lead to enhanced strategies for combating TB by enhancing the hosts immune response and addressing the challenges associated with current treatment regimens.

CHAPTER 1:

INTRODUCTION

1. Introduction

1.1 Tuberculosis, a global health concern

Tuberculosis (TB), caused by the bacterium *Mycobacterium tuberculosis* (*Mtb*), remains a global health concern, affecting millions of people annually (Goletti et al., 2024). TB is one of the leading causes of death worldwide, only surpassed by COVID-19 during the 2020 pandemic (Goletti et al., 2024; Tiwari and Martineau, 2023). TB has been known to have existed since ancient times, with *Mtb* identified by Robert Koch in 1882 as the causative agent of TB. Approximately one-third of the world's population is infected with *Mtb*, with 10 million people developing TB annually. In 2022 alone, TB caused 1.3 million deaths, highlighting its continued significance as a threat to global health (WHO, 2023). It is estimated that 5-10% of those individuals infected with *Mtb* will develop active TB disease, which may eventually lead to death (Carranza et al., 2020). In 2022 alone, the World Health Organization (WHO) reported 410 000 cases of Multidrug-resistant TB (MDR-TB) globally, with 62 000 cases in Africa (WHO, 2023). Additionally, extreme drug-resistant TB (XDR-TB) affects an estimated 9.7% of MDR-TB patients (Ndlovu and Marakalala, 2016).

TB is spread through the air from person to person during actions that create aerosols laden with *Mtb*, such as coughing and sneezing by an individual with active TB (Tiwari and Martineau, 2023). These aerosols travel through the air and may be inhaled by a vulnerable individual, who could then become infected with *Mtb* and potentially develop active TB (Churchyard et al., 2017). Once inhaled, *Mtb* bacilli travel through the respiratory system and take residence in the lungs. In some individuals, the innate immune system may completely eradicate the *Mtb* bacilli, resulting in the clearance of the infection (Carranza et al., 2020). Alternatively, a sustained response from both the innate and adaptive arms of the immune system may control bacterial replication, causing the *Mtb* bacilli to remain dormant within the lungs of an infected individual. This leads to a state known as 'Latent TB infection' (LTBI) (Carranza et al., 2020; Migliori et al., 2021). LTBI can also be described as a state of infection where the bacteria remain dormant and are unlikely to progress to clinical disease in the foreseeable future. However, if the immune system fails to contain the infection, LTBI can progress into active TB disease. Active TB is characterised by increased bacterial replication and clinical symptoms such as fever, anorexia, loss of appetite, persistent cough, night sweats, microbiological evidence of infection, radiographical abnormalities and anaemia (Drain et al., 2018; Loddenkemper et al., 2016). Recent developments have identified an intermittent stage of infection between LTBI and active TB, referred to as subclinical TB. This state of infection is characterised by the absence of the clinical symptoms associated with active TB and microbiological and radiographic abnormalities, except those typically associated with active TB disease (Drain et al., 2018).

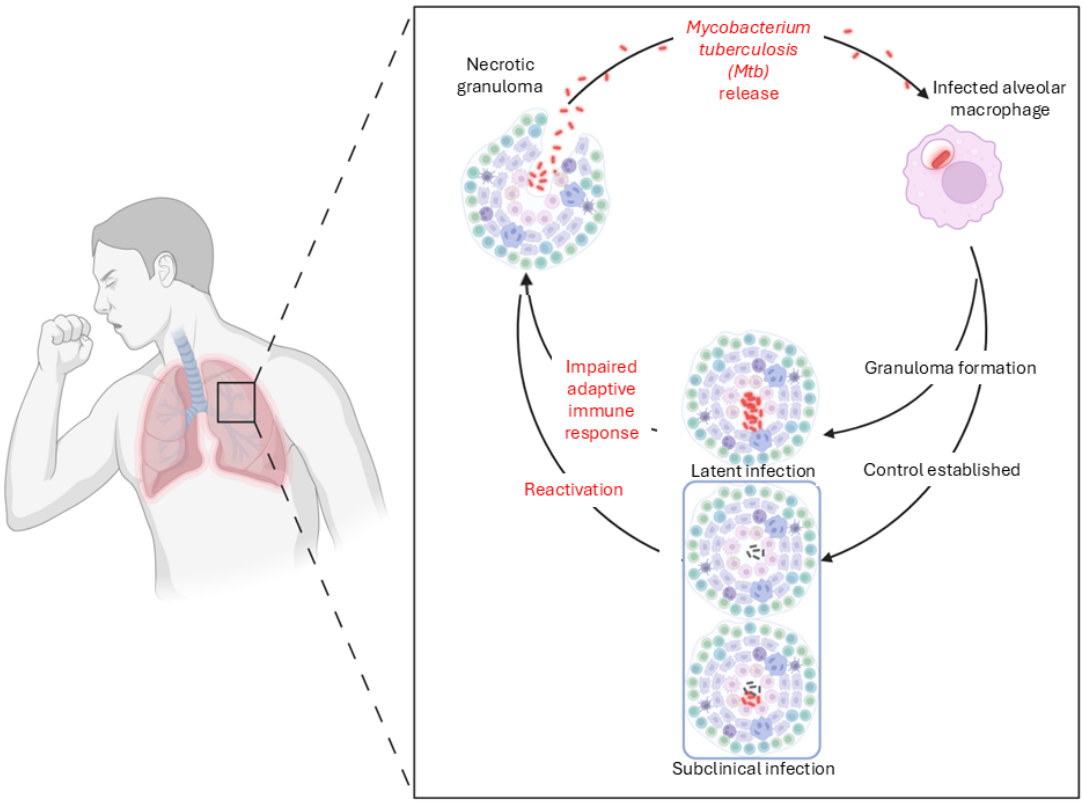

Figure 1.1: **Progression of tuberculosis from latent Infection to active disease and dissemination.** This diagram illustrates the stages of TB progression, beginning with the initial infection. The granuloma develops caseous necrosis as the infection progresses from LTBI to subclinical TB to active TB or from LTBI to active TB, forming a necrotic core. Further progression leads to cavitary granuloma formation, resulting in active TB and, eventually, dissemination and infection of a new host. (Created in Biorender.com)

1.2 Current Tuberculosis Treatment and Drug Resistance

One of the biggest challenges in eradicating TB is drug-resistant TB (Ndlovu and Marakalala, 2016). Currently, treatment for drug-susceptible TB consists of the use of first-line anti-tubercular drugs such as rifampicin, ethambutol, pyrazinamide, and isoniazid (Bendre et al., 2021). However, drug-resistant TB is a significant threat, with resistance to first-line drugs known as MDR-TB (Seung et al., 2015). MDR-TB cannot be cured with standard first-line treatment and requires the use of second-line antitubercular drugs consisting of injectable drugs (amikacin, kanamycin, streptomycin and capreomycin), fluoroquinolones (levofloxacin and moxifloxacin), oral bacteriostatic drugs (cycloserine, ethionamide, prothionamide and para-aminosalicyclic acid) or drugs which have limited information on efficacy and long-term safety (bedaquiline, linezolid, clofazimine, amoxicillin, imipenem) (Bendre et al., 2021; Seung et al., 2015). The term XDR-TB is used to describe *Mtb* strains which are resistant to first-line drugs and one or more fluoroquinolones, as well as any of the second-line injectable drugs (Alsayed and Gunosewoyo, 2023; Seung et al., 2015).

Current TB treatment efforts face significant challenges due to factors such as adverse drug reactions, side effects, lengthy treatment strategies, and issues with patient adherence. The existing first-line TB treatment regimen involves a lengthy duration of at least 6 months, while second-line treatment for MDR-TB may require 18-24 months (Bendre et al., 2021; Ndlovu and Marakalala, 2016). As with most drug regimens, TB treatment can induce several unfavourable side effects, including nausea, vomiting, diarrhoea, skin rashes, loss of appetite, and joint pain. These adverse effects can disrupt treatment plans and may contribute to the development of drug-resistant strains of *Mtb* (Kim et al., 2021; Maranatha and Bahri, 2020; Seung et al., 2015). The combination of these side effects, coupled with a prolonged treatment duration, can lead to non-adherence among TB patients, which increases the risk of treatment failure and recurring infections (Kim et al., 2021). Furthermore, the rise of drug-resistant TB strains is a global health concern, as it necessitates the use of second-line drugs, which are more expensive to manufacture and may carry the risk of drug toxicity (Gygli et al., 2017).

Currently, the Bacillus Calmette-Guérin (BCG) vaccine is the only authorised vaccine for use as a TB prevention strategy. The BCG vaccine is composed of a weakened form of *Mycobacterium bovis* and is administered to infants at birth (Srivastava et al., 2023). BCG has been used as a vaccine against TB for over a century and has been reported to have varying efficacy rates of 0-80% in preventing TB. However, studies indicate that the preventative effect of the vaccine declines from birth to adulthood, leaving individuals susceptible to pulmonary TB. As a result, there is a dire need for developing a more effective vaccine against TB (Khandelia et al., 2023; Srivastava et al., 2023).

1.3 Complications associated with tuberculosis

An array of adverse complications is associated with TB disease due to its ability to disseminate beyond the lungs and infect various organs and tissues, a condition known as extrapulmonary TB (EPTB). EPTB may or may not result in a display of clinical pulmonary TB symptoms (Moule and Cirillo, 2020). Lymphadenitis, an infection of the lymph nodes, is the most widespread form of EPTB, occurring in 50% of patients with EPTB cases. Pleural TB, an infection of the pleura lining the lungs, affects 18% of individuals who experience EPTB. Pott's Disease is an infection of the spine leading to spinal TB that occurs in 6% of individuals with EPTB. EPTB may also disseminate and cause infections in the bones and joints (Baykan et al., 2022; Moule and Cirillo, 2020). Central nervous system (CNS) EPTB, a rare but severe form, occurs in 3% of patients and can exist as tuberculoma, TB meningitis, an abscess, or encephalitis (Baykan et al., 2022; Leonard, 2017). Renal EPTB can cause obstructive kidney injury and lead to renal failure (De Francesco Daher et al., 2013). The most fatal form of EPTB, miliary TB, results from *Mtb* bacilli entering the bloodstream and spreading throughout the body, leading to widespread infection and the development of TB lesions in various organs (Moule and Cirillo, 2020).

Infection with *Mtb* triggers a complex immune response, inducing an inflammatory reaction. To effectively combat the disease, a delicate balance of inflammation is essential. An insufficient

inflammatory immune response can increase bacterial load, while excessive inflammation may be associated with heightened fatality risks or other adverse health outcomes (Krug et al., 2021). Uncontrolled inflammation can exacerbate the progression of TB. In the advanced stages of the disease, individuals with TB may experience fibrosis or nodular filtrates, cavitation, necrosis, or a combination of these pathologies. Some of these pathologies may lead to permanent lung damage, resulting in persistent complications even after the disease is cured (Ravimohan et al., 2018; Tiwari and Martineau, 2023).

Patients living with pulmonary TB may experience several complications even after microbial cure, leading to permanent lung damage. These complications include post-TB lung disease (PTLD), pulmonary dysfunction, and susceptibility to further respiratory infections (Hsu et al., 2020; Ravimohan et al., 2018). Pulmonary dysfunction can cause extreme breathlessness and may result in respiratory-related mortality. TB survivors may develop chronic obstructive pulmonary disorder (COPD), pneumonia, bronchiectasis, haemoptysis, and scar carcinoma (Hsu et al., 2020; Ravimohan et al., 2018; Gupta et al., 2016).

TB-related lung damage encompasses conditions such as pulmonary cavitation and fibrosis, which lead to lung tissue remodelling, respiratory defects, impaired gas exchange, long-term lung injury and thickening of the lung walls. In cases of caseous necrosis, resident cells within the alveoli, along with the blood vessels and bronchi, are destroyed (Kayongo et al., 2023; Ravimohan et al., 2018). A study by Hunter *et al.* (2011) showed that the necrotic tissue is eventually expelled through coughing, leaving gas-filled spaces surrounded by collagen in the place of the necrotic tissue. In addition, studies using resected lung tissue from TB patients have highlighted these anomalies (Hunter, 2011; Tiwari and Martineau, 2023). Post-TB complications frequently diminish a patient's quality of life, and lung damage and tissue remodelling due to uncontrolled inflammation can potentially be fatal (Nuwagira et al., 2022; Ravimohan et al., 2018).

1.4 Human Immunodeficiency Virus and Tuberculosis Co-infection

Human immunodeficiency virus (HIV) and TB coinfection is a lethal combination, as both HIV and TB accelerate the severity of the other. HIV infection hampers the strength of the immune system, leaving individuals living with HIV more susceptible to contracting TB (Pooranagangadevi and Padmapriyadarsini., 2022). It has been estimated that there are 14 million people living with HIV (PLWH) who are co-infected with *Mtb*. This is because HIV infection increases the susceptibility to develop active TB by twenty times, which may be a result of weakened immunity during HIV infection, which increases the risk of being infected with *Mtb* and increases the risk of the reactivation of LTBI (Bruchfeld et al., 2015). Currently, 88% of patients with active TB are coinfected with HIV (Nigam et al., 2022). A distinct characterisation of HIV infection is the depletion of cluster of differentiation (CD)4^+ T cells, which function as a reservoir for HIV. This is a significant contributing factor in the

increased risk of developing active TB during HIV infection, as $CD4^+$ T cells play an essential role in the defence against invading pathogens (Ahmed et al., 2016). TB continues to be the highest cause of death amongst HIV-infected individuals globally, emphasising the urgent need for successful HIV-TB coinfection treatment (Nigam et al., 2022).

There are several complications which arise in the treatment of HIV and TB coinfection. These include the need for separate healthcare providers to manage each condition, drug toxicities, the risk of drug-drug interactions, and poor patient adherence due to the large number of medications required to treat both HIV and TB (Pooranagangadevi and Padmapriyadarsini, 2022). Additionally, individuals who are undergoing treatment for HIV and TB are at risk for developing TB-immune reconstitution inflammatory syndrome (TB-IRIS), which is an inflammatory condition that results in a significantly increased immune response during *Mtb* infection. TB-IRIS commonly arises at the onset of treatment with anti-retroviral treatment (ART) in individuals infected with HIV (Lanzafame and Vento, 2016). This condition may further lead to the worsening of individuals infected with TB through the development of new TB lesions or aggravating of initial lesions (Lanzafame and Vento, 2016). TB-HIV coinfection presents significant challenges in the concurrent treatment of these conditions, emphasising the need for an improved treatment strategy for the integrated treatment and control of both these diseases (Nigam et al., 2022)

1.5 Cellular interplay in the immune response *to Mycobacterium tuberculosis* infection

Mtb spreads from person to person through the transmission of *Mtb-infected* aerosols. Once inhaled, *Mtb* migrates through the respiratory system until it encounters the lungs. Resident alveolar macrophages (AM), located in the alveolar spaces of the lung, serve as the first line of defence against *Mtb* (Sasindran and Torrelles, 2011). AMs possess receptors termed 'pathogen recognition receptors' (PRRs) which recognise 'pathogen-associated molecular patterns' (PAMPs). Several PRRs recognise *Mtb*, including Nucleotide-binding oligomerization domain containing protein (NOD) 2 and C-type lectin receptors (CLRs) such as Dectin-1, and Toll-like receptor (TLR)2, TLR4, TLR9, possibly TLR8. These PRRs recognise components of *Mtb,* such as peptidoglycan and glycolipids (Alsayed and Gunosewoyo, 2023; Van Crevel et al., 2011; Zhuang et al., 2024).

Some TLRs are located on the cell surface, such as TLR2 and TLR4, while others are found inside the cell, such as TLR7, TLR8 and TLR9. TLR2 forms a heterodimer with either TLR1 or TLR6 and recognises *Mtb* cell wall glycolipids, including lipoproteins, mannosides, and lipomannan. TLR4 is activated by recognising heat shock protein (HSP) 60/65, whereas TLR9 recognises unmethylated CpG motifs found in bacterial deoxyribonucleic acid (DNA) (Sasindran and Torrelles, 2011; Van Crevel et al., 2011). TLR7 and 8 generally function to recognise single-stranded ribonucleic acid (RNA) from pathogens; however, studies report that TLR7/8 is upregulated in the presence of *Mtb*. This suggests that TLR7/8 is involved in intracellular signalling during the immune response to *Mtb*. However, the

mechanism by which TLR7/8 recognises *Mtb* is currently unknown (Sasindran and Torrelles, 2011; Van Crevel et al., 2011).

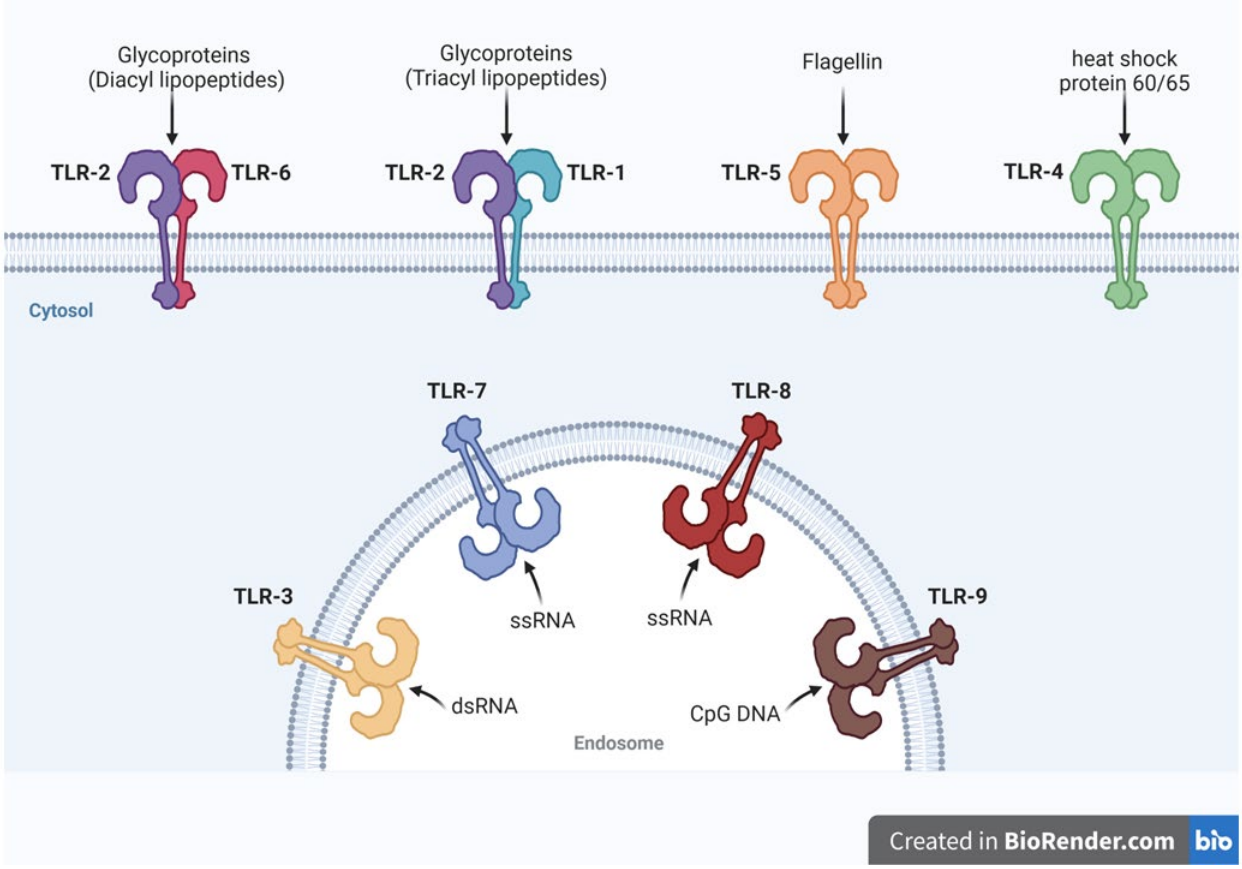

Figure 1.2: **Recognition of *Mtb* antigens by their respective TLRs during innate immunity.** TLRs function to recognise PAMPs associated with invading pathogens. This diagram illustrates the various components of *Mtb* and delineates the specific TLRs which they bind upon activation of the innate immune system.

The recognition of *Mtb* components by PRRs elicits the activation of the innate immune response through signal transduction pathways, such as the nuclear factor kappa-light chain-enhancer of activated B-cell (NF-κB) signalling cascade, via the activation of the adaptor protein myeloid differentiation primary-response protein 88 (MyD88). This activates downstream signalling, leading to the production of pro-inflammatory cytokines and chemokines. AMs subsequently phagocytose *Mtb* bacilli, leading to bactericidal effects such as the release of the pro-inflammatory cytokines (e.g. Tumour necrosis factor (TNF)-α, interleukin (IL)-6 and IL-1β, IL-12), reactive oxygen species (ROS), reactive nitrogen species (RNS) and the induction of autophagy. These processes initiate antimicrobial functions aimed at bacterial clearance (Sasindran and Torrelles, 2011; Zhuang et al., 2024). *Mtb* may then be cleared from the lungs or multiply, resulting in the death of AMs (Sasindran and Torrelles, 2011).

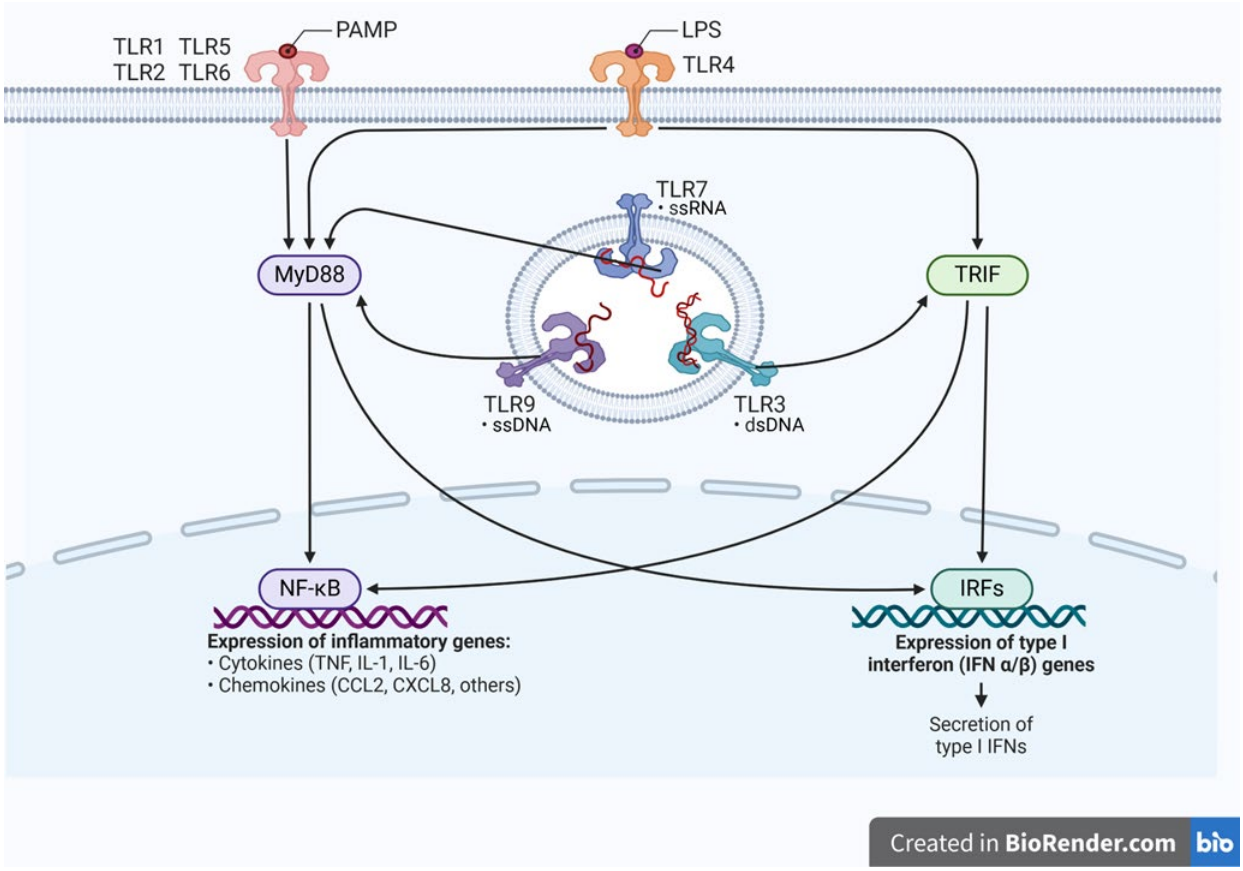

Figure 1.3: **Activation of TLRs by *Mtb* components elicits the activation of the inflammatory pathways, such as the NF-κB pathway, through signal transduction.** Recognition of *Mtb* components by TLRs leads to the initiation of intracellular pathways. This stimulates signal transduction and ultimately leads to the production of pro-inflammatory cytokines through pathways such as NF-κB and mitogen-activated kinase pathways.

Mtb evades the innate immune system by employing various survival mechanisms. These include suppressing the host's immune inflammatory response, preventing cytotoxic molecules like ROS and RNS, and critically blocking the process of autophagy (Olive and Sassetti, 2018; Sasindran and Torrelles, 2011). The cell wall of *Mtb* bacilli is composed of the plasma membrane, the cell wall core and the outermost layer which is made up of glycolipids (i.e. lipomannan, lipoarabinomannan (LAM), trehalose dimycolate, phospholipids, glycopeptidolipids, trehalose monomycolate, phosphatidylinositol, mannosides, sulfolipids, phthiocerol dimycocerosate (PDIM), and pthioceroldimycocerosates) and mycolic acids. The high lipid content in the outer layer of *Mtb*, as well as the presence of mycolic acid, creates extreme hydrophobic conditions, offering resilience to the bacilli against defence from the complement system, hydrophilic antibiotics and oxidative damage (Ghazaei, 2018; Jacobo-Delgado et al., 2023; Shukla et al., 2014). The hydrophobic conditions of Mtb assist in the evasion of recognition by the innate immune system by concealing PAMPs using PDIM and sulfoglycolipids, preventing recognition by TLRs, specifically TLR2. This ultimately inhibits the production of downstream pro-inflammatory cytokines (Dulberger et al., 2020; Jacobo-Delgado et al.,

2023). As mentioned, *Mtb* is phagocytosed by AMs, resulting in the formation of the phagosome, which under normal circumstances would fuse with the lysosome (Glick et al., 2010; Sasindran and Torrelles, 2011). However, studies report that the bacilli inhibit phagosome maturation and persist within the phagosome, preventing phagosome-lysosome fusion using the surface protein, LAM (Shukla et al., 2014). Autophagy is a cellular recycling process in which unwanted materials are transported to lysosomes for degradation (Levine et al., 2011). However, *Mtb* cleverly prevents the acidification of the autophagosome, a critical step for its fusion with the lysosome, using various mechanisms. This ultimately prevents autophagy, allowing *Mtb* to continue replicating within AMs (Chandra et al., 2022). For example, studies have reported that *Mtb* uses its secretion system ESX-1 to inhibit autophagy from occurring by modulating the host's autophagy system (Chandra et al., 2022; Romagnoli et al., 2012). *Mtb* not only prevents autophagy and maturation of the lysosome, but it also regulates the host cellular environment to permit its survival further. Several studies show that *Mtb* neutralises and forms a protective barrier against host-secreted ROS and RNS (Tyagi et al., 2015). This is possible due to the lipids located on the cell wall, the release of the secretory redox buffer ergothionine, and secretory antioxidant enzymes such as catalase and superoxide dismutase. Ultimately counteracting the efforts of the immune system to eliminate *Mtb* (Tyagi et al., 2015). The persistence of *Mtb* within phagocytes eventually leads to cell death as a last resort of immune defence by phagocytes. Apoptosis, a programmed cell death modality, is associated with a controlled reduction of bacterial replication. During apoptosis, the cell membrane remains intact and prevents the release of harmful substances into the surrounding environment (Behar et al., 2011; Martin et al., 2012). However, *Mtb* inhibits apoptosis to evade the immune system, and virulent strains of Mtb favour the induction of necrosis.

Necrosis is a cell death modality characterised by the disruption of the plasma membrane, during which cellular contents are released into the extracellular environment, resulting in the spread of *Mtb* bacilli and ultimately infecting surrounding cells. Necrosis encourages immune evasion and bacterial spread, and further increases inflammation within the surrounding tissue (Behar et al., 2011; Martin et al., 2012). Another cell death modality, which could occur due to the inhibition of apoptosis, is efferocytosis. During efferocytosis, neighbouring macrophages engulf apoptotic cells, which then undergo a more controlled cell death, clearing the infection and reducing inflammation (Behar et al., 2011; Martin et al., 2012).

Failure of the AM to eliminate *Mtb* results in the activation of the adaptive immune system. Infected AMs disseminate to other areas of the pulmonary interstitium, resulting in the infection of cells, such as monocyte-derived and tissue-resident macrophages, dendritic cells and neutrophils (Chandra et al., 2022). Dendritic cells (DCs) internalise and process *Mtb* bacilli. The infected DCs migrate to the lymph node, where T-cells are activated through antigen presentation via an interaction between the major histocompatibility complex (MHC) class II and the T-cell receptor (TCR). During this interaction, the costimulatory molecules, CD40, located on DCs, bind to their ligand to further ensure the full activation

of T-cells (Chandra et al., 2022; Zhuang et al., 2024). A tailored immune response is then initiated, accompanied by cytokine signalling, specifically IL-12, which drives the $CD4^+$ T cells to differentiate into T helper cells (Th1). Th1 cells migrate to the site of the infection and release interferon-gamma (IFN-γ), IL-2 and TNF-α. The release of IFN-γ further signals the activation of macrophages, promoting bacterial clearance of *Mtb* (Zhuang et al., 2024).

Ongoing cytokine release at the site of infection results in persistent immune signalling. This leads to the recruitment of an influx of immune cells such as monocytes, neutrophils, natural killer (NK) cells, T-cells, B-cells, fibroblasts, mast cells, eosinophils, endothelial cells and epithelial cells (Cronan, 2022). The recruited cells then organise into a structure called a granuloma, containing the infection and preventing its spread to other tissues (Alsayed and Gunosewoyo, 2023; Sasindran and Torrelles, 2011; Tiwari and Martineau, 2023). Macrophages located in the centre of the granuloma undergo differentiation into epithelioid macrophages, foamy macrophages and multi-nucleated giant (MG) cells and tightly interlock with one another and aggregate with neighbouring cells (Cronan, 2022; Tiwari and Martineau, 2023). The granuloma, characterised by a solid organised morphology, facilitates a latent infection in which patients exhibit no clinical symptoms of TB. The bacterial load of *Mtb* decreases, bacterial replication halts, and *Mtb* persists in a dormant state where the bacilli remain in a resting metabolic state under stressful conditions while evading the host's immune response. This state may indicate either complete bacterial clearance or conditions in which *Mtb* bacilli are contained (Chandra et al., 2022; Verma et al., 2022).

1.6 Secondary infection and disease progression in Tuberculosis

Studies indicate that the centre of the granuloma is rich in lipids and largely hypoxic due to the surrounding layer of cells (Ndlovu and Marakalala, 2016). The conditions within the granuloma are hypoxic and laden with constant inflammatory responses to control *Mtb* replication. However, this leads to tissue damage within the granuloma (Belton et al., 2016; Rustad et al., 2009). *Mtb* is known to inhibit apoptosis in favour of necrotic cell death, which may lead to bacterial dissemination and replication, as mentioned previously (Chandra et al., 2022). These factors lead to the formation of a 'cheese-like' necrotic core termed caseum, leading to the development of a 'caseous granuloma'. Foamy macrophages, which are composed of an accumulation of lipid droplets, surround the necrotic core of the granuloma. An imbalance in the host's lipid metabolism may contribute to further disease progression (Alsayed and Gunosewoyo, 2023).

The necrotic core harbours *Mtb* bacilli and may provide favourable conditions for bacterial dormancy. However, the destruction of the granuloma causes the caseous core to soften and liquefy, subsequently resulting in cavitation and the formation of a 'cavitary granuloma' (Alsayed and Gunosewoyo, 2023; Ndlovu and Marakalala, 2016). The bacteria are revived, and the host develops a state of active TB and exhibits symptoms of clinical disease. Due to cavitation, the viable *Mtb* migrates to the airways and is

released in the form of aerosols when the host coughs. This aids the transmission of *Mtb* to a new susceptible host (Alsayed and Gunosewoyo, 2023; Ndlovu and Marakalala, 2016).

The progression of active TB is intricately influenced by both the host's immune response and the pathogenic characteristics of *Mtb* (Divangahi et al., 2018). Factors such as substance abuse, poor diet, smoking, HIV co-infection, comorbidities/non-communicable diseases, age, genetic susceptibility, and immune suppressive medication may further weaken the host immune response. These factors may subsequently result in the reactivation of *Mtb* and the development of active TB (Alsayed and Gunosewoyo, 2023).

Conversely, *Mtb* plays a crucial role in disease progression by modulating multiple cell death pathways in the host, including necrosis, apoptosis, pyroptosis, and ferroptosis (Rahlwes et al., 2023). These mechanisms allow *Mtb* to evade complete elimination, survive within host cells and spread. Additionally, *Mtb* utilises both non-protein and protein virulence factors to strengthen its ability to evade the host's immune responses, set up survival tactics to trigger active disease, disseminate within the host, migrate through the airways and establish an infection in new hosts (Rahlwes et al., 2023).

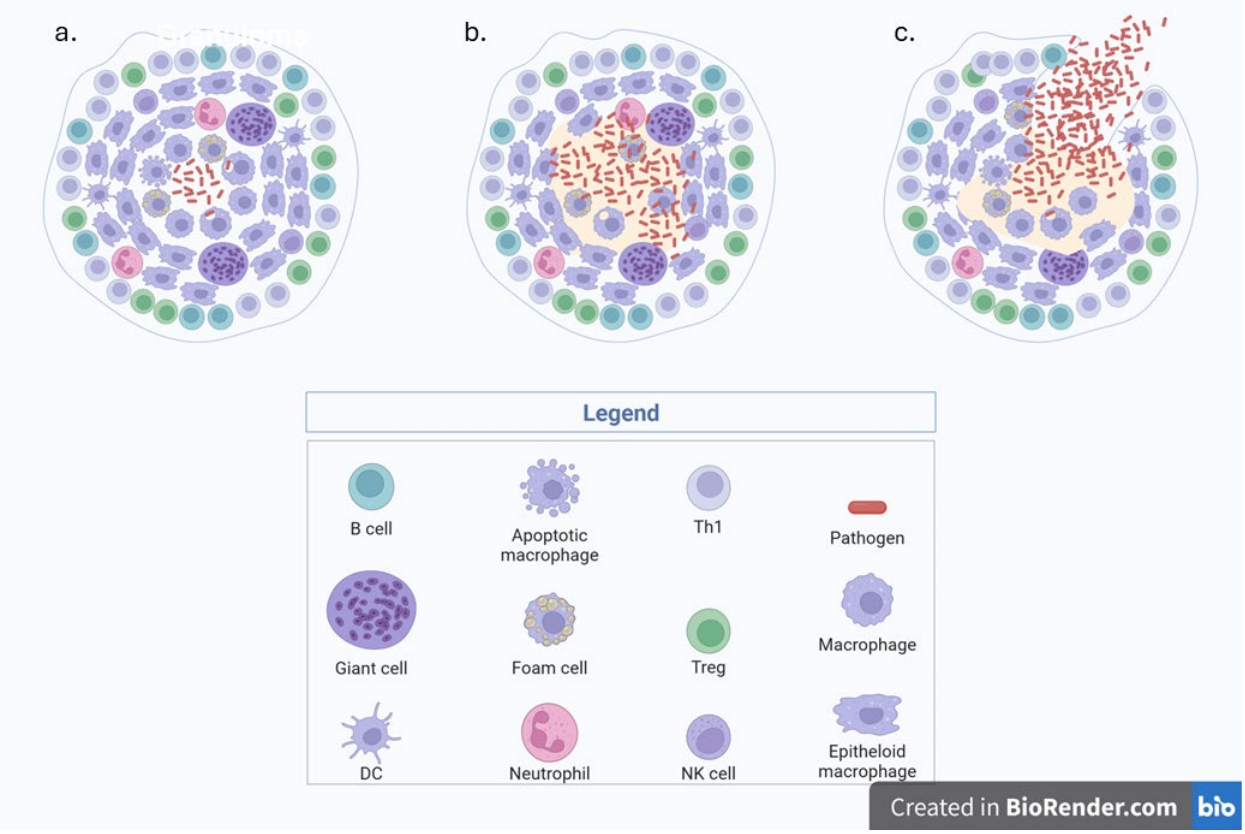

Figure 1.4: **Stages of granuloma formation in tuberculosis and associated immune cells**. This figure illustrates the progression of granulomas in TB infection. (a) Solid granuloma: Characterised by a dense cluster of immune cells working to contain the infection. (b) Necrotising granuloma: Shows the central area of necrosis surrounded by macrophages, foamy macrophages and multinucleated giant cells, reflecting tissue damage (in yellow) and the ongoing inflammatory response. (c). Cavitary/disseminating granuloma: Displays the advanced

stage where the granuloma has developed a central cavity due to tissue destruction, with *Mtb* bacilli potentially spreading to new areas. This stage includes a range of immune cells, such as neutrophils and T-cells, indicating active infection and dissemination.

1.7 Inflammation, cytokines and their role in tissue remodelling and damage

As mentioned previously, *Mtb* elicits an extreme immune response that causes significant tissue damage and aids in its spread to a new host. However, if left unmodulated, the host immune response results in tissue remodelling (Belton et al., 2016). TNF-α, which is released from the onset in the immune response to *Mtb* infection, stimulates the release of metalloproteinase (MMP)-1 and MMP-9. MMPs are known to degrade the extracellular matrix components, eventually leading to tissue remodelling and destruction (Ravimohan et al., 2018; Sabir et al., 2019). Excessive release of TNF-α may also result in cavitation and fibrosis, which is excessive scar tissue within granulomas (Sabir et al., 2019). Fibrosis leads to stiffening of the lung tissue and reduces lung function. The release of the pro-inflammatory cytokine IL-1β signals the production of MMP-1 and thus contributes to ECM degradation and tissue damage. Persistent release of IL-1β can result in cavitation of the granuloma and, eventually, fibrosis (Ravimohan et al., 2018; Sabir et al., 2019; Schönbeck et al., 1998).

Transforming growth factor (TGF)-β is another cytokine involved in tissue repair and fibrosis. The release of TGF-β signals the production and release of TNF-α. This effect further increases the inflammatory response (Ravimohan et al., 2018; Santoso et al., 2023). TGF-β is involved in amplifying tissue repair and, therefore, initiates the production of increased extracellular matrix (ECM) proteins and collagen, and according to studies, TGF-B is said to be a key mediator in fibrogenesis. This leads to fibrosis formation within the lung (Ravimohan et al., 2018; Santoso et al., 2023). The hypoxic environment within the granuloma results in the release of hypoxia-inducible factor (HIF)-1α, which is crucial in the host response to hypoxia (Belton et al., 2016). HIF-1α also stimulates the release of MMPs, which promote tissue remodelling and angiogenesis, as highlighted in various studies (Belton et al., 2016). Additionally, the release of IFN-γ, IL-6, IL-12, and IL-8, along with MMPs, contributes to lung necrosis due to increased inflammation, eventually leading to cavitation (Ravimohan et al., 2018).

These factors lead to complications mentioned in section 1.3 and may also lead to cavitary lung disease (Urbanowski et al., 2020). This can cause patients to develop drug-resistant TB, increase transmission rates, require prolonged antibiotic treatment to treat secondary infections and necessitate intense monitoring to ensure a successful treatment prognosis (Urbanowski et al., 2020). In severe cases where cavitary disease persists despite medical treatment and bacterial cure, surgical interventions may be necessary to remove localised disease and prevent further complications (Urbanowski et al., 2020).

1.8 Host-directed therapies

The WHO has set a sustainable development goal (SDG) 3 to ensure healthy lives and well-being for all at all ages. In addition to this SDG, WHO has also developed the End TB Strategy that aims to end the TB epidemic by the year 2030, aiming to reduce the number of deaths due to TB by 90% and the TB incidence rate by 80% (Arinaminpathy et al., 2023). However, challenges such as complications associated with TB, lengthy treatment strategies, drug-resistant *Mtb* strains, complications related to TB and the complex and costly development of new vaccines highlight the need for a revised treatment strategy (Gygli et al., 2017; Ndlovu and Marakalala, 2016). Moreover, current antimycobacterial treatment solely targets *Mtb* and does not mitigate inflammation-associated pathology during TB (Hayford et al., 2020). Consequently, there is growing interest in HDTs as a treatment strategy to address TB (Ndlovu and Marakalala, 2016). HDTs are drugs which are used in conjunction with antimycobacterial drugs to enhance the host immune response against *Mtb*, modulate inflammation and reduce tissue damage, which is often seen in TB (Zumla et al., 2016). This approach may lead to successful treatment outcomes, reduce mortality and morbidity, facilitate long-term recovery, shorten treatment duration, and prevent additional clinical complications associated with TB (Hayford et al., 2020). The host's innate and adaptive system against *Mtb* determines whether the infection will progress from LTBI to an active TB disease state. Factors such as increased inflammation, immunocompromising conditions, stress, poor access to health care, poor living conditions, comorbidities and poor lifestyle decisions affect the host's ability to eliminate disease-causing pathogens and treatment outcomes (Zumla et al., 2016).

HDTs offer potential benefits by enhancing the host's cellular response to pathogens, which target microbial factors which cause damage within the host and initiate innate and adaptive immune processes, as well as immunological memory (Zumla et al., 2016). HDTs may be beneficial in that they may be used to combat the pathogen by targeting the host's immune mechanisms to combat the infection (Kilinç et al., 2021). Mycobacteria have established various mechanisms to evade the host's immune system, enabling the bacteria to survive and replicate within the host. Targeting the host's immune response to curb these mechanisms may aid bacterial clearance (Kilinç et al., 2021). *Mtb* prevents phagosome maturation by inhibiting the fusion of the phagosome with the lysosome. Targeting this pathway with the aid of HDTs to enhance phagosome maturation may be beneficial in clearing the infection. *Mtb* also evades the host's immune system by preventing autophagy from occurring. Targeting autophagy through the activation of host PRRs may also be a strategy for HDTs enhancing the elimination of *Mtb* (Matteucci et al., 2022; Stek et al., 2018). Next, improving the release of ROI/RNI species, which exert direct antimicrobial effects on phagocytosed *Mtb*, resulting in the elimination of *Mtb*, may also be a promising strategy for HDT (Jeong et al., 2022; Kilinç et al., 2021). The release of ROS/RNI may further be increased through the activation of PRRs. However, it is vital to prevent excessive release of these antimicrobial mediators as this may result in unwanted cell death

during *Mtb* infection. Furthermore, Mtb has been reported to favour necrotic cell death to enable its dissemination. In contrast, apoptotic cell death assists in the control of *Mtb*, as when macrophages undergo apoptosis, the cell membrane is kept intact, and *Mtb* is contained (Jeong et al., 2022; Ndlovu and Marakalala, 2016). Activation of TLRs has been said to favour apoptotic cell death, and therefore, compounds enhancing the occurrence of apoptosis may be potential HDTs (Jeong et al., 2022).

On the other hand, HDTs may also alleviate tissue damage caused by the inflammatory immune response. One promising area for developing HDTs aimed at inflammation during TB is cytokine inhibition of excessive inflammatory signals by balancing cytokine responses in a way that clears the infection and favours the host. This can include the inhibition of cytokines such as TNF-α, IL-1β and IL-6 (Young et al., 2020). In addition to cytokine inhibition, anti-inflammatory agents that enhance anti-inflammatory pathways or block pathways that result in downstream production of pro-inflammatory pathways may also be beneficial during TB. This can assist in maintaining immune efficacy while preventing tissue pathology (Tobin, 2015). Several agents targeting various immune response mediators in TB have been evaluated as HDTs for pulmonary TB, including corticosteroids, phosphodiesterase inhibitors, cytokine inhibitors, doxycycline, Vitamin D and Vitamin A (Tiwari and Martineau, 2023).

1.9 Repurposing Anti-inflammatory Drugs as Host-directed Therapies in Tuberculosis: Mechanisms, Clinical Evidence and Future Direction

Inflammation is a critical factor influencing the outcomes of TB treatment (Cubillos-Angulo et al., 2022; Zumla et al., 2016). However, as discussed in section 1.7, excessive inflammation can potentially harm the host by contributing to lung tissue pathology (Zumla et al., 2016). This has spurred interest in anti-inflammatory drugs as potential HDTs during TB infections. Such therapies, including anti-inflammatory agents, offer the potential benefit of limiting tissue damage and improving the quality-of-life post-recovery (Zumla et al., 2016).

Drug repurposing involves the utilisation of existing drugs to treat conditions other than their intended purpose due to drug-target interactions (Maitra et al., 2016). Anti-inflammatory drugs can target cytokines such as TNF-α, TGF-β and IL-1β, thereby modulating their release and limiting lung damage (Krug et al., 2021). Several drugs are undergoing clinical trials or have shown benefits to be repurposed as potential HDTs for TB, as detailed in Table 1.

Repurposing anti-inflammatory drugs shifts the therapeutic focus from traditional antituberculosis agents, which primarily target the bacteria, to addressing the host's immune response (Zumla et al., 2016). This approach aims to mitigate extreme inflammation, preserve host tissue integrity and potentially enhance the immune response to facilitate antimycobacterial clearance (Cubillos-Angulo et al., 2022).

Moreover, the safety and efficacy of some of these drugs have already been established by the Food and Drug Administration (FDA) approval for conditions such as asthma, arthritis, and immune disorders

(Zumla et al., 2016). This regulatory approval reduces the time and cost associated with developing new antibiotics from scratch and, in some instances, may include extensive safety and efficacy testing (Krug et al., 2021).

Therefore, this study aims to evaluate the effects of anti-inflammatory drugs through high-throughput screening. This research seeks to identify drugs that could be repurposed as adjunctive host-directed treatment for TB, aiming to decrease lung damage resulting from TB-associated inflammation and bolster the host's immune response against *Mtb*.

Table 1: **Displaying drugs which have undergone and are currently undergoing clinical trials to be repurposed as host-directed therapies for TB**.

Drug	Drug Target	Mechanism of action and potential benefits in Tuberculosis	Reference
Ibuprofen	COX-1 and COX-2	• Non-selective cox inhibitor utilized for pain relief, treating inflammation, rheumatoid arthritis, and fevers • Modulates the production of lipid mediators derived from arachidonic acid • Reduces the size and number of lung lesions • Decrease in bacterial load and long-term survival	(Arias et al., 2023; Kroesen et al., 2017)
Doxycycline	MMP	• Inhibits the activation of MMPs in TB infection contributing to reduced tissue damage • Exhibits anti-mycobacterial properties	(Krug et al., 2021b)
Acetylsalicylic acid	COX-1 and COX-2	• Non-selective COX-inhibitor with anti-inflammatory effects • Inhibits Thromboxane A2 production and platelet activation related to pro-inflammatory states • Limits TNF-α release by interacting with LXA_4, thus reducing inflammation	(Arias et al., 2023; Kroesen et al., 2017)
Imatinib	Tyrosine Kinases	• Induces myeloid cell differentiation and myelopoiesis • Reduction of bacterial load and number of lesions • Increased autophagy via phagosome acidification	(Tobin, 2015)
Metformin	AMPK	• Reduces TB intensity and anti-inflammatory • Reduced the number of TB related deaths in diabetic patients • Modulates the expression of HIF-α • Enhances bacterial clearance properties in TB	(Krug et al., 2021b; Tiwari and Martineau, 2023b)
Verapamil	Calcium Channel inhibitor	• The inhibition of MTB efflux pumps results in disrupting bacterial membrane integrity and increases the effects of anti-TB drugs • Enhances macrophage immunity via increased drug uptake	(Chen et al., 2018)

1.10 Rationale, aims and objectives

1.10.1 *Rationale*

Tuberculosis, caused by the infectious agent *Mycobacterium tuberculosis*, is currently treated with antibiotics that target the bacteria. Additionally, BCG is the only vaccine used as a preventative measure against TB. TB treatment is often prolonged and may result in adverse side effects, leading to poor treatment adherence. Furthermore, patients frequently endure long-term lung damage due to TB-associated harm, resulting in lifelong complications. The WHO has established a target to eliminate TB by 2030. Consequently, this study aims to evaluate the effects of anti-inflammatory drugs and TLR immunomodulatory compounds through high-throughput screening to identify drugs that could serve as adjunctive host-directed treatments for TB by reducing lung damage and enhancing the host's immune antimicrobial response.

1.10.1 ***Aims***

I: High-throughput screening of anti-inflammatory agents and their potential to reduce TB-associated inflammation and bacterial replication in PBMCs, along with analysing the effects of TLR modulation to increase the inflammatory immune response and their effects on bacterial load during Mtb infection in THP-1 cells.

II: Analysis of candidate anti-inflammatory drugs and candidate TLR immunomodulatory agents as modulators of inflammatory immune response and bacterial clearance in a biomimetic three-dimensional (3D) model of TB-induced granulomas.

III: Characterization of the spatial expression of the candidate drug target protein and the candidate TLR immunomodulatory agent’s target protein in association with TB pathogenesis in resected TB-diseased lung.

1.10.3 *Objectives*

Aim I objectives

- Co-culture blood mononuclear cells (PMBCs) with anti-inflammatory drugs chosen from a drug screening library and infect the cells with the *Mtb* H37Rv strain. To concurrently culture THP-1 cells treated with TLR immunomodulatory agents, and infect these cells with the luminescent *Mtb* strain, H37Rv LUX.
- To evaluate the effects of the anti-inflammatory drugs and TLR immunomodulatory agents on inflammation within the *Mtb*-infected PBMCs and THP-1 cells using enzyme-linked immunosorbent assay (ELISA) to measure the concentration of the inflammatory cytokines, TNF-α, IL-1β, and IL-6.

- To determine the effect of the TLR immunomodulatory agents on bacterial replication using luminometry and the luminescent *Mtb* H37Rv LUX strain.
- To shortlist candidate drugs for further analysis in Aim II based on their ability to reduce inflammation and, in the case of TLR modulatory agents, enhance bacterial clearance as determined in Aim I.

Aim II objectives

- To set up a 3D biomimetic model of the TB granuloma using a collagen-alginate matrix and PBMCs infected with H37Rv LUX. This will mimic the events during *Mtb* infection in the lung and analyse the effects of the shortlisted anti-inflammatory drug and TLR immunomodulatory agent in the 3D model of the granuloma.
- To determine the effects of the shortlisted anti-inflammatory drugs on inflammation during *Mtb* infection by measuring the level of inflammatory cytokines, TNF-α, IL-1β, IFN-γ, and IL-6, production in the 3D model using ELISA.
- To determine the effect of the shortlisted drugs on bacterial replication by obtaining OD readouts from the luminescent bacteria using luminometry.

Aim III objectives

- To validate the colocalization of the shortlisted drugs' target protein and the TLR immunomodulatory agents' target in the inflammation induced by *Mtb* infection using immunofluorescence on TB-diseased lung tissue with severe immunopathology.

1.11. Potential impact

This study will provide valuable insight into pathways associated with pathology during TB. By identifying these pathways, the research may reveal potential targets for alleviating TB-associated pathology, particularly in the context of developing HDTs. This approach offers an alternative strategy to current TB treatment, targeting the host's immune response while simultaneously aiding in bacterial clearance. Furthermore, the findings of this study could contribute to the WHO SDG to end TB, providing a new strategy to advance TB treatment. Additionally, the candidate drugs and TLR immunomodulatory agents may undergo further clinical investigation to assess their potential as HDTs, ultimately contributing to more comprehensive TB treatment strategies and improving treatment outcomes.

CHAPTER 2:

METHODS AND MATERIALS

2. Methods and materials

2.1 Cell culturing, small-molecule compound treatment and *Mtb* infection:

Study setting and ethics

This study was conducted at the Africa Health Research Institute, under the CUBS study, which has been approved by the Biomedical Research Ethics Committee (BREC) at the University of KwaZulu-Natal (BE022/13), with participants recruited from the KwaDabeka Clinic and Prince Zulu Communicable Disease Centre. KwaZulu-Natal is currently the province with the highest incidence rate of TB in South Africa (Kasprowicz et al., 2011). Approximately 30 participants were enrolled by a qualified nurse, with the procedure thoroughly explained to all potential participants, which included the collection of whole blood, long-term storage, and the use of these samples for further research purposes. Once written informed consent was obtained from each participant, the participants were enrolled in the study. For this study, a healthy control cohort was recruited, with eligibility confirmed through a negative QuantiFERON test. In addition, LTBI (QuantiFERON positive, GeneXpert negative) and active TB (GeneXpert positive) participant groups were enrolled.

2.1.1 *H37RV Mtb growth conditions*

Middlebrook 7H9 media preparation

To prepare 500 ml of Middlebrook 7H9 media supplemented with 0.5% glycerol, 0.05% Tween 80, and 10% OADC, an amount of 2.35 g of Middlebrook 7H9 broth (Becton, Dickinson and Company, USA) was dissolved in 450 ml of deionized water (dH_2O). Next, a volume of 2.5 ml of 40% glycerol (Sigma Aldrich, USA) was added to the solution. This was then autoclaved for 15 minutes at 121 °C and cooled to the touch. Upon cooling, 50 ml of BBL™ Middlebrook OADC Enrichment (Becton, Dickinson and Company, USA) and 1.25 ml of 20% Tween 80 (Sigma Aldrich, USA) were added to the media. The media was then sterilised using a Corning 1L filtering system with a 0.2 µm membrane (Corning, USA) and stored at 4 °C.

Growth conditions for the Mycobacterium tuberculosis H37Rv strain

A glycerol stock of the *Mtb* H37RV laboratory pathogenic strain (gifted by the Rubin lab at the Harvard School of Public Health, USA) was thawed, and 1 ml of the H37Rv *Mtb* stock was added into 5 ml of Middlebrook 7H9 media. The culture (now referred to as starter culture) was incubated at 37 °C with continuous shaking at 150 revolutions per minute (RPM) for 5 days. Hereafter, a subculture was prepared by taking 1 ml of the starter culture and adding it to 9 ml of Middlebrook 7H9 media. The subculture was incubated at 37 °C with continuous shaking at 150 RPM for 3-4 days until the subculture reached an optical density at wavelength of 600 nm (OD_{600}) of 0.8.

2.1.2 *PBMC isolation*

A volume of 10 ml of whole blood was collected by the field nurse in ethylenediaminetetraacetic acid (EDTA) tubes and labelled with a unique participant identification number (PID). The tubes were kept at 18-25 °C before use. A total of three tubes were collected from each participant and transported at environmental temperature from the collection site. PBMC isolation was performed based on the Ficoll-Histopaque density gradient centrifugation, in which the cells were distributed in the solution according to the density difference between PBMCs and elements found in blood. This was conducted as follows:

A volume of 10 ml of whole blood was diluted with 25 ml of 1X phosphate-buffered saline (PBS) (Gibco, United Kingdom). The diluted blood was slowly layered at an angle onto 15 ml of Histopaque (Sigma-Aldrich, USA). The tube was transferred to the centrifuge with caution and centrifuged at 800 x *g* for 30 minutes with the acceleration set to maximum and the deceleration off. This was performed to separate the elements of the whole blood. The top layer, consisting of plasma, was carefully removed from the tube and discarded. Hereafter, the buffy coat, containing PBMCs, was carefully aspirated in circular motions to avoid disruption of the bottom layer, consisting of red blood cells. The buffy coat collected was dispensed into a centrifuge tube and combined with the buffy coat collected from each tube of blood from the same PID. This was topped up to 50 ml with 1X PBS and centrifuged at 300 x *g* for 10 minutes with the acceleration and deceleration set at maximum. The supernatant was discarded, and the pellet was resuspended in 10 ml 1X PBS. A cell count was performed using the Trypan blue dye exclusion assay by mixing 10 µl of the cell suspension and 10 µl of Trypan blue dye (Gibco, USA) and placing 10 µl of this mixture onto a haemocytometer. A cell count was performed by counting the live cells (clear cells). The total number of cells suspended in 1X PBS was calculated using equations 1 and 2 in section 2.4. The tube was then centrifuged at 300 x *g* for 10 minutes with both the acceleration and deceleration set to maximum. The supernatant was discarded, and the cells were used immediately or cryopreserved. The cryopreservation processing involved resuspending the cells in 10 ml freeze media, consisting of 10% dimethyl sulfoxide (DMSO) (Sigma-Aldrich, USA) and 90% fetal bovine serum (FBS) (Gibco, United Kingdom). The cell suspension was aliquoted into 1 ml volume cryovials and stored at 5-10 million cells/ml. The PBMCs were stored in liquid nitrogen until further use.

Media preparation and thawing of PBMCs

R10 media was prepared using Roswell Park Memorial Institute (RPMI) medium 1640 (Gibco, United Kingdom) supplemented with 10% FBS and 10 mM HEPES (Sigma-Aldrich, United Kingdom) and 1X GlutaMax™-1 (Gibco, USA). The PBMCs were rapidly thawed by placing the vial into a water bath set at 37 °C for 30 to 60 seconds or until a small bit of ice remained. Hereafter, 1 ml of pre-warmed media was quickly added to the PBMCs to dilute the concentration of DMSO and to wash the PBMCs. Next, the PBMCs were transferred to a 15 ml centrifuge tube containing 5 ml of pre-warmed R10 media. The initial cryovial was washed with an additional 1 ml of media, and this was transferred to the 15 ml

centrifuge tube. The PBMCs were centrifuged at 400 *x* g for 10 minutes at 4°C. The supernatant was discarded, and the pellet was resuspended in 1 ml of pre-warmed R10 media. The PBMCs were then counted using the Trypan blue dye exclusion assay as described above. The PBMCs were diluted to obtain a concentration of 100 000 cells/200 µl. A volume of 200 µl per well of PBMC suspension was then added to a 96-well cell culture plate (Corning, USA)

2.1.3 *Drug Treatment and Infection of PBMCs*

Following the addition of PBMCs to a 96-well plate, a volume of 1 µl of 10 mM drugs of interest (as detailed in Table 2, MedChemExpress, USA) was added into the allocated wells to achieve a final concentration of 40 µM of the allocated drug. An amount of 1 µl R10 media was added to the control wells. The cell culture plates were incubated for 2 hours at 37 °C with 5% CO_2 in an incubator set at 90% humidity. The previously prepared H37Rv subculture, grown to an OD_{600} of 0.8, was collected into a centrifuge tube and centrifuged at 2 400 x *g* for 10 minutes. The supernatant was discarded, and the pellet was resuspended in 10 ml of R10 media. The OD_{600} was measured, and the required dilutions were performed to obtain a concentration of 20 000 000 cells/ml. After achieving the desired concentration, 50 µl of the H37Rv *Mtb* suspension was added to the allocated wells to obtain a multiplicity of infection (MOI) of 10. Additionally, 50 µl of R10 media was added to the control wells. A final volume of 250 µl in each well was obtained. The plates were then incubated for 3 days at 37 °C with 5% CO_2 and 90% humidity.

Table 2: **Drugs Screened and Their Targets.**

No.	Drug	Target	Catalogue No.
1	1,4-Chrysenequinone	Aryl Hydrocarbon Receptor	HY-111441
2	Balsalazide	Interleukin Related; STAT	HY-B0667
3	C-176	STING	HY-112906
4	CAY 10465	Aryl Hydrocarbon Receptor	HY-112627
5	Chloropyramine hydrochloride	FAK; Histamine Receptor; VEGFR	HY-B1305
6	Clemizole (hydrochloride)	HCV; HCV Protease; Histamine Receptor	HY-30234A
7	Diclofenac	COX	HY-15036
8	Ebastine	Histamine Receptor	HY-B0674
9	Etoricoxib	COX	HY-15321
10	Flufenamic acid	AMPK; Calcium Channel; Chloride Channel; COX; Potassium Channel	HY-B1221
11	Guaiacol	COX; NF-κB	HY-N1380
12	Histamine (phosphate)	Histamine Receptor	HY-A0129
13	Ibuprofen	COX	HY-78131
14	IFN alpha-IFNAR-IN-1 (hydrochloride)	IFNAR	HY-12836A
15	INCB 3284	CCR	HY-15450A
16	Indomethacin	Autophagy; COX	HY-14397
17	Interferon receptor inducer-1	IFNAR	HY-112189
18	IRAK-1-4 Inhibitor I	IRAK	HY-13329
19	ITE	Aryl Hydrocarbon Receptor	HY-19317
20	JNJ-5207852	Histamine Receptor	HY-12190
21	Loratadine	Histamine Receptor	HY-17043
22	Loxoprofen	COX	HY-B0578

23	MK-886	FLAP	HY-14166
24	Naproxen	Autophagy; COX	HY-15030
25	Neochlorogenic acid	COX; Interleukin Related; NF-κB; TNF Receptor	HY-N0722
26	PF-543 (Citrate)	SPHK	HY-15425A
27	Plerixafor	CXCR	HY-10046
28	Quiflapon sodium	FLAP	HY-50714
29	RS 504393	CCR	HY-15418
30	Salicylic acid	Autophagy; COX; Mitophagy	HY-B0167
31	seco-Isolariciresinol Diglucoside	Keap1-Nrf2; NF-κB; NOD-like Receptor (NLR)	HY-N0727
32	SKI II	SPHK	HY-13822
33	Sodium Salicylate	Autophagy; COX	HY-B0167A
34	Suplatast (Tosilate)	Interleukin Related	HY-17002
35	Tapinarof	Aryl Hydrocarbon Receptor	HY-109044
36	Tyrphostin A1	Interleukin Related	HY-16668
37	Vadimezan	Interleukin Related; STING	HY-10964
38	WZ811	CXCR	HY-15478
39	Vadimezan	Interleukin Related; STING	HY-10964
40	TAM-X1	Interleukin Related	HY-19969
41	Adelmidrol	COX; NF-κB; PPAR	HY-B1026
42	Avacopan	Complement System	HY-17627
43	BEC (hydrochloride)	Arginase	HY-19548A
44	Betahistine (dihydrochloride)	Histamine Receptor	HY-B0524A
45	Cetirizine (dihydrochloride)	Histamine Receptor	HY-17042A
46	CU CPT 22	Toll-like Receptor (TLR)	HY-108471
47	CU-CPT-9a	Toll-like Receptor (TLR)	HY-112667
48	Eucalyptol	5-HT Receptor; Interleukin Related; Potassium Channel; TNF Receptor	HY-N0066
49	Gardiquimod trifluoroacetate	HIV; Toll-like Receptor (TLR)	HY-103697A

50	Ginsenoside Rd	Calcium Channel; COX; Cytochrome P450; NF-κB	HY-N0043
51	Imiquimod	Autophagy; Toll-like Receptor (TLR)	HY-B0180
52	MCC950 (sodium)	NOD-like Receptor (NLR)	HY-12815A
53	Methylthiouracil	ERK; Interleukin Related; NF-κB; TNF Receptor	HY-B0513
54	Motolimod	Toll-like Receptor (TLR)	HY-13773
55	Mulberroside A	Interleukin Related; TNF Receptor; Tyrosinase	HY-N0619
56	Nodinitib-1	NOD-like Receptor (NLR)	HY-18639
57	Olopatadine (hydrochloride)	Histamine Receptor	HY-B0426A
58	Reparixin (L-lysine salt)	CXCR	HY-15252
59	Troxerutin	NOD-like Receptor (NLR)	HY-N0139
60	VGX-1027	Interleukin Related	HY-15507
61	Y-320	Interleukin Related	HY-15898
62	AM679	FLAP	HY-14460
63	Chloroquine (diphosphate)	Autophagy; Toll-like Receptor (TLR)	HY-17589
64	L-NAME (hydrochloride)	NO Synthase	HY-18729A
65	Veratric acid	COX	HY-N2007
67	AMD 3465 (hexahydrobromide)	CXCR; HIV	HY-15971
68	APY0201	Interleukin Related; PIKfyve	HY-15982
69	Azelastine (hydrochloride)	Histamine Receptor	HY-B0462
70	Baohuoside I	Apoptosis; CXCR	HY-N0011
71	CU-CPT-8m	Toll-like Receptor (TLR)	HY-112050
72	Cyproheptadine (hydrochloride sesquihydrate)	5-HT Receptor; Histamine Receptor	HY-B1165
73	Desloratadine	Histamine Receptor	HY-B0539
74	Diacerein	Interleukin Related	HY-N0283
75	Eltrombopag	Thrombopoietin Receptor	HY-15306
76	Fiboflapon	FLAP	HY-15874
77	GIBH-130	Interleukin Related	HY-101860

78	Ginsenoside Rg3	Amyloid-β; COX; NF-κB; Potassium Channel; Sodium Channel	HY-N0603
79	Ginsenoside Rh1	Interleukin Related; PPAR; TNF Receptor	HY-N0604
80	Hydroxychloroquine sulfate	Parasite; Toll-like Receptor (TLR)	HY-B1370
81	Indole-3-carbinol	Aryl Hydrocarbon Receptor; NF-κB	HY-N0170
82	Leukadherin-1	Complement System	HY-15701
83	Lornoxicam	COX	HY-B0367
84	MF63	PGE synthase	HY-13283
85	Nimesulide	COX	HY-B0363
86	Oxaprozin	COX; NF-κB	HY-B0808
87	PF-4136309	CCR	HY-13245
88	Resatorvid	Autophagy; Toll-like Receptor (TLR)	HY-11109
89	SB290157 (trifluoroacetate)	Complement System	HY-101502A
90	Sinensetin	PGE synthase; TNF Receptor	HY-N0297
91	Vesatolimod	Toll-like Receptor (TLR)	HY-15601
92	Vidofludimus	Interleukin Related	HY-14908
93	DL-Norvaline	Arginase; Endogenous Metabolite	HY-W010510
94	Ginsenoside Rc	GABA Receptor; Interleukin Related; TNF Receptor	HY-N0042
95	Ginsenoside Rb1	Autophagy; IRAK; Mitophagy; Na+/K+ ATPase; NF-κB	HY-N0039
96	Skatole	Aryl Hydrocarbon Receptor; p38 MAPK	HY-W007355
97	Benzydamine (hydrochloride)	PGE synthase	HY-30235A

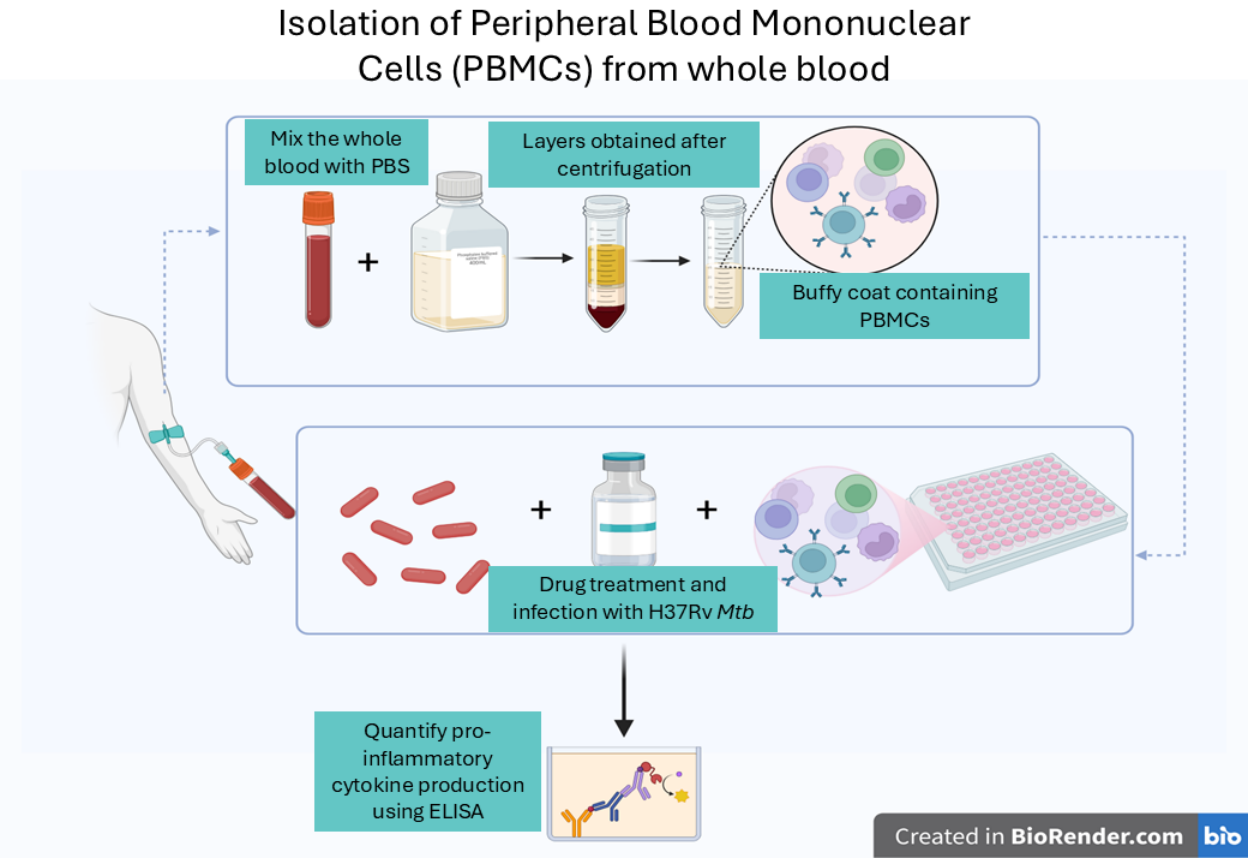

Figure 2.1. **Schematic representation of the experimental flow for high-throughput drug screening of small-molecule compounds.** Cytokine production was analysed using ELISA after drug treatment and infection with H37Rv *Mtb*.

2.1.4 *Collection of PBMC supernatants*

The PBMC supernatant was collected 3 days after infection by aspirating the contents of each well and transferring it to appropriately labelled microcentrifuge tubes. To pellet any remaining cells and debris, the PBMC suspension was centrifuged at 16 000 x *g* for 5 minutes. The supernatant obtained was transferred into a respective labelled Corning® Costar® Spin-X® centrifuge tube filter (Corning, USA) and centrifuged at 16 000 x *g* for 5 minutes. The filtered flow-through was collected and aliquoted into microcentrifuge tubes. The aliquoted supernatant was stored at -80 °C for further use.

2.1.5 *Enzyme-linked immunosorbent assay (ELISA) for cytokine detection after drug treatment*

ELISA was utilised to detect and quantify the level of pro-inflammatory cytokines (specifically IL-1β, IL-6, and TNF-α,) in the supernatant collected upon drug treatment and *Mtb* infection of PBMCs. This was performed using BD OptEIA Human ELISA kits (BD Biosciences, USA) for each of the specified cytokines. This was conducted as follows:

ELISA buffer preparation

A coating buffer consisting of 0.2 M Sodium carbonate, pH 9.5, was prepared by adding 6 capsules of Carbonate-Bicarbonate Buffer (Sigma-Aldrich, USA) to 150 ml of dH_2O. Next, 500 ml of assay diluent consisting of phosphate-buffered saline (PBS) with 10% FBS was prepared by adding 50 ml 10X PBS (Gibco, United Kingdom) and 50 ml FBS to 400 ml dH_2O. An amount of 5 L wash buffer, PBS with 0.05% Tween-20, was prepared by adding 500 ml 10X PBS and 2.5 ml Tween-20 (Sigma-Aldrich, USA) to 4.5 L dH_2O. A stop solution, consisting of 2M H_2SO_4, was prepared by adding 6.396 ml of 10.38 M Sulfuric acid (Sigma-Aldrich, USA) to 53.602 ml dH_2O. The buffers were stored at 4 °C until required for use or up to 3 days after preparation.

ELISA

A volume of 44 µl of capture antibody was diluted in 11 ml of coating buffer or as indicated by the manufacturer's instructions. This was performed for each of the antibodies of interest. A volume of 100 µl of the diluted capture antibody was added to each well of the respective 96-well plates to coat the plates. The plates were then sealed and incubated overnight at 4 °C. Hereafter, the coated plates, wash buffer, and assay diluent were allowed to reach room temperature (RT). Upon reaching RT, the contents of the plates were decanted. The plates were washed 3 times using 300 µl/well of the previously prepared wash buffer. The plates were dried by gently banging them on a paper towel. The plates were then blocked by adding 200 µl of Assay diluent into each well, followed by a 1-hour incubation period at RT. After incubation, the contents of the plates were decanted, and the plates were washed as previously described. Next, the standards were prepared by diluting the required volumes of standard for each cytokine in 300 µl of assay diluent, as indicated in Table 3. The standards were then serially diluted by adding 300 µl of the previously diluted standard to 300 µl of assay diluent to obtain the standard concentration range specified in Table 3. An amount of 100 µl of sample or standard was added to the respective wells. The plates were incubated at RT for 2 hours. During the incubation period, a working detector solution was prepared by diluting 44 µl of detection antibody and 44 µl Streptavidin-horseradish peroxidase conjugate (Sav-HRP) in 11 ml assay diluent for the respective cytokines (IL-6, TNF-α, and IFN-γ). For IL-1β, 11 µl of detection antibody only was diluted in 11 ml of assay diluent. Upon the 2-hour incubation period, the contents of the plates were decanted, and the plates were washed 5 times. It was ensured that all the wash buffer was removed from the plates by gently blotting the plates on paper towel. A volume of 100 µl working detector solution (Detection Antibody + SAv-HRP or Detection Antibody only for IL-1β) was added to each well. The plates were sealed and incubated for 1 hour and were washed 7 times (5 times for the IL-1β) with 300 µl/well wash buffer. For the IL-1β plate, 44 µl of Sav-HRP was diluted with 11 ml assay diluent, and 100 µl of this was added into each well. This was incubated for 30 minutes. A volume of 100 µl of substrate solution

(Tetramethylbenzidine (TMB) and hydrogen peroxide), 1-Step™ TMB ELISA Substrate Solutions (Thermo Fisher Scientific, USA) was added to the other plates. The plates were sealed and incubated for 30 minutes in the dark at RT. Hereafter, 50 µl of previously prepared stop solution was added to each well. Upon completion of the 30-minute incubation for IL-1β, the plate was washed 7 times, and the rest of the steps were completed for the IL-1β. The absorbance of all the plates was measured using a microplate reader, within 30 minutes of adding the stop solution, at 450 nm with a wavelength correction of 570 nm. The values obtained were used to determine the concentration of IL-1β, IL-6, TNF-α, and IFN-γ.

Table 3: **Stock Concentrations of Cytokines and Standard Curve Ranges.**

Cytokine	Stock concentration (ng/ml)	Diluted stock volume (µl)	Working concentration (ng/ml)	Standard curve concentration range (ng/ml)
TNF-α	34	17.65	1	1.0 - 0.0
IL-6	205	0.88	0.3	0.3 - 0.0
IL-1β	60	5.0	0.5	0.5 - 0.0

2.1.6 *THP-1 cell culture maintenance*

Media preparation and thawing of THP-1 cells

THP-1 cells, a human leukemia monocytic cell line isolated from a one-year-old patient with monocytic leukemia, are used as an *in vitro* model to gain insight into the biochemistry, physiology, and drug delivery of monocytes and/or macrophages (Liu et al., 2023). THP-1 cells, which were gifted by the Sigal lab (AHRI, Durban), were cultured and maintained using protocols described by Tsuchiya *et al*., with adaptations (Tsuchiya et al., 1980).

THP-1 cells were cultured and maintained in RPMI medium 1640 supplemented with 10% FBS, 4.5 M g/L D-glucose (Gibco, United Kingdom), 10 mM HEPES, 1 mM Sodium Pyruvate (Sigma-Aldrich, USA), 0.05 mM β-mercaptoethanol (Gibco, United Kingdom), and 1X Glutamax (Gibco, United Kingdom). The RPMI medium was warmed to 37 °C in a water bath. Next, a vial of cryogenically frozen THP-1 cells was retrieved from liquid nitrogen and thawed by placing the vial in a water bath set at 37 °C for 20 seconds or until a small amount of ice remained. The cells were diluted with 1 ml of warm RPMI-1640 media and transferred to a 15 ml centrifuge tube containing 5 ml of RPMI-1640 media. The cryovial was then washed with an additional 1 ml of media, and this was transferred to the centrifuge tube. Hereafter, the cells were centrifuged at 400 *x* g for 5 minutes at room temperature. The supernatant was discarded, and the cells were

resuspended in 5 ml of media. A cell count was performed using the Trypan blue dye exclusion assay, and the cells were seeded at a concentration of 1×10^5 cells/ml in a T25 tissue culture flask (Corning, USA), ensuring that the cell suspension did not exceed 20 ml. The cells were then placed in an incubator at 37 °C with 5% CO_2 for 3 days. After 3 days, the confluency of the cells was analysed under a microscope, and the Trypan blue dye exclusion assay was performed to confirm the confluency of the cells. Once the cells reached a confluency of 1×10^6 cells/ml, the cells were sub-cultured using a split ratio of 1:3 and placed in an incubator at 37 °C with 5% CO_2. Fresh media was added to the cells every 3-4 days, and a cell density of $5 \times 10^5 – 8 \times 10^5$ cells/ml was maintained. The cells were not sub-cultured past the 5th passage to ensure alterations to the cell morphology did not occur.

2.1.7 *THP-1 differentiation and drug treatment with Toll-like receptor modulators to assess effects on bacterial killing*

The cell suspension was transferred into a 50 ml Falcon tube and centrifuged at 400 *x* g for 5 minutes. The supernatant was discarded, and the pellet was resuspended in 5 ml of fresh warm media. A cell count was performed using the Trypan blue dye exclusion assay, and the cell suspension was diluted to obtain a cell density of 5×10^5 cells/ml. Hereafter, 200 µl of the cell suspension was added into each well of a 96-well cell culture plate to obtain a final concentration of 100 000 cells/200 µl. To differentiate the THP-1 cells from monocytes to macrophages, 1 µl of 5 µM of phorbol-12-myristate-13-acetate (PMA) was added to each well to obtain a final concentration of 25 nM PMA in each well. The cells were incubated at 37 °C with 5% CO_2 for 3 days. Thereafter, cell differentiation from monocytes to macrophages was confirmed by examining the cell morphology with the aid of a microscope. Upon confirmation of differentiation, the media was discarded, and the cells were washed using 250 µl of 1X PBS. This was repeated three times to ensure that all the PMA was removed. A volume of 200 µl of fresh media was added to each well, and the cells were incubated for 24 hours at 37 °C with 5% CO_2. This was performed to allow the cells to undergo a recovery period due to PMA-induced stress. Following the recovery period, 1 µl of the TLR modulatory agents, displayed in Table 4, was added to the respective wells. The cells were then incubated for 2 hours at 37 °C with 5% CO_2.

Table 4: **Summary of Immunomodulatory Drugs Screened and Their Respective Targets.**

No.	Drug	Target	Catalogue No.
1	Resiquimod	Toll-like Receptor (TLR)	HY-13740
2	Atractylenolide I	JAK; STAT; Toll-like Receptor (TLR)	HY-N0201
3	Chloroquine (diphosphate)	Autophagy; Toll-like Receptor (TLR)	HY-17589
4	CU-CPT-9b	Toll-like Receptor (TLR)	HY-112051
5	CU-CPT-8m	Toll-like Receptor (TLR)	HY-112050
6	Hydroxychloroquine sulfate	Parasite; Toll-like Receptor (TLR)	HY-B1370
7	Vesatolimod	Toll-like Receptor (TLR)	HY-15601
8	Imiquimod	Autophagy; Toll-like Receptor (TLR)	HY-B0180
9	Motolimod	Toll-like Receptor (TLR)	HY-13773
10	CU-CPT-9a	Toll-like Receptor (TLR)	HY-112667
11	CU CPT 22	Toll-like Receptor (TLR)	HY-108471
12	Toll-like receptor modulator	Toll-like Receptor (TLR)	HY-10018
13	Gardiquimod trifluoroacetate	HIV; Toll-like Receptor (TLR)	HY-103697A

2.1.8 *Growth conditions of Mycobacterium tuberculosis H37Rv LUX strain*

Middlebrook 7H9 media supplemented with 0.5% glycerol, 0.05% Tween-80, 10% OADC, and 25 µg/ml of kanamycin sulfate (Sigma-Aldrich, USA) was prepared as previously described in section 2.1.1. Hereafter, a starter culture for the bioluminescent *Mtb* H37Rv LUX strain expressing a luxABCDE operon from *P. luminescence* (Gifted from the Steyn Lab) was prepared. This was done by thawing a 1 ml glycerol stock of H37Rv, which was pipetted into 5 ml of Middlebrook 7H9 media previously prepared. The starter culture was then incubated at 37 °C with 5% CO_2 and shaken at 150 RPM for 5 days. After 5 days, 1 ml of the starter culture was transferred into 9 ml of Middlebrook 7H9 media supplemented with 25 µg/ml of kanamycin to prepare a subculture. The subculture was incubated and shaken at 150 RPM at 37 °C with 5% CO_2 for 3 days until the subculture reached an OD_{600} of 0.8. This system allowed for the constitutive emission of luminescence without the need for any additional substrates.

2.1.9 *Treatment and infection of THP-1 cells with H37Rv LUX strain to determine the antimicrobial effects of the TLR modulators*

THP-1 cells, which were cultured and treated with TLR modulatory agents displayed in Table 4, were infected with the H37Rv LUX strain as described in section 2.1.3. and incubated for 4 hours. Hereafter, the infected THP-1 cells were washed three times with 250 µl of 1X PBS to remove any extracellular H37Rv LUX. The cell culture plate was then transferred to a luminometer, where the luminescence was measured. The luminescence measured was directly proportional to the amount of H37Rv LUX present at the time of measurement, as facilitated by the luxABCDE operon expressed by the strain. This provided insight into the anti-bacterial properties of macrophages aided by TLR modulators as potential targets for adjunctive TB vaccine development.

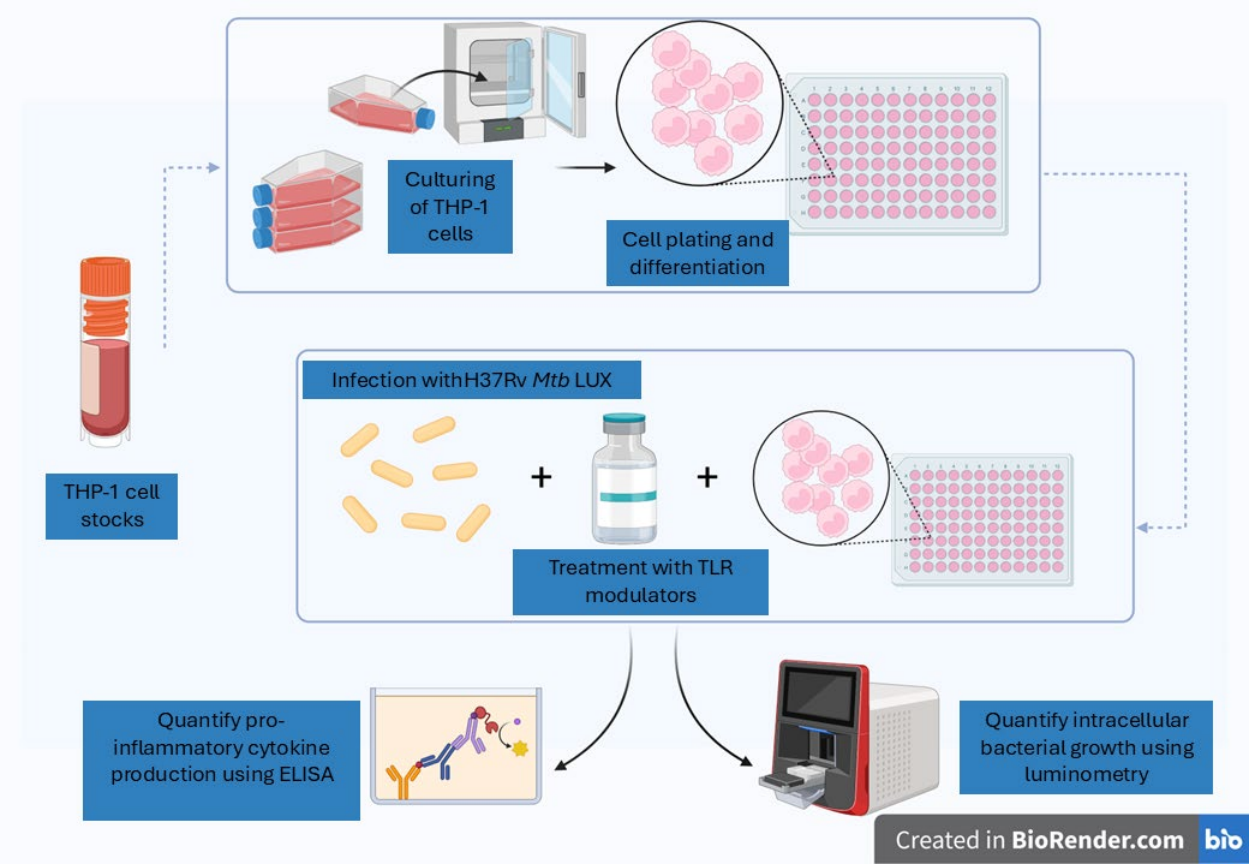

Figure 2.2: **Schematic representation of the experimental flow for screening of TLR immunomodulatory agents.** Cytokine production was analysed using ELISA after drug treatment and infection with H37Rv *Mtb* LUX. Luminometry was used to measure intracellular growth of *Mtb* after TLR modulation.

2.1.10 *Assessment of inflammatory response in PBMCs treated with Toll-like receptor modulators*

To assess the effects of the TLR modulator agents, TLR M, CU-CPT-9a, chloroquine (diphosphate), or a combination of CU-CPT-9a and chloroquine (diphosphate), PBMCs were thawed and cultured, then treated with 20 µM TLR modulatory agents as described in section 2.1.7 The PBMCs were incubated for 3 days at 37 °C with 5% CO_2 in an incubator set at 90% humidity. After the incubation, the supernatant was collected, and ELISA was performed as described in section 2.1.5.

2.2 Evaluating the effects of chosen drugs in an *in vitro* 3D granuloma-like model

A 3D microsphere model, using bio-electrospray technology, was set up to form a biomimetic physiologically relevant *in vitro* 3D granuloma-like tissue cell culture system and gain closer insight into the potential effects of selected drugs in alleviating pathology. This was performed using techniques described by Tereza *et al*. (2017) (Tezera et al., 2017).

2.2.1 *Day 1: Buffer preparation, Equipment Autoclaving, and Alginate Preparation*

In preparation for setting up the 3D model, the following items were autoclaved: five 150 ml Duran® borosilicate crystalising glass beakers with spouts (DWK Life Sciences, Germany), five pieces of 1 cm magnetic stirrers, six Female Luer Thread Style Connectors (VWR, USA), 3 pairs of Nalgene™ Polypropylene Scissor-Type forceps (Thermo Fisher Scientific, USA), tissue paper, and 3 pieces of 45 cm sterile silicon tubes (Thermo Fisher, USA). Next, 50 ml of 3% Ultrapure sodium alginate PRONOVA™ UP MVG (Novamatrix, Norway) in Hanks' Balanced Salt Solution (HBSS) without Ca/Mg (Gibco, United Kingdom) was prepared in aseptic conditions. The solution was vortexed for 3 minutes to partially dissolve the alginate. This was placed on a roller mixer overnight at 4°C. Subsequently, 1 M Calcium Chloride was prepared by dissolving 147 g of Calcium chloride anhydrous (Thermo Scientific, USA) and 23.8 g of HEPES (Sigma-Aldrich, United Kingdom) in 1 L of dH_2O, and the pH was adjusted to 5-6. This was to be used as a precipitation bath solution. The solution was sterilised using a 0.22 µm filter and stored at RT. Next, 50 ml of 0.05 N Sodium hydroxide (Sigma-Aldrich, United Kingdom) in 0.2 M HEPES was prepared by mixing 2.5 ml NaOH with 10 ml 1 M HEPES and adding 37.5 ml Ultrapure distilled water (Gibco, United Kingdom). The solution was filter sterilised using a 0.22 µm filter and stored at RT.

2.2.2 *Day 2: Preparation of Alginate-Collagen Mixture and Peripheral Blood Mononuclear Cells Extraction*

A volume of 30 ml of a collagen-alginate mix was prepared by combining 15 ml of the previously prepared 3% alginate with 1.35 ml of 0.05 N NaOH in 0.2 M HEPES and 2.7 ml of 7.5% Sodium bicarbonate (Gibco, United Kingdom). This mixture was filter sterilised using a 0.22 µm syringe-driven filter (Merck, Ireland). After filtering, 10.95 ml of human collagen type 1 (3 mg/ml, Advanced Biomatrix, USA) was added to the mixture. This was performed to obtain a collagen-alginate mixture consisting of 50% 3% alginate, 4.5% 0.05 N NaOH in 0.02 HEPES, 9% of 7.5% $NaHCO_3$, and 36.5% human collagen. Hereafter, 25 ml of this mixture was aliquoted into five different Sterlin™ 7 ml polystyrene Bijou containers (Thermo Fisher, USA), with each container receiving a total of 5 ml. This was stored at 4 °C until required.

PBMCs were isolated using the Ficoll-Histopaque density gradient centrifugation as described in section 2.1.2 until the completion of the first wash of the buffy coat. Before the final wash, the cells were resuspended in 50 ml of HBSS without Ca/Mg, and 15 µl of the cell suspension was used for cell counting using the Trypan Blue dye exclusion assay. The appropriate number of cells was taken from the cell suspension (25 million cells/5 ml of alginate). This was centrifuged at 320 × *g* for 8 minutes at 4 °C. The supernatant was discarded, and the PBMCs were resuspended in 30 ml of RPMI medium. The PBMCs were infected with H37Rv LUX *Mtb* using an MOI of 0.1, using the protocol described in section 2.1.3. The infected cells were transferred into a T75 cell culture flask (Corning, USA) and

incubated overnight at 37 °C with 5% CO_2. On the other hand, the 25 million uninfected cells (healthy control) sample was added to a T25 cell culture flask and incubated overnight at 37 °C with 5% CO_2.

2.2.3 *Day 3: Preparation of Cell Encapsulation Setup for Bio-electrospray*

In preparation for the cell encapsulation, 100 mM $CaCl_2$ was prepared using the 1 M $CaCl_2$ solution and diluting it with HBSS without Ca/Mg. This was used as a working solution for the $CaCl_2$ gelling bath. The flasks containing the PBMCs were removed from the incubator, and the cells were transferred to two separate 50 ml centrifuge tubes. A volume of 5 ml of Versene (Gibco, United Kingdom) was added to each of the flasks, as a detachment solution, and this was incubated for 8-10 minutes at 37°C with 5% CO_2. Upon completion of the incubation, 5 ml of HBSS without Ca/Mg was added to the flasks to dilute the effects of the Versene. The bottom of the flask was carefully scraped using a cell scraper to resuspend the remaining cells. The remaining contents of each flask were added to the allocated 50 ml centrifuge tubes. The flasks were rinsed with 10 ml HBSS without Ca/Mg, which was then added to the allocated centrifuge tubes. The cells were centrifuged at 320 × *g* for 8 minutes. The supernatant was carefully discarded, and the cells were resuspended in HBSS without Ca/Mg (i.e., 50 µl per 5 x 10^6 cells). The collagen-alginate mixture was obtained from the fridge, and the cells were added to the respective 7 ml Bijou container of collagen-alginate mix. This was done by adding 25 million cells/5 ml of alginate. This was stored at 4 °C until required for cell encapsulation.

2.2.4 *PBMC encapsulation*

The bead generator (Nisco Engineering, Switzerland) was set up as described by Tezera et al. (2017). The syringe driver was set to a speed of 10 ml/h. A magnetic stirrer was placed into a borosilicate beaker. The silicon tubes with female Luer thread style connectors at each end and nozzles were connected to the needle in the arm of the encapsulator. An empty 150 Borosilicate glass beaker with a 1 cm magnetic stirrer was placed under the encapsulator. Hereafter, 50 ml of HBSS without Ca/Mg was passed through the tube with the aid of a 20 ml syringe to wash the system and ensure that the needle was connected correctly and there were no leaks present in the system. The arm was dried using sterile tissue. Next, 5 ml of the collagen-alginate mixture containing PBMCs was slowly aspirated into a 5 ml syringe while preventing the formation of air bubbles. The syringe was connected to the tube using the connector attached at the end of the tube. The syringe plunger was pushed gently until the solution reached the bead generator needle. A volume of 80 ml of 100 mM $CaCl_2$ in HBSS without Ca/Mg was added to a new clean borosilicate beaker containing a clean magnetic stirrer. The beaker was placed under the arm of the encapsulator. The syringe was then placed in the syringe driver while ensuring that the driving screw contacted the end of the syringe. The doors of the bead generator were closed. The voltage was set to 7 kV, and the stirrer was set to 70%. The voltage and stirrer were then turned on, and the syringe driver was started. Once the syringe was empty, a second batch of PBMC-collagen-alginate was injected to drive the mixture present in the dead space through the encapsulator needle. Once the second batch

of the PBMC-collagen-alginate mixture reached the dead space of the tubing, the bead generator was paused. Hereafter, the syringe was replaced with a syringe containing 5 ml of HBSS without Ca/Mg. The bio-electrospray was initiated and allowed to run until all the PBMC-collagen-alginate was dispensed into the gelling bath, until no spheroids were being formed. The bead generator was stopped, and the microspheres were decanted into a 50 ml Falcon tube. The microspheres were allowed to settle, and the supernatant was removed using a Pasteur pipette. The Falcon tube was topped up to 50 ml with HBSS with Ca/Mg. The tube containing the microspheres was placed in a Falcon tube rack to allow the microspheres to settle, and the HBSS was removed. The microspheres were then washed with HBSS with Ca/Mg twice by adding HBSS with Ca/Mg and then removing using a Pasteur pipette. This process was repeated for each of the treatment conditions. When changing between different treatment conditions, it was ensured that a clean Borosilicate beaker, magnetic stirrer, silicone tube, and fresh 100 mM $CaCl_2$ were used during cell encapsulation.

The microspheres obtained were aliquoted into sterile Eppendorf tubes using a sterile Pasteur pipette. To avoid the microspheres from settling, it was ensured that the Falcon tube containing microspheres was continuously agitated to keep a constant concentration of microspheres in the media. For each condition, 1 ml of microspheres were aliquoted into each Eppendorf tube. Next, 700 µl of RMPI media supplemented with 10% FBS, 4.5 M g/L D-glucose, 10 mM HEPES, 1 mM Sodium Pyruvate, 0.05 mM β-mercaptoethanol, and 1X Glutamax was added to each of the Eppendorf tubes.

2.2.*5 Drug treatment of microspheres with candidate drugs*

To obtain a final drug concentration of 40 µM, 6.8 µl of the candidate drugs (stock: 10 mM) selected from Aim I was added to the respective microspheres. These were Tam-X1 and Toll-like receptor modulator (TLR M). The microspheres were then placed in an incubator set at 37°C with 5% CO_2. The final conditions consisted of Control (uninfected microspheres), H37Rv *Mtb* (infected untreated microspheres), Tam-X1-treated microspheres and TLR M-treated microspheres. This was then utilised for downstream analysis. The supernatant of each of the different microspheres was collected on day 3, day 10, and day 20 after treatment. This was performed by transferring the supernatant into a respective labelled Corning Costar Spin-X centrifuge tube filter and centrifuging at 16 000 x g for 5 minutes to remove any H37Rv present in the supernatant. The flow-through of each tube was collected and aliquoted into allocated microcentrifuge tubes. This was then stored at -80 °C for downstream assays.

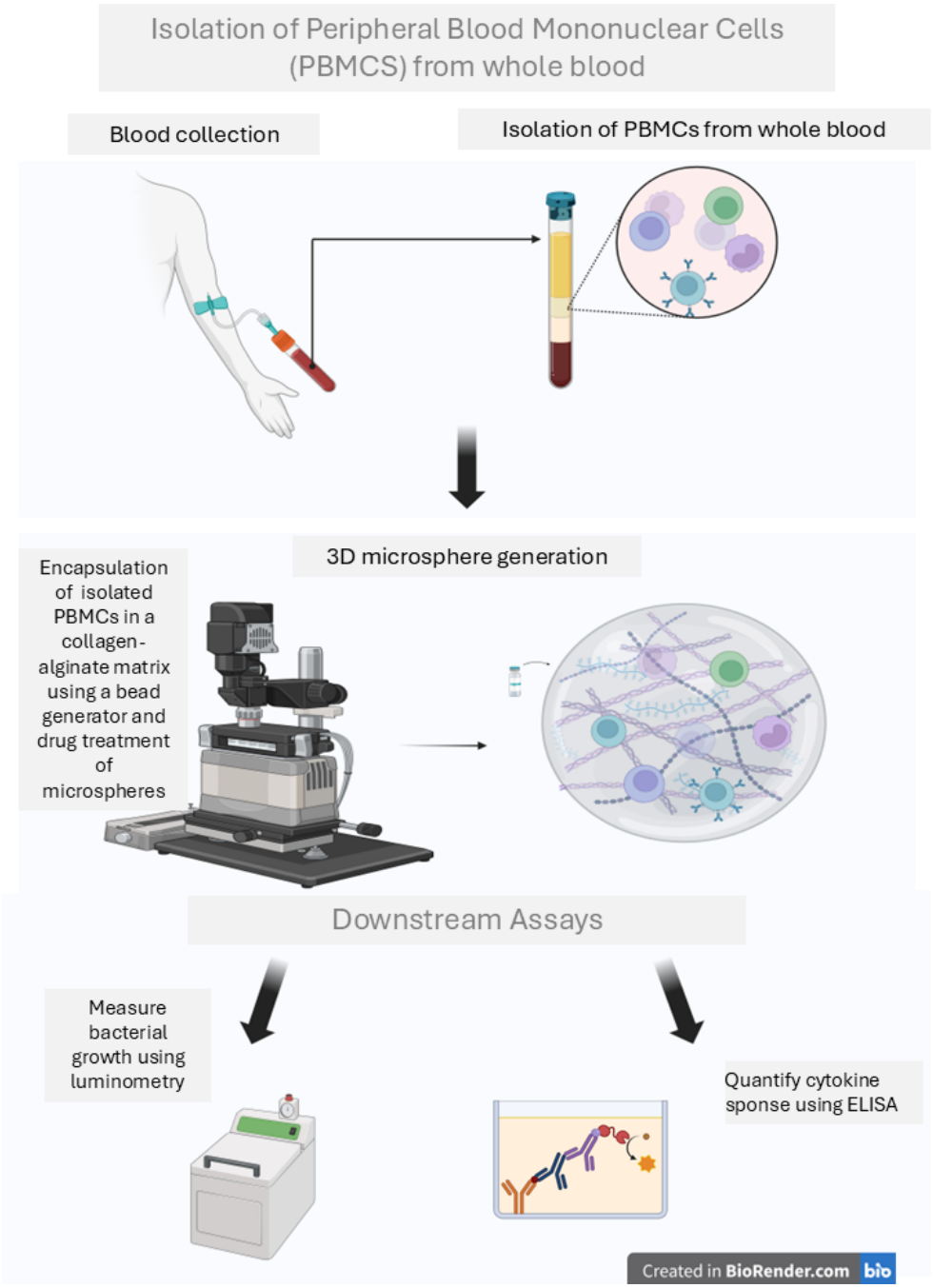

Figure 2.3: **Schematic representation of the experimental flow used to construct a biomimetic 3D collagen-alginate model to determine the effects of the selected drugs on inflammation and intracellular bacterial growth during *Mtb* infection using ELISA and luminometry.**

2.2.6 *Luminometry*

Luminometry was performed as previously described in section 2.1.9 to measure bacterial killing after treatment with the drugs. The luminescence of the H37Rv LUX strain was measured every day for 7 days and then every third day until day 20.

2.2.7 *ELISA*

The supernatant collected on day 3 and day 10 was used to measure the expression of the pro-inflammatory cytokines, IL-6 and IL-1β, as described in section 2.1.5. This was performed to measure cytokine production to gain insight into the effects of the drugs on reducing inflammation during *Mtb* infection.

2.3 Analysis of the colocalization of drug targets and inflammation in resected lung tissue of TB patients with lung damage

Immunofluorescence is a technique that allows the visualisation of various molecules present in cells and tissue with the aid of fluorescently tagged antibodies (Im et al., 2019). This technique was used to analyse the target of the various drugs of interest and their spatial relation to inflammation within the granuloma of resected lung tissue of TB patients.

Study setting and tissue sample collection

Lung tissue samples (n=14) were obtained from patients living with TB who have undergone lung resection due to severe TB-associated lung damage, through the Africa Health Research Institute (AHRI) lung study at a collaborating hospital called King Dinizulu Hospital Complex located in Durban, South Africa. This study was approved by the BREC at the University of KwaZulu-Natal (BE019/13). Succeeding the lung resection, tissue blocks were categorised by the operating surgeon, ranging from the most to least diseased ("non-affected," "mildly affected," and "severely affected") sections of the tissue section removed. This was performed by macroscopic estimation based on appearance. A PID was given to each patient upon receiving their written consent. Each of the sections was then preserved in 10% Formaldehyde solution (Sigma-Aldrich, USA).

2.3.1 *Formalin removal from fixed tissue and tissue embedding*

The lung tissue obtained was dissected to select appropriate sections for downstream analysis and placed into labelled cassettes. This was transferred to the Microm STP 120 Spin Tissue Processor (Thermo Fisher, USA), and the tissue sections were processed according to the manufacturer's instructions. This was performed to remove the 10% Formalin solution from the tissue. The tissue sections were then removed from the cassettes and transferred to the HistoStar Embedding Station (Thermo Fisher, USA). The Embedding station was turned on and allowed to heat up. Each tissue section was placed into a clean base mold and transferred to the hotspot below the liquid paraffin dispenser. The mold was filled with liquid paraffin until the tissue was completely covered. Working quickly, the tissue was oriented using forceps and securely covered with a cassette lid, and additional paraffin was added to cover the cassette lid. The mold was then placed onto the cold plate for chilling to solidify the wax. Upon solidification, the wax block was removed from the mold and the tissue was sectioned at a width of 5 µM using a microtome (Leica Biosystems, USA). The tissue sections obtained

were placed onto X-tra™ Adhesive Micro Slides (Leica Biosystems, USA). The slides were placed in an incubator set at 65 °C for 2 hours to melt the wax from the tissue sections.

2.3.2 *Hematoxylin and Eosin staining*

Hematoxylin and Eosin (H&E) staining was performed on formalin-fixed paraffin-embedded tissue. To remove paraffin, the slides were submerged in xylene twice, for 5 minutes each. To prevent distortion of the tissue and gradually remove water, the tissue underwent ethanol dehydration by immersing the slides in 100% ethanol, 95% ethanol, and finally, 70% ethanol. Each ethanol step was repeated twice, with an incubation period of 5 minutes. To prepare the tissue for staining, the slides were soaked in dH_2O for 5 minutes. The slides were then submerged in hematoxylin for 5 minutes and washed using tap water for 5 minutes. Next, the slides were immersed in Eosin for 2 minutes and rinsed with 95% ethanol for 30 seconds. The slides were then soaked in 100% ethanol twice for 1 minute. Finally, the slides were submerged in xylene for 1 minute. Mounting media was added to the tissue, and coverslips were cautiously placed on top of the tissue. The slides were scanned using the Hamamatsu NanaZoomer 2.0Rs scanner (Hamamatsu Photonics, Japan). Once scanned, the H&E-stained tissues were analysed using NDP.view2 Plus Image viewing software (Hamamatsu Photonics, Japan) and images were generated.

2.3.4 *Immunofluorescence staining*

To visualise the co-localization of the shortlisted drugs' target with inflammation in TB-diseased lung tissue, multi-coloured immunofluorescence was performed.

A volume of 1 L of 1X Target Retrieval Solution was prepared by diluting 30 ml 50X EnVision™ FLEX Target Retrieval Solution, High pH (containing Tris/EDTA, pH 9, Agilent Technologies, Denmark) in 970 ml of dH_2O. This was added into the Dako PT Link, which was used to deparaffinize, rehydrate, and perform antigen retrieval of the embedded tissue sections. The slides were added into the Dako PT Link and the machine was set to 2 hours and turned on. After performing antigen retrieval, the slides were washed by soaking in 1X Envision™ Flex wash buffer (Agilent Technologies, Denmark) for 10 minutes. A hydrophobic barrier was drawn around the tissue section using the ImmEdge® pen (Vector Laboratories, USA) to ensure that the reagents remain localised on the tissue section. Next, the tissue was covered with 300 µl of Peroxidase-Blocking solution (Agilent Technologies, Singapore) for 10 minutes to inhibit the activity of endogenous peroxidases present in the tissue. The slides were then submerged in the wash buffer for 10 minutes (2X 5 minutes). To ensure the prevention of non-specific binding, 300 µl of a second blocking buffer consisting of 0.05 g Bovine Serum Albumin + 0.5 ml Goat Serum + 4.5 ml wash buffer was applied to the tissue and incubated for 20 minutes. The slides were then soaked in the wash buffer for 10 minutes (2X 5 minutes). The primary antibody of interest was diluted according to the manufacturer's recommendations, as displayed in Table 5. A volume of 300 µl of the diluted primary antibody of interest was added to the tissue and incubated for 40 minutes.

Following the incubation, the slides were soaked in the wash buffer for 10 minutes (2X 5 minutes). An amount of 3 drops of Opal Polymer (HRP: Ms + RB) (Akoya Biosciences, USA) was then added to the tissue and incubated for 20 minutes. This served as a secondary antibody to be conjugated to the primary antibody. To label the first primary antibody, a fluorochrome Opal 520 reagent with a wavelength of 494/525 nm (FITC–green) was diluted using 1X Plus Amplification Diluent (Akoya Biosciences, USA) at 1:200 according to the manufacturer's recommendations. A volume of 300 µl of the diluted fluorochrome was applied to the tissue and incubated for 10 minutes. The tissue was rinsed with wash buffer using a Pasteur pipette and then soaked in wash buffer for 10 minutes (2X 5 minutes). To add a second antibody of interest, antigen retrieval was performed. Firstly, 1X Antigen Retrieval buffer was prepared by diluting 50 ml of AR6 Buffer (pH 6, Akoya Biosciences, USA) with 450 ml dH_2O. This was preheated to boiling temperature and added to a microwave-safe container. The slides were placed in a rack and submerged in the 1X Antigen Retrieval buffer. The container was placed in the microwave, which was set on high for 2 minutes, followed by low for 5 minutes, and lastly, medium for 10 minutes. The slides were then cooled by placing the container in running tap water for 20 minutes until cooled to RT. Next, the slides were soaked in wash buffer for 5 minutes to equilibrate the tissue. The tissue was then blocked to prevent non-specific binding using 300 µl of blocking buffer previously prepared. The second primary antibody at a concentration recommended by the manufacturer (as seen in Table 5) was added to the tissue following the steps previously mentioned. This was incubated overnight at 4 °C. The following day, the diluted antibody solution was rinsed using the wash buffer with a Pasteur pipette. The slides were then soaked in the wash buffer for 10 minutes (2X 5 minutes). The Opal polymer secondary antibody was added to the tissue and incubated for 20 minutes. Hereafter, a second fluorochrome, Opal 570 reagent (AKOYA Biosciences, USA), with a wavelength of 550/570 nm (TRITC–yellow), was diluted with 1X Plus Amplification buffer at 1:200 according to the manufacturer's recommendations. A volume of 300 µl of the diluted fluorochrome was added to the tissue and incubated for 10 minutes. To add a third antibody, antigen retrieval using the 1X AR6 Buffer was performed as previously described. After antigen retrieval, 300 µl of the third antibody, diluted using the manufacturer's guidelines (described in Table 5), was added to the tissue and incubated for 45 minutes. Next, 3 drops of Opal polymer secondary antibody were added to the tissue and incubated for 20 minutes. Opal 620 reagent with a wavelength of 676/694 nm (Cy5-Red) was diluted with 1X Plus Amplification buffer at 1:200 according to the manufacturer's recommendations. A volume of 300 µl of the fluorochrome was added to the tissue, and this was incubated for 10 minutes. Once the incubation was completed, one drop of Spectral 4'6-diamidino-2-phenylindole (DAPI) (Akoya Biosciences, USA) was added to 1 ml of wash buffer. The diluted DAPI solution was added to the tissue and incubated for 5 minutes at RT. The slides were washed by soaking in the wash buffer for 10 minutes (2X 5 minutes). Lastly, three drops of Dako fluorescence mounting media (Agilent Technologies, USA) were added to the tissue, and the coverslips were placed on the tissue with caution. To view the fluorescently labelled tissue, the slides were scanned using the NanoZoomer S60 Digital slide scanner

(Hamamatsu Photonics, Japan). Once scanned, the fluorescently labelled tissues were analysed using NDP.view2 Plus Image viewing software (Hamamatsu Photonics, Japan) and images were generated.

Table 5: **Antibodies and Their Concentrations for Multi-coloured Immunofluorescent Staining of Resected TB lung Tissue.**

Antibody	Concentration	Manufacturer	Catalogue No.
Anti-TLR 7	1:100	Abcam, United Kingdom	ab124928
Anti-TLR 8	1:100	Abcam, United Kingdom	ab228962
Anti-MyD88	1:500	Abcam, United Kingdom	ab133739
Anti-IL-6	1:500	Abcam, United Kingdom	ab6672
Anti-IL-5	1:200	Abcam, United Kingdom	ab25034
Anti-IL-5Rα	1:1000	Abcam, United Kingdom	ab237716

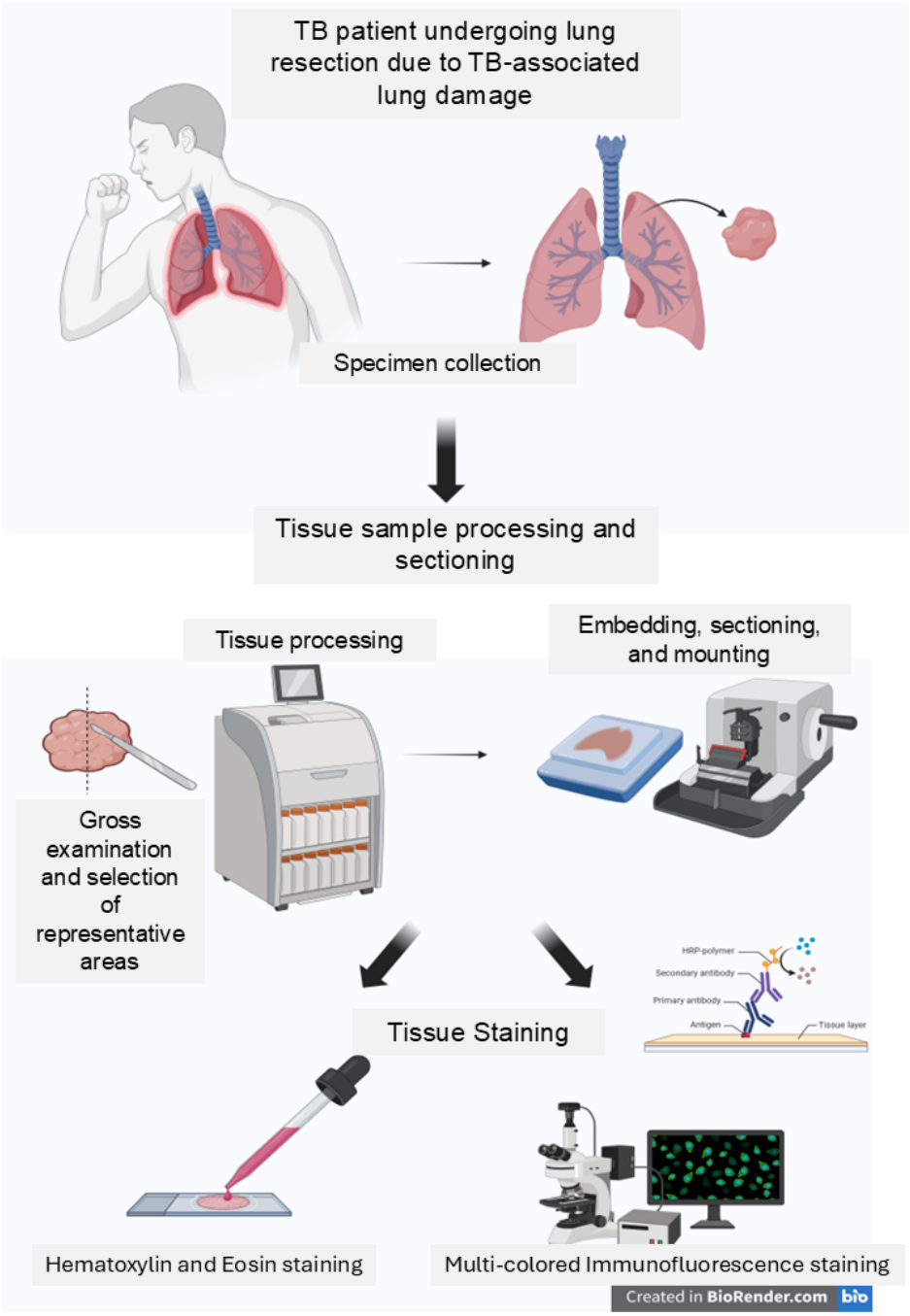

Figure 2.4: **Schematic representation of the experimental flow followed for histopathological analysis to characterise the drug targets in association with TB pathogenesis.** H&E was used to characterise cellular subsets located in the lung tissue, whereas immunofluorescence was used to stain for the protein target of the drug, to spatially analyse its association with pathology in the TB-diseased lung.

2.4 Equations.

1. Cells/ml = (total number of cells in outer 4 corners/4) × 2 ×10 000
2. Total cells = cell/ml × total volume cells are resuspended in

2.5 Statistical Analysis

Data obtained was analysed using Microsoft® Excel® (Version 2408 Build 16.0.17928.20114) and GraphPad Prism (Version 10.0.3). Drug-treated groups were compared to the positive control (*Mtb* + PBMC) using unpaired t-tests with Welch's correction to assess statistical significance, with p-values defined as significant at $p < 0.05$. Images obtained from H&E staining and immunofluorescence were analysed using NDP.view2 Plus Image viewing software.

CHAPTER 3:

PART A: RESULTS

HIGH-THROUGHPUT SCREENING OF SMALL-MOLECULE COMPOUNDS TO IDENTIFY AGENTS WITH THE POTENTIAL TO REDUCE INFLAMMATION DURING *Mtb* INFECTION.

3. Results: Part A

3.1 High-throughput Screening of small-molecule compound library to identify drugs with the potential to reduce inflammation during *Mtb* infection

To investigate the effects of anti-inflammatory drugs as potential host-directed therapies to alleviate severe inflammation during tuberculosis, PBMCs from healthy donors were collected, infected with H37Rv *Mtb*, and treated with small-molecule compounds from a screening library. The effects on the production of pro-inflammatory cytokines, IL-1β, IL-6 and TNF-α, after a 3-day incubation period were then quantified using ELISA.

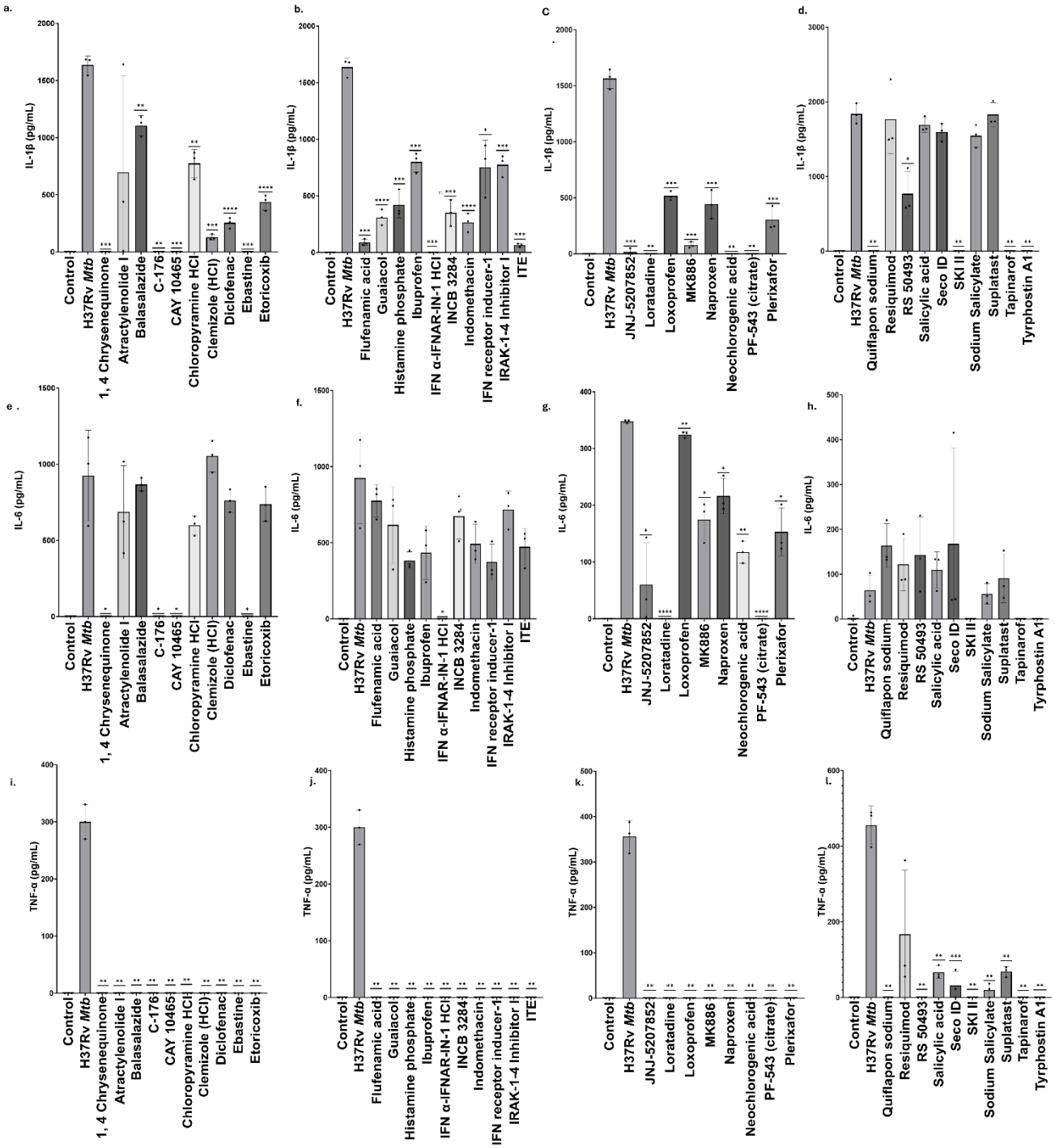

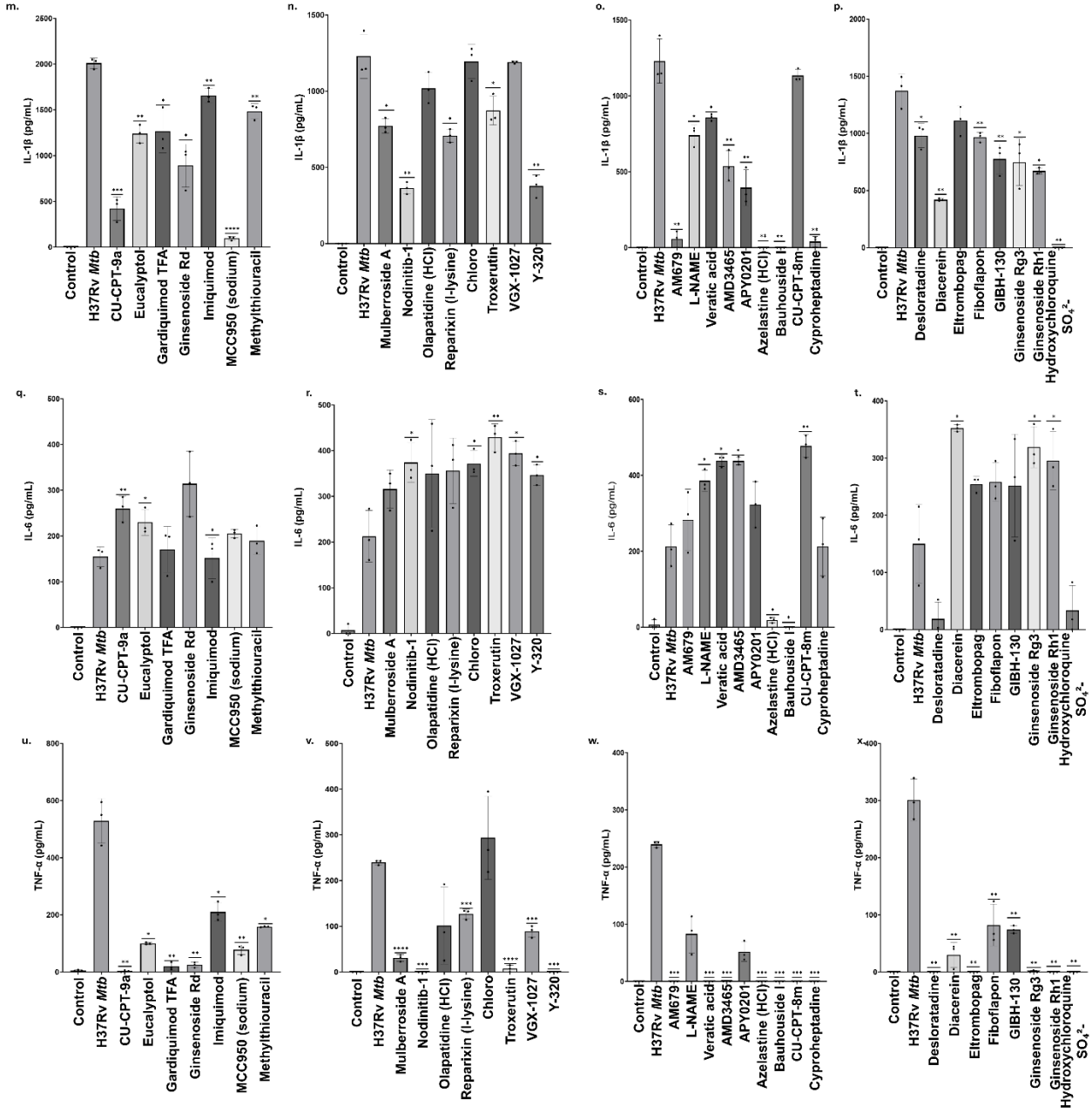
m.
IL-1β (pg/mL)
Control
H37Rv Mtb
CU-CPT-9a
Eucalyptol
Gardiquimod TFA
Ginsenoside Rd
Imiquimod
MCC950 (sodium)
Methylthiouracil
n.
IL-1β (pg/mL)
Control
H37Rv Mtb
Mulberroside A
Nodinitib-1
Olapatidine (HCl)
Reparixin (l-lysine)
Chloro
Troxerutin
VGX-1027
Y-320
o.
IL-1β (pg/mL)
Control
H37Rv Mtb
AM679
L-NAME
Veratic acid
AMD3465
APY0201
Azelastine (HCl)
Bauhouside I
CU-CPT-8m
Cyproheptadine
p.
IL-1β (pg/mL)
Control
H37Rv Mtb
Desloratadine
Diacerein
Eltrombopag
Fiboflapon
GIBH-130
Ginsenoside Rg3
Ginsenoside Rh1
Hydroxychloroquine
SO4 2-
q.
IL-6 (pg/mL)
Control
H37Rv Mtb
CU-CPT-9a
Eucalyptol
Gardiquimod TFA
Ginsenoside Rd
Imiquimod
MCC950 (sodium)
Methylthiouracil
r.
IL-6 (pg/mL)
Control
H37Rv Mtb
Mulberroside A
Nodinitib-1
Olapatidine (HCl)
Reparixin (l-lysine)
Chloro
Troxerutin
VGX-1027
Y-320
s.
IL-6 (pg/mL)
Control
H37Rv Mtb
AM679
L-NAME
Veratic acid
AMD3465
APY0201
Azelastine (HCl)
Bauhouside I
CU-CPT-8m
Cyproheptadine
t.
IL-6 (pg/mL)
Control
H37Rv Mtb
Desloratadine
Diacerein
Eltrombopag
Fiboflapon
GIBH-130
Ginsenoside Rg3
Ginsenoside Rh1
Hydroxychloroquine
SO4 2-
u.
TNF-α (pg/mL)
Control
H37Rv Mtb
CU-CPT-9a
Eucalyptol
Gardiquimod TFA
Ginsenoside Rd
Imiquimod
MCC950 (sodium)
Methylthiouracil
v.
TNF-α (pg/mL)
Control
H37Rv Mtb
Mulberroside A
Nodinitib-1
Olapatidine (HCl)
Reparixin (l-lysine)
Chloro
Troxerutin
VGX-1027
Y-320
w.
TNF-α (pg/mL)
Control
H37Rv Mtb
AM679
L-NAME
Veratic acid
AMD3465
APY0201
Azelastine (HCl)
Bauhouside I
CU-CPT-8m
Cyproheptadine
x.
TNF-α (pg/mL)
Control
H37Rv Mtb
Desloratadine
Diacerein
Eltrombopag
Fiboflapon
GIBH-130
Ginsenoside Rg3
Ginsenoside Rh1
Hydroxychloroquine
SO4 2-

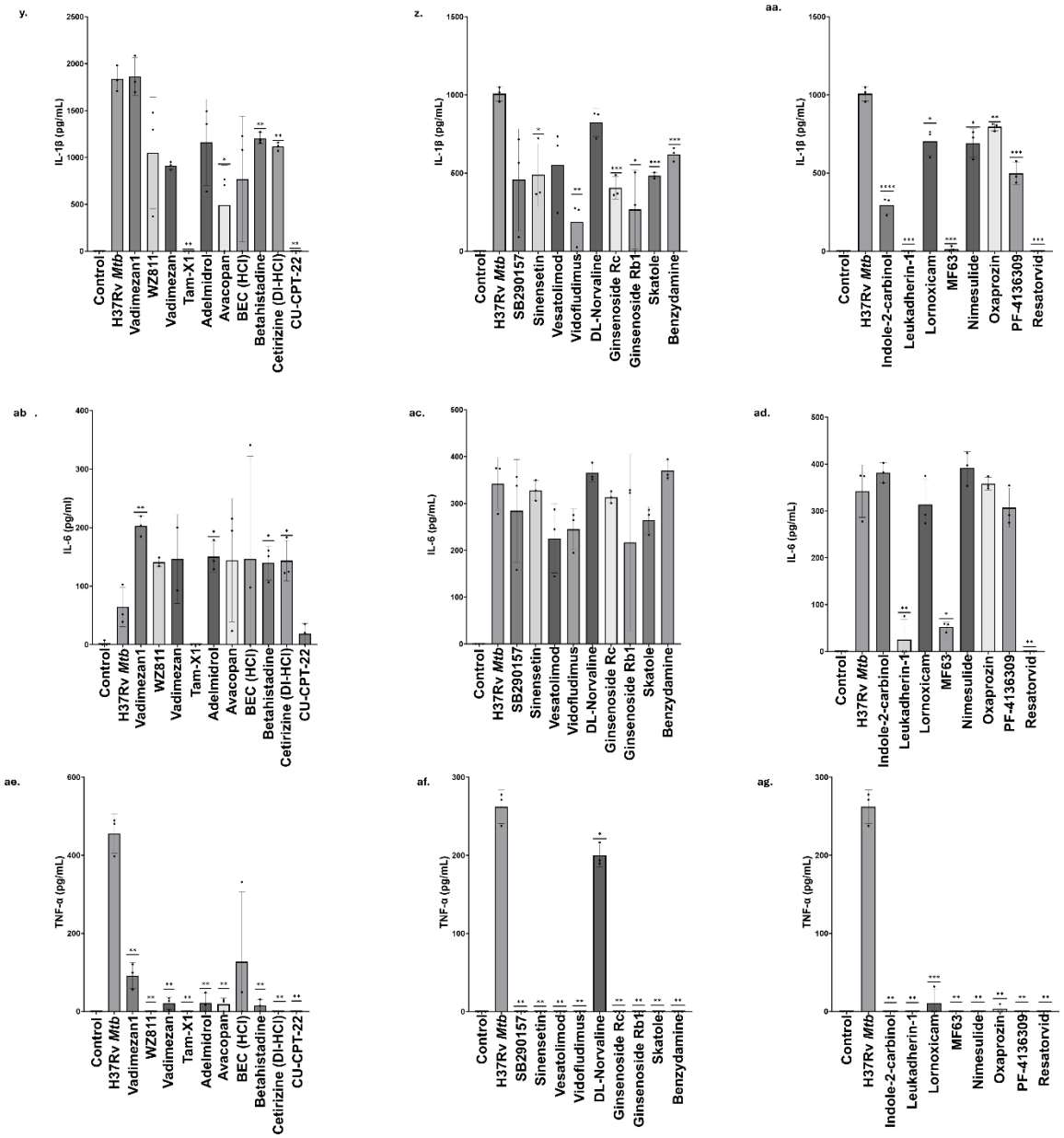

Figure 3.1. **High-throughput screening of anti-inflammatory small-molecule compounds in PBMCs infected with Mtb H37Rv 3 days post-infection.** Cytokine levels of IL-1β, IL-6 and TNF-α were quantified using ELISA. Statistical analysis was conducted using a t-test with Welch's correction to compare PBMCs infected with H37Rv *Mtb* and treated with drugs to PBMCs infected solely with H37Rv *Mtb* (untreated control). Three replicates were performed for each group, and the mean values were plotted. Error bars represent the standard deviation of the mean. Significant differences are indicated as follows: *p ≤ 0.05, ** p ≤ 0.01, ***p ≤ 0.001 and ****p ≤ 0.0001).

Figure 3.1 displays a representation of the results obtained. Treatment of H37Rv *Mtb*-infected cells with several drugs significantly reduced IL-1β to undetectable concentrations compared to the H37Rv *Mtb*-

infected cells (control) not treated with drugs. Notable drugs included: **1,4 Chrysenequinone** (Fig. 3.1.a.), **C-176** (Fig. 3.1.a;), **CAY-10465** (Fig. 3.1.a), **IFN alpha-IFNAR-IN-1 HCl** (Fig 3.1.b.), **JNJ-5207852** (Fig. 3.1.c.), **Loratadine** (Fig. 3.1.c), **Neochlorogenic acid** (Fig. 3.1.c.), **PF-543 citrate** (Fig. 3.1.c.), **Quiflapon sodium** (Fig. 3.1.d.), **SKI II** (Fig. 3.1.d.), **Tapinorof** (Fig 3.1.d.), **Tyrphostin A1** (Fig. 3.1.d.), **Azelastine** (Fig. 3.1.o.), **Bauhouside I** (Fig. 3.1.o.), **Hydroxychloroquine sulfate** (Fig. 3.1.p.), **Tam-X1** (Fig. 3.1.y.), **CU-CPT-22** (Fig. 3.1.y.), **Leukaherin-1** (Fig. 3.1.aa.), and **Resatorvid** (Fig. 3.1. aa.).

For IL-6, significant reductions to undetectable levels were observed with: 1.4 **Chrysenequinone** (Fig. 3.1.e.), **C-176** (Fig. 3.1.e.), **CAY-10465** (Fig. 3.1.e.), **Ebastine** (Fig. 3.1.e.), **IFN alpha-IFNAR-IN-1 HCl** (Fig. 3.1.f.), **Loratadine** (Fig. 3.1.g.), **PF-543 citrate** (Fig. 3.1.g.), **Bauhouside I** (Fig. 3.1.s.), and Resatorvid (Fig. 3.1.ad.). However, drugs like **Tapinorof** (Fig. 3.1.h), **Tyrphostin A1** (Fig. 3.1.h.), and **Tam-X1** (Fig. 3.1.ab.) showed reductions in IL-6; these were not significantly different to the untreated control group due to variability.

Additionally, several drugs resulted in a significant reduction of TNF-α compared to the untreated control. These include the following drugs shown in Figure 3.1.i.: **1,4 Chrysenequinone**, **Atractylenolide I**, **Balasalazide**, **C-176**, **CAY 10465**, **Chloropyramine HCl**, **Clemizole HCl**, **Diclofenac**, **Ebastine**, and **Etoricoxib**. From Figure 3.1.j, the following resulted in a significant reduction in the production of TNF-α**: Flufenamic acid**, **Guaciacol**, **Histamine phosphate**, **Ibuprofen**, **IFN alpha-IFNAR-IN-1 HCl**, **INCB 3284**, **Indomethiacin**, **Interferon inducer-1**, **IRAK-1-4 inhibitor**, and **ITE**. In Figure 3.1.k, **JNJ-5207852**, **Loratadine**, **Loxoprofen**, **MK886**, **Naproxen**, **Neochlorogenic acid**, **PF-543 citrate**, and **Plerixafor** resulted in a significant reduction in the release of TNF-α. Next, **Quiflapon sodium**, **RS50493**, **SKI II**, **Tapinorof**, and **Tyrphostin A1**, displayed in Figure 3.1.l, all significantly reduced TNF-α. Similarly, treatment with each of the drugs displayed in Figure 3.1.u resulted in a significant reduction of TNF-α. Figure 3.1.v shows that **Nodinitib-1** and **Y-320**, significantly decreased the production of TNF-α. In addition to this, Figure 3.1.w showed that **AM679**, **Veratic acid**, **AMD3465**, **Azelastine**, **Bauhouside I**, **CU-CPT-8m**, and **Cyproheptadine** all significantly decreased the expression of TNF-α. Figure 3.1.ae shows the significant reduction of TNF-α as a result of treatment with: **WZ 811**, **Tam-X1**, **Citirizine (DI-HCl)**, and **CU-CPT-22**. Likewise, Figure 3.1.x which includes **Desloratadine**, **Eltrombopag**, **Ginsenoside Rg3**, **Ginsenoside Rh1**, and **Hydroxychloroquine sulfate** showed the same effect. In Figure 3.1.ae, treatment with each of the drugs resulted in a significant reduction in TNF-α except **BEC (HCl)**. Lastly, Figure 3.1.af and Figure 3.1.ag both display the significant reduction of TNF-α by **SB 290152**, **Sinensetin**, **Vesatolimod**, **Vidofludimus**, **Ginsenoside Rc**, **Ginsenoside Rb**, **Skatole**, **Benzydamine, Indole-2-carbinol**, **Leukadherin-1**, **MF-63**, **Nimesulide**, **Oxaporozin**, **PF-4136309**, and **Resatorvid**.

Overall, **1,4 Chrysenequinone**, **C-176**, **CAY-10465**, **Ebastine**, **IFN alpha-IFNAR-IN-1 HCl**, **Loratidine**, **PF-543**, **SKI-II**, **Tapinorof**, **Tyrphostin A1**, **Tam-X1**, **CU-CPT-22** and **Bauhouside I** displayed reduction in the production of IL-1β, IL-6 and TNF-α. In contrast, several other drugs (shown in Fig. 3.1) resulted in a significant reduction in the production of these cytokines. Although this was reduced to undetectable levels in one or two of the cytokines measured, it did not reduce the production of all three cytokines. Whereas **Tam-X1** displayed a constant reduction in each of the cytokines during Mtb infection. This led to further investigation of this agent.

3.2 **Effects of Tam-X1 on intracellular bacterial growth during *Mtb* infection in a 3D biomimetic model**

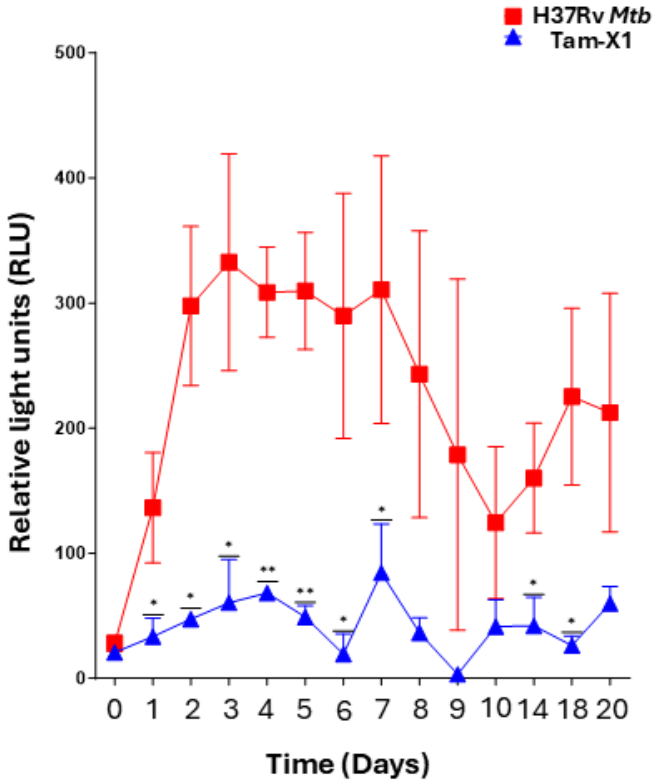

Figure 3.2. **Tam-X1 significantly enhances bacterial killing during *Mtb* infection.** Luminescence released by H37Rv *Mtb* LUX was measured via luminometry over 20 days to assess the effects of **Tam-X1** on bacterial killing in PBMCs infected with H37Rv LUX *Mtb* in a 3D collagen-alginate biomimetic infection model. Three replicates were performed, and the mean values were plotted. Error bars represent the standard deviation of the mean. A t-test with Welch's correction was used to determine statistical significance. Significant differences between the treated group (Tam-X1-shown in blue) and the untreated control group (H37Rv *Mtb*-shown in red) are indicated as follows: *$p \leq 0.05$, ** $p \leq 0.01$, ***$p \leq 0.001$ and ****$p \leq 0.0001$.

High-throughput screening identified **Tam-X1** as one of the most effective drugs in significantly reducing *Mtb*-induced inflammatory responses in *Mtb*-infected PBMCs. Due to its unique ability to inhibit type 2 cytokine, IL-5, from binding to its receptor IL-5R (Morokata et al., 2002), the drug was

further investigated to assess its potential role during TB pathogenesis. **Tam-X1** was explored to determine its effects on bacterial growth during *Mtb* infection in a biomimetic 3D collagen-alginate spheroid model. Luminescence was measured over 20 days post-infection. The amount of luminescence measured was directly proportional to the amount of luminescent *Mtb* present in the model at the time of measurement. As shown in Fig. 3.2, the effects of treatment with **Tam-X1** on bacterial growth were evident from day 1 up to day 20 when compared to the untreated infected control group. The group treated with **Tam-X1** displayed an overall lower amount of *Mtb* present as compared to the untreated control group. Taken together, the data indicate that **Tam-X1** effectively inhibits the increase in *Mtb* bacterial growth in infected PBMCs *in vitro*.

When taking a closer look, the group treated with **Tam-X1** displayed a slow growth of the bacteria, as evidenced by the amount of luminescent *Mtb* present up to day 3. Although this was significantly lower than that of the H37Rv *Mtb* control group. From day 4 to day 6, the bacterial load in the **Tam-X1**-treated cells displayed a decreasing trend, remaining significantly lower than in the untreated control cells. However, on day 7, the **Tam-X1**-treated group displayed an increasing trend in bacterial load. Following this, the Tam-X1-treated group displayed a downward trend in bacterial load, ultimately reaching no detectable bacteria, although this result was not significant due to variability in the control group. After day 9, an upward trend in bacterial load was observed, which stabilised until day 14. A significant downward trend was noted from day 14 to day 18, followed by another upward trend observed from day 18 to day 20.

Overall, **Tam-X1** treatment resulted in a significantly lower bacterial load, as indicated by decreased luminescence, compared to the untreated H37Rv *Mtb* control group. This suggests that treatment with **Tam-X1** aids in enhancing host anti-mycobacterial response. Next, we investigated the effects of **Tam-X1** on inflammation during *Mtb* infection.

3.3 Analysis of the effects of Tam-X1 on systemic inflammation during *Mtb* infection in a 3-dimensional biomimetic model

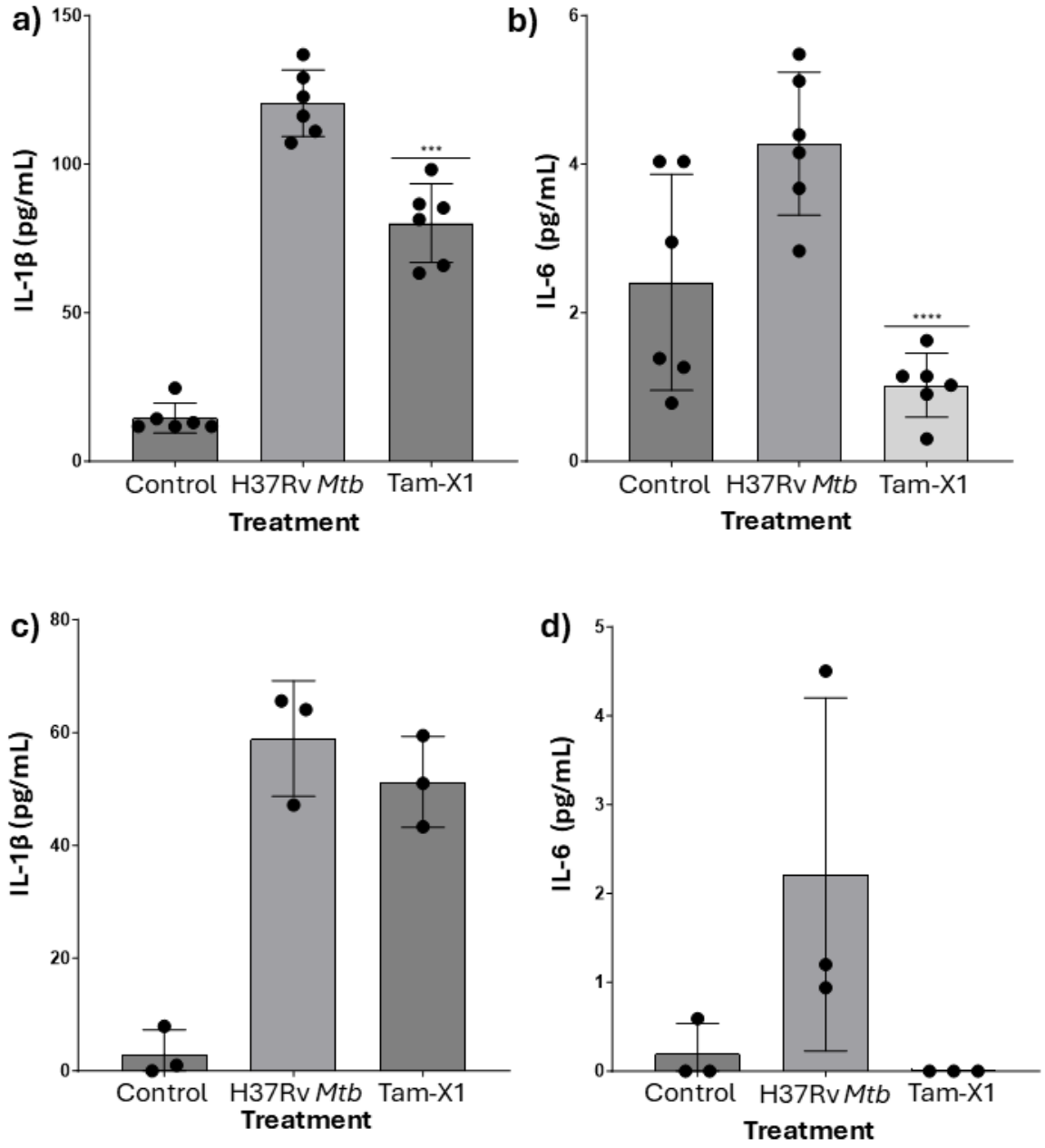

Figure 3.3. **Tam-X1 significantly reduces inflammation during Mtb infection in the 3D biomimetic collagen-alginate model.** The pro-inflammatory cytokines IL-6 and IL-1β were measured using ELISA after treatment with Tam-X1. Three replicates were performed, and the mean values were plotted. The error bars represented the standard deviation of the mean value. Significant differences between the treated group (Tam-X1) and the untreated group (H37Rv *Mtb*) were determined using the t-test with Welch's correction, and significance is indicated as follows: *$p \leq 0.05$, ** $p \leq 0.01$, ***$p \leq 0.001$ and ****$p \leq 0.0001$. Graphs a) and b) represent data from the supernatant obtained on day 3, while graphs c) and d) represent data from the supernatant collected on day 10.

The 2D monolayer culture models, although widely used, cannot mimic the complex interactions that take place in a tissue microenvironment (Li et al., 2023; Riedl et al., 2017). Therefore, we made use of a 3D biomimetic collagen-alginate model to replicate the physiological microenvironment of lung tissue during *Mtb* infection (Li et al., 2023; Wang et al., 2017).

To evaluate the effects of **Tam-X1** treatment on inflammation during *Mtb* infection, supernatants were collected from the 3D biomimetic spheroid model on days 3 and 10. ELISA was performed to measure the concentration of IL-1β and IL-6 released in the supernatants collected, as these cytokines are a part of the inflammatory response associated with TB. The results obtained on day 3 indicated that treatment with **Tam-X1** significantly reduced the release of both IL-1β (Fig. 3.3.a) and IL-6 (Fig. 3.3.b) compared to the untreated H37Rv *Mtb* control. Additionally, on day 10 (Fig. 3.3.c and Fig. 3.3.d), the group treated with Tam-X1 exhibited a downward trend in the release of IL-6 and IL-1β compared to the untreated control group.

The significant reduction in the production of pro-inflammatory cytokines when PBMCs within the 3D biomimetic model were treated with **Tam-X1**, depicted the potential ability of this agent to reduce inflammation during *Mtb* infection and prompted further exploration into the relationship between IL-5 and IL-5Ra, particularly regarding their association with TB-associated pathology within lung tissue.

3.4 **Histopathological analysis of Tam-X1 target in association with *Mtb*-infected lung tissue and its pathological implications**

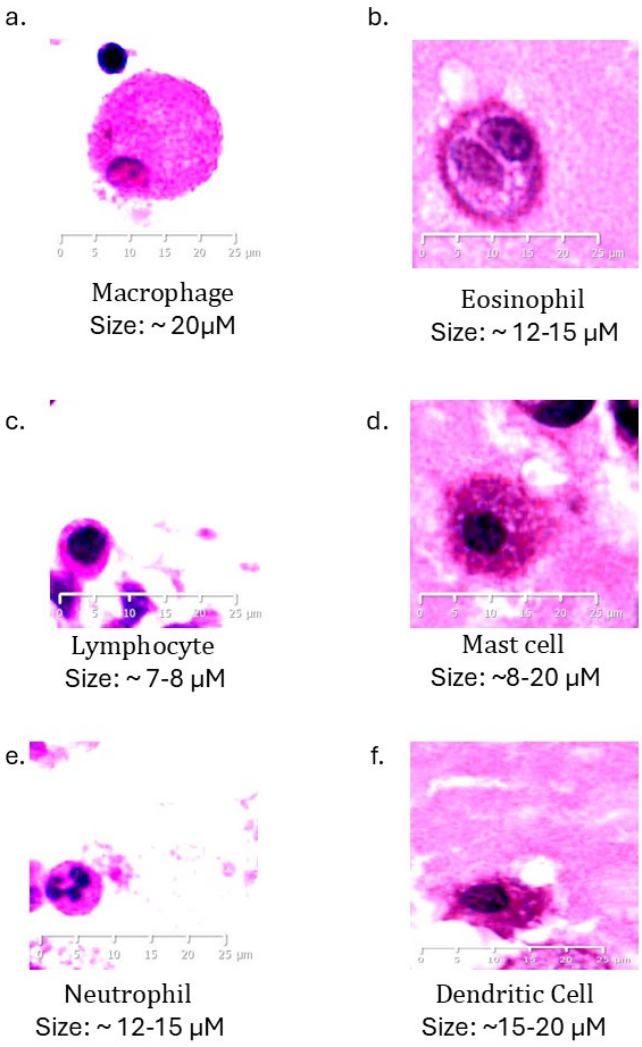

Figure 3.4: **Characterisation of immune cell subsets in lung tissue infected with TB via H&E.** Resected lung tissue obtained from a TB patient who underwent surgery for severe TB-associated damage was stained with H&E. Immune cells were identified based on their size and morphology (both cellular and nuclei). The nuclei were stained blue-purple by haematoxylin stain, and the cytoplasm was stained pink-red by eosin stain. Images were captured using a NanoZoomer 2.0Rs digital slide scanner at 40x magnification, with the cells identified using 80x zoomed-in magnification of the images. The scale bars represent appropriate lengths for each image.

Resected lung tissue from a patient who underwent lung surgery due to severe TB-associated damage, was stained using H&E to identify various cell types present within the tissue. Macrophages (Fig. 3.4.a) were identified based on their round shape and oval-indented nucleus, which was located eccentrically. They were further identified based on the size, which was ~20 μM in diameter, with a foamy cytoplasm. Eosinophils (Fig. 3.4.b) were identified based on their bi-lobed nucleus and granular cytoplasm. The granules of eosinophils were stained pink due to their eosinophilic nature, and the cytoplasm between

granules was stained blue. They were further identified by their size, which was 12-15 μM in diameter. Lymphocytes (Fig. 3.4.c) were identified based on their diameter, which was 7-8 μM, their round shape and their large nucleus. Next, mast cells (Fig. 3.4.d) were identified based on their granular cytoplasm and oval, irregular shape. They were further identified based on their size, which was 8-20 μM. Neutrophils (Fig. 3.4.e) were identified based on their multilobed nucleus with three or more lobes and granular cytoplasm, along with their diameter of 12-15 μM. Dendritic cells (Fig. 3.4.f) were identified based on the morphology, which comprises branched cytoplasmic projections and a size ranging between 15-20 μM. These findings were then used for the identification of cells in the analysis of microscopic images obtained after immunofluorescent staining of proteins of interest.

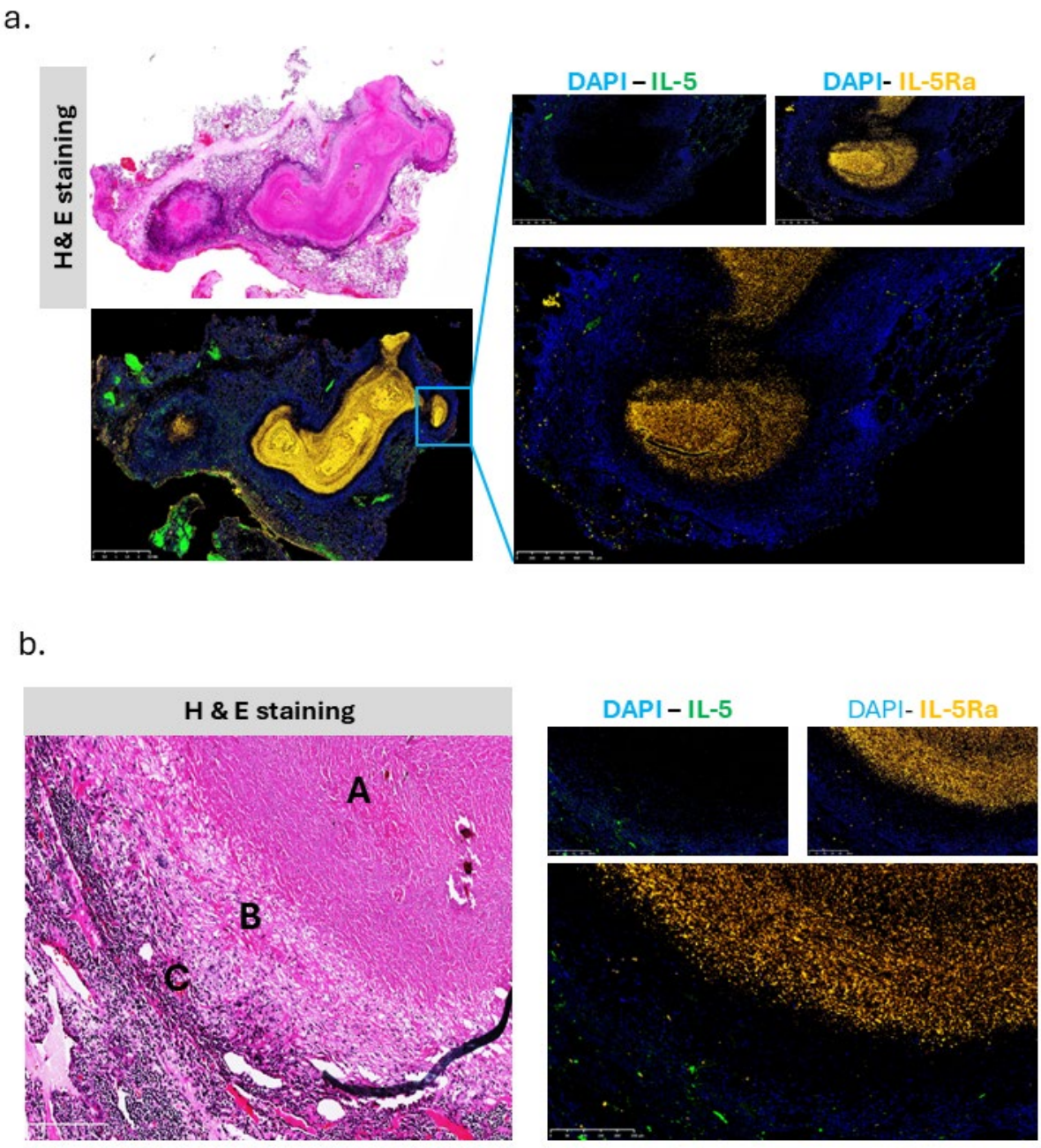

Figure 3.5: **IL-5Rα is associated with the necrotic areas of caseating granulomas in TB-diseased lung.** Immunofluorescence staining was performed to visualise (a-c) the localisation of IL-5Rα in resected TB lung tissue from patients who underwent surgery due to severe TB-associated lung damage. Immunofluorescence was performed to target IL-5 (green), IL-5Rα (yellow) and IL-6 (red). Nuclei were counterstained with DAPI (blue). H&E staining was performed to identify various cell types and different regions of the granuloma. Images were captured using a NanoZoomer S60 digital slide scanner at varying magnifications, with the scale bars representing appropriate lengths for each panel. Merged images illustrate the relationship between IL-5 and IL-5Rα release, highlighting their roles in mediating inflammation within the lung tissue during *Mtb* infection. A = necrotic core. B = Macrophage-rich region (inner cellular region). C = Lymphocytic cuff (outer cellular region)

Immunofluorescence was performed on resected lung tissue obtained from patients with TB who underwent surgery due to severe TB-associated pathology to identify the association of the target of

Tam-X1, IL-5Rα, and its associated pathway with inflammation-mediated pathology. The lung biopsies obtained had varying degrees of granulomas, with the size of the granuloma indicating the severity of the lesion. From Figure 3.5.a, it was observed that IL-5Rα was more abundantly expressed within the caseum of the granuloma than the macrophage-rich region or the lymphocytic cuff. It was also seen that IL-5Ra was associated with larger caseating granulomas. Additionally, the early caseating granuloma shows low levels of IL-5Rα. IL-5Rα was particularly associated with the necrotizing areas of the granuloma in higher levels (Fig. 3.5.b), in contrast to the cellular outer layers of the granuloma. Conversely, IL-5 was not expressed in the caseum but was more abundantly found in other regions of the tissue, particularly the cells found in the alveolar epithelium and spaces, with sparse expression observed in the lymphocytic cuff (outer cellular region) surrounding the granuloma. This may indicate that cells expressing IL-5Rα are associated with inflammatory processes, which result in tissue remodelling during *Mtb* infection.

a.

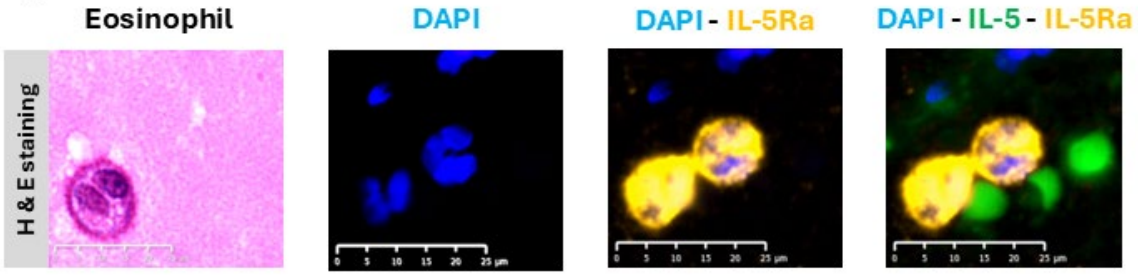
Eosinophil
DAPI
DAPI - IL-5Ra
DAPI - IL-5 - IL-5Ra
H & E staining

b.

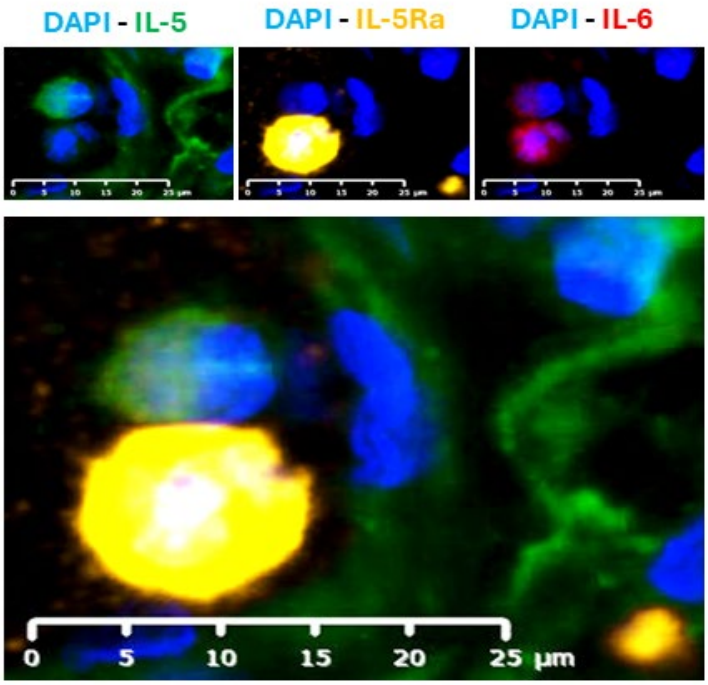
DAPI - IL-5
DAPI - IL-5Ra
DAPI - IL-6
0
5
10
15
20
25 µm

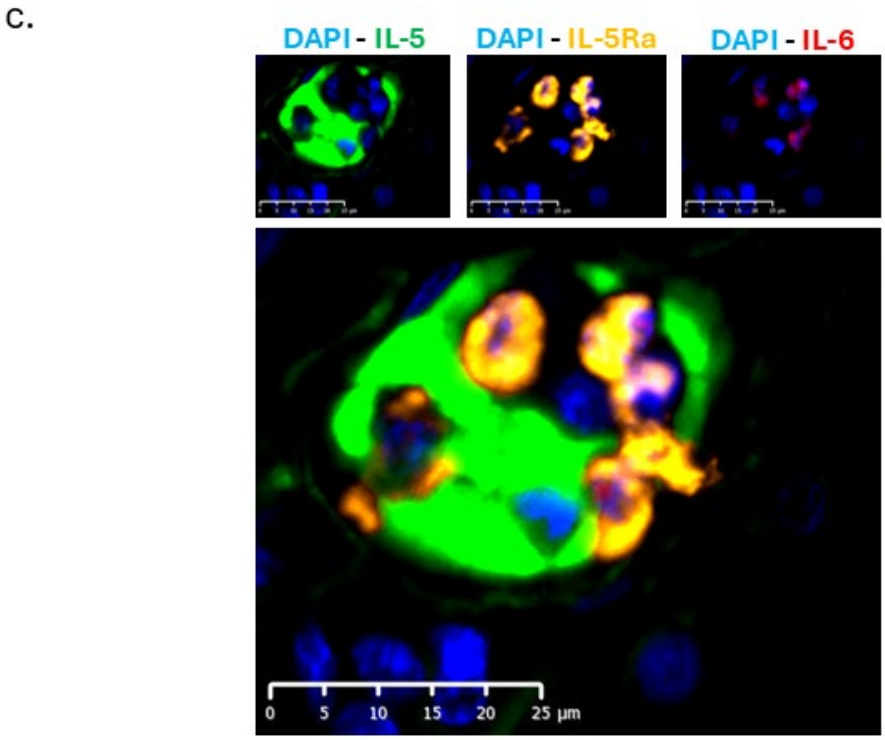

Figure 3.6: **IL-5Rα is highly expressed in eosinophil-like cells and associates with inflammation mediated by IL-6 through IL-5 signalling. Immune cells expressing IL-5Rα form aggregates in the presence of IL-5.** Immunofluorescence staining was performed to visualise (a-c) the localisation of IL-5Rα in resected TB lung tissue from patients who underwent surgery due to severe TB-associated lung damage. Immunofluorescence was performed to target IL-5 (green), IL-5Rα (yellow) and IL-6 (red). Nuclei were counterstained with DAPI (blue). H&E staining was performed to identify various cell types. Images were captured using a NanoZoomer S60 digital slide scanner at varying magnifications, with the scale bars representing appropriate lengths for each panel. Merged images illustrate the relationship between IL-5 and IL-5Rα release and the inflammatory marker IL-6, highlighting their roles in mediating inflammation within the lung tissue during *Mtb* infection.

Moreover, IL-5Rα was predominantly expressed in eosinophil-like cells compared to other cell types within the tissue (Fig. 3.6.a). These IL-5Rα-expressing cells appeared to be interacting with those releasing IL-5. Notably, these cells displayed expression of IL-6 in the nuclei (Fig. 3.6.b). This analysis may imply that cells releasing IL-5Rα are potentially activated via the binding of IL-5 to drive an inflammatory response through the release of IL-6. Additionally, immune cells expressing IL-5Rα formed aggregates in the presence of IL-5 (Fig. 3.6.c), co-localizing with it in the alveolar spaces of the lung and within cellular mass surrounding the granuloma, which may suggest early granuloma formation. Taken together, the data suggests that IL-5/IL-5Rα-mediated signalling by eosinophils drives inflammatory responses, potentially contributing to the formation of TB-induced granulomas.

a.

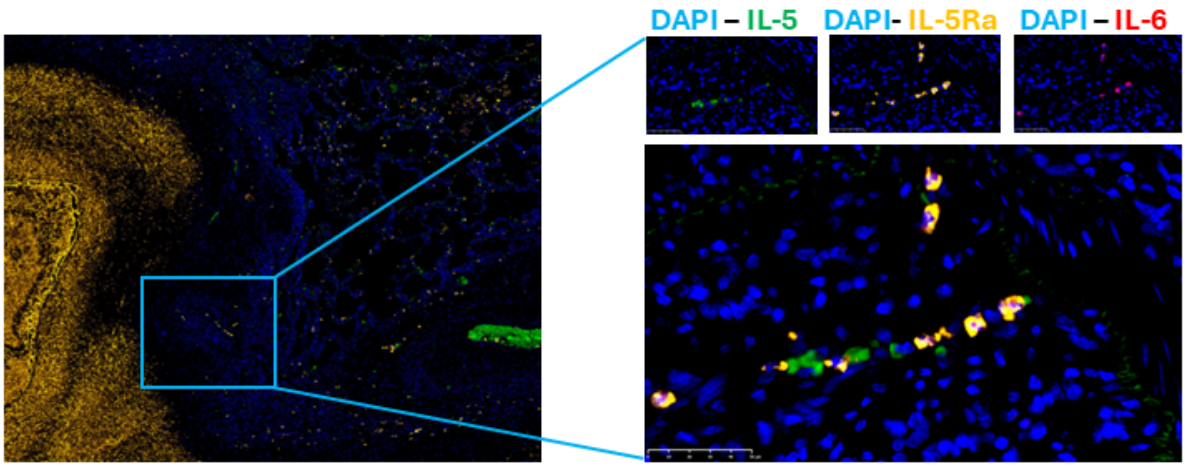
DAPI – IL-5
DAPI- IL-5Ra
DAPI – IL-6

b.

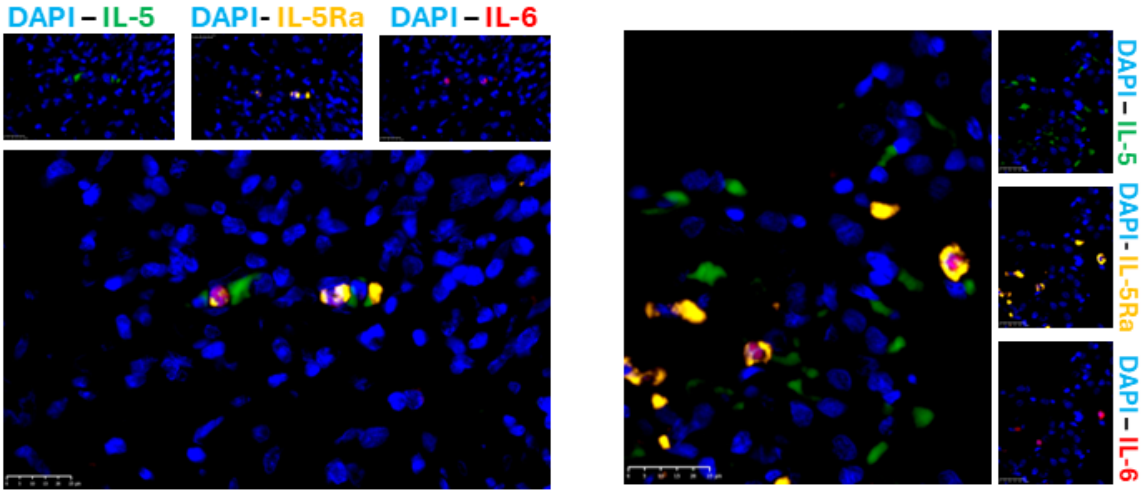
DAPI – IL-5
DAPI- IL-5Ra
DAPI – IL-6
DAPI – IL-5
DAPI- IL-5Ra
DAPI – IL-6

c.

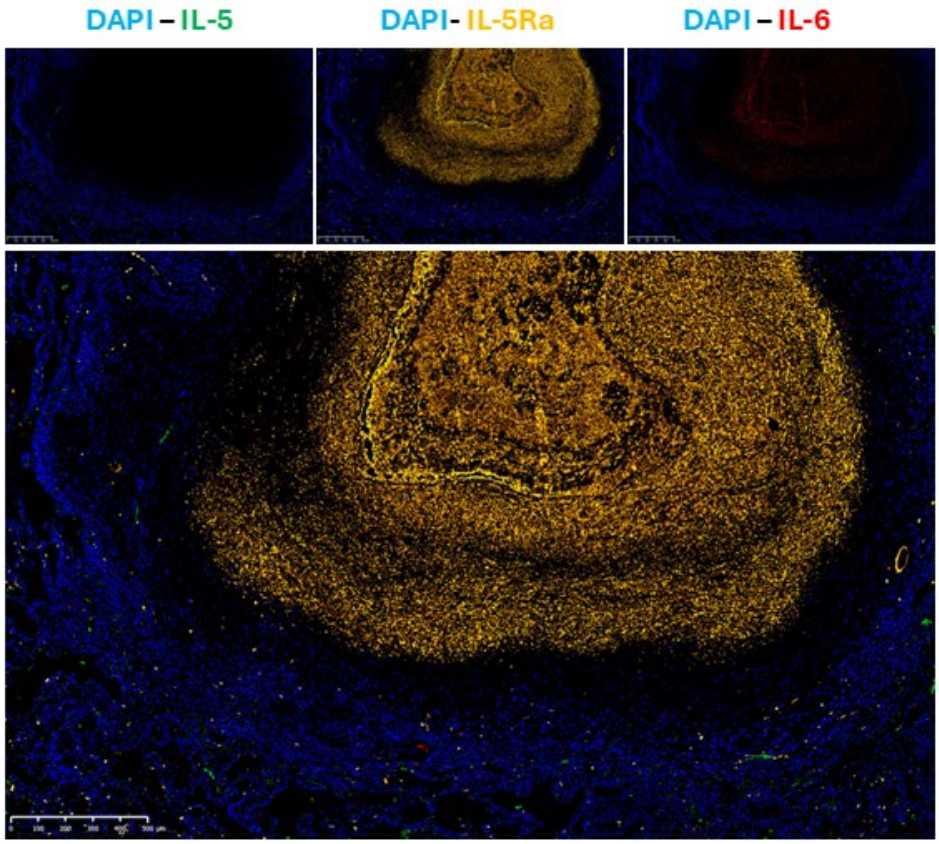

Figure 3.7: **IL-5Rα associates with IL-6-mediated inflammation in the caseum of the TB granuloma. Some immune cells expressing IL-5, IL-5Rα and IL-6 are localised outside the caseum of the granuloma.** Immunofluorescence staining was performed to visualise (a-c) the localisation of IL-5Rα in resected TB lung tissue from patients who underwent surgery due to severe TB-associated lung damage. Immunofluorescence was performed to target IL-5 (green), IL-5Rα (yellow) and IL-6 (red). Nuclei were counterstained with DAPI (blue). Images were captured using a NanoZoomer S60 digital slide scanner at varying magnifications, with the scale bars representing appropriate lengths for each panel. Merged images illustrate the relationship between IL-5 and IL-5Rα release and the inflammatory marker IL-6, highlighting their roles in mediating inflammation within the lung tissue during *Mtb* infection.

Cells expressing IL-5Rα, which co-localised with IL-6 and interacted with IL-5-expressing cells, were localised near the caseum in the macrophage-rich layer of the granuloma (Fig. 3.7.a). It was also seen that IL-6 was localised in the nuclei region of the cells, with IL-5 localised around the nucleus. These cells displayed a pattern resembling linear clustering near the caseum, which may indicate a chemotactic response by these cells toward the caseum through the signalling of IL-5. Finally, IL-5Rα and IL-6 co-localised within the caseum of the granuloma (Fig. 3.7.b and Fig. 3.7.c), showing higher expression in this region compared to other lung areas. This observed expression pattern suggests that the immune

response from cells expressing IL-5Rα leads to tissue remodelling during *Mtb* infection through the release of IL-6 via IL-5 signalling.

CHAPTER 4:

PART A: DISCUSSION

4. Discussion

TB is currently one of the world's leading causes of mortality, with 1.25 million deaths in 2023 and a total of 10.8 million cases reported in 2023 (WHO, 2024). The current prescribed treatment used to manage TB consist of rifampicin, isoniazid, pyrazinamide, and ethambutol, along with second-line drugs (Ndlovu and Marakalala, 2016; Zhao et al., 2023). However, one of the main challenges faced is the emergence of drug-resistant strains, such as MDR-TB and XDR-TB, alongside disease progression driven by severe inflammation (Huang et al., 2024). This inflammation can exacerbate lung damage and worsen patient outcomes, especially in immunocompromised individuals. Consequently, there is a critical need for improved treatment strategies to combat these challenges (Ndlovu and Marakalala, 2016).

Host-directed therapies, which have gained interest in recent years, aim to target the host's immune response to prevent lung damage and enhance the defence against *Mtb,* (Tobin, 2015). In this work, we have focused on screening existing anti-inflammatory drugs, some of which have been approved for other inflammatory diseases, as potential repurposed host-directed therapeutics for TB. Our screening identified several promising small-molecule compounds that could potentially reduce the severe inflammation associated with the host's immune response to *Mtb*, particularly an IL-5 antagonist. Furthermore, targeting this pathway not only reduced inflammation but also resulted in a significant decrease in bacterial load during *Mtb* infection. Additionally, we observed that the compound's target protein was spatially associated with disease pathogenesis in resected TB lung tissue.

From our screening of anti-inflammatory agents in PBMCs during *Mtb* infection, several compounds showed a reduction in the production of IL-1β, IL-6 and TNF-α. These compounds included 1,4 Chrysenequinone, C-176, CAY-10465, Ebastine, IFN alpha-IFNAR-IN-1 HCl, Loratidine, PF-543, SKI-II, Tapinorof, Tyrphostin A1, Tam-X1, CU-CPT-22 and Bauhouside I. In contrast, some other anti-inflammatory agents tested reduced the expression of primary pro-inflammatory cytokines that control bacteria but not consistently across all three cytokines. Notably, Tam-X1 consistently reduced all three cytokines to undetectable levels during *Mtb* infection. Given this, we decided to further investigate the effects of Tam-X1 as a potential host-directed therapy.

Tam-X1, a compound composed of 2,3-dimethoxy-6,6-dimethyl-5,6-dihydrobenzo[7,8]indolizino[2,3-b]quinoxaline (referred to in this thesis as Tam-X1), acts as an IL-5 inhibitor. It has been shown to selectively block the binding of IL-5 to human peripheral eosinophils and eosinophilic HL-60 clone 15 cells. Tam-X1 functions as an IL-5 antagonist by competitively binding to the IL-5 receptor (IL-5R), ultimately preventing IL-5 from binding to its receptor (Morokata et al., 2002). IL-5 is primarily produced and expressed by Th2 cells along with NK cells, mast cells, eosinophils, $CD34^{+}$ progenitor cells and type 2 lymphoid cells (Bagnasco et al., 2017; Roufosse, 2018; Varricchi et al., 2016). The IL-5R, found on the surface of basophils and eosinophils, is a heterodimer composed of two subunits. The

alpha chain subunit, IL-5Rα, specifically binds IL-5 and is highly expressed on the surface of eosinophils. In contrast, the beta subunit, IL-Rβc, is non-specific and binds to IL-5, as well as granulocyte-macrophage colony-stimulating factor (GM-CSF) and IL-3 (Pelaia et al., 2019). When IL-5 binds to IL-5Rα, the IL-5βc subunit is recruited to the complex, ultimately forming the IL-5/IL-5Rα/IL-5RβC complex. The IL-5Rβc subunit is associated with Janus kinase (JAK)1, while the IL-5Rα subunit is associated with JAK2. The binding of IL-5 activates JAK2 by binding to IL-5R, which in turn activates signal transducers and activators of transcription (STAT) 1,3 and 5 (Pelaia et al., 2019). This cascade of events leads to eosinophil activation, eosinophil survival, and eosinophilopoiesis through the modulation of transcription genes. Additionally, the binding of IL-5 to IL-5R may regulate gene transcription by activating pathways such as p38 mitogen-activated protein kinase (MAPK), Ras/Raf-ERK MAP kinases through JAK2 signalling and NF-κB, and phosphoinositide 3-kinase (PI3K) through JAK1 activation which leads to the production of pro-inflammatory cytokines (Pelaia et al., 2019; Takatsu, 2011).

Tam-X1, a quinoxaline derivative, has been reported to exhibit anti-tubercular effects (Chandra et al., 2024; Morokata et al., 2002.; Raphoko et al., 2021). Similarly, clofazimine, another quinoxaline derivative, is part of the second-line drugs used to treat MDR-TB (Raphoko et al., 2021). Studies have shown that quinoxaline derivatives exert anti-mycobacterial effects by inhibiting RNA synthesis through binding to the CpG sites on DNA (Palos et al., 2018; Ramalingam et al., 2010). However, further work may be required to understand the mechanisms underlying this effect fully. As a result, we further investigated the role of Tam-X1 on inflammation and bacterial load during TB in a 3D-biomimetic collagen-alginate model. It was observed that treatment with Tam-X1 resulted in a significantly reduced bacterial load, as indicated by decreased luminescence, compared to the untreated H37Rv *Mtb* control group. This suggests that treatment with Tam-X1 facilitates bacterial clearance during *Mtb* infection. This supports our hypothesis that treatment with Tam-X1 reduced intracellular bacterial growth and prompted further investigation into the effects of Tam-X1 on inflammation during *Mtb* infection.

Further to this, we observed that Tam-X1 significantly reduced the production of IL-1β and IL-6 in PBMCs within the 3D biomimetic model infected with *Mtb*, suggesting its potential ability to reduce inflammation during *Mtb* infection. The decrease in pro-inflammatory cytokines following Tam-X1 treatment in our study may be linked to the reduction of *Mtb* due to its anti-mycobacterial effects (Chandra et al., 2024). This could also be attributed to the fact that Tam-X1 inhibits the binding of IL-5 to its receptor IL-5R on immune cells expressing IL-5R, thereby preventing these cells' differentiation, maturation, activation, and survival. Literature indicates that some immune cell populations can produce pro-inflammatory cytokines such as IL-6 and IL-1β through the activation of the NF-κB pathway and p38 MAPK pathways, mediated by the JAK-STAT signalling cascade following IL-5 binding to IL-5Rα (Pelaia et al., 2019; Sastre et al., 2018). Therefore, the reduction in pro-inflammatory

cytokines observed with Tam-X1 treatment may be attributed to the inhibition of inflammatory immune cell activation. Similarly, a study performed by Ou *et al.* (2024) showed that Tam-X1 reduced IL-1β production in a dextran sulphate sodium-induced colitis model in mice and decreased IL-1β expression in lipopolysaccharide (LPS)-primed macrophages (Ou et al., 2024). These findings, along with the reduction in pro-inflammatory cytokines observed in our study, support a role for Tam-X1 in reducing inflammatory signalling. Further research is required to fully elucidate the effects of Tam-X1 on the inflammatory immune response during *Mtb* infection. These results validate our findings in *Mtb*-infected PBMCs and support our hypothesis that this drug has the ability to reduce inflammation associated with *Mtb* infection. This prompted further investigation into the relationship between IL-5 and IL-5Rα and its spatial association with TB-associated pathology in lung tissue.

It was previously reported that the pathological response to TB is characterised by compartmentalisation of inflammatory mediators during the development of the granuloma. The caseum is more enriched with pro-inflammatory proteins, while cellular regions are more enriched with anti-inflammatory responses (Hawn et al., 2013; Marakalala et al., 2016; Tobin, 2015). We, therefore, hypothesised that targeting IL-5R using Tam-X1 may also influence granulomatous development during TB. In this study, we observed that IL-5Rα was more abundantly expressed within the caseum of the granuloma than in the macrophage-rich region or the lymphocytic cuff. Notably, it was particularly associated with the necrotising areas in the necrotic core of the granuloma. IL-5Rα, as previously mentioned, is the alpha chain of the IL-5R, which specifically binds to IL-5. This receptor is present on the surface of both eosinophils and basophils (Elena-Pérez et al., 2021). During tuberculosis, cells within a granuloma can undergo necrotic cell death, resulting in the formation of a caseating granuloma. This process can lead to remodelling of the granuloma, which may eventually lead to a cavitary granuloma, facilitating the spreading of bacteria (Ndlovu and Marakalala, 2016). Therefore, the presence of IL-5Rα-expressing cells in the caseating core of the granuloma suggests that these cells are strongly associated with the inflammatory process driving tissue remodelling during *Mtb* infection.

Conversely, IL-5 was not expressed in the caseum but was more abundantly found in other regions of the tissue, particularly the cells found in the alveolar epithelium spaces, with sparse expression observed in the lymphocytic cuff surrounding the granuloma. IL-5, produced mainly by Th2 T-cells, is essential for the growth, activation, and survival of eosinophils. IL-5 is further known to act as a chemoattractant to eosinophils, recruiting these cells to the site of inflammation, where they are activated (Sastre et al., 2018; Varricchi et al., 2016). Consistent with our findings, the interaction of IL-5 with IL-5Rα was primarily observed in cells exhibiting the morphology of eosinophils, characterised by a bilobed nucleus and an overall diameter of approximately 12-15 μM as identified by H&E (Sastre et al., 2018). The presence of IL-5 outside the caseum, particularly within the lymphocytic cuff, suggests that IL-5 may play a role in recruiting eosinophils to the core of the granuloma.

Our study observed that IL-6 co-localized with IL-5Rα-expressing eosinophil-like cells, which interacted with IL-5. A study by Hamid *et al*. (1992) demonstrated that IL-6 is indeed released by eosinophils (Hamid et al., 1992). Similarly, literature reports that eosinophils produce various cytokines, which are then stored within their granular proteins, including IL-6 (Gaur et al., 2022; Babu et al., 2019). Eosinophils have the ability to release various cytokines that promote T-cell proliferation and polarization toward Th1 or Th2 states (Blanchard and Rothenberg, 2009). A study by Spencer *et al*. (2009) demonstrated that human eosinophils release cytokines associated with both Th1 and Th2 immune responses, including TNF-α, IL-6 and IFN-γ (Babu et al., 2019; Spencer et al., 2009). Activated eosinophils also interact with multiple immune cells, such as macrophages, T-cells, neutrophils, basophils, dendritic cells, and B cells, which may contribute to a Th1 immune response (Sastre et al., 2018). Our findings suggest that IL-5 signalling promotes the release of IL-6 in eosinophil-like cells. These cells were also observed forming aggregates in the presence of IL-5 within less diseased regions of the alveolar spaces, which may indicate early granuloma formation. Interestingly, a study by Bohrer *et al.* (2022) showed that eosinophils are part of the early immune response to *Mtb* infection of AM and may be among the first cells recruited to the site of infection (Bohrer et al., 2022). This could explain the cellular aggregates observed in our study. Together, these data suggest that IL-5/IL-5Rα-mediated signalling by eosinophil-like cells may contribute to the inflammatory responses, potentially playing a role in the formation of TB-induced caseous granulomas.

Cells expressing IL-5Rα, which co-localized with IL-6 and interacted with IL-5-expressing cells, were predominantly localized near the caseum in the macrophage-rich layer of the granuloma. These cells exhibited a linear clustering pattern toward the caseum of the granuloma, suggesting that IL-5 may actively be recruiting these eosinophil-like cells towards the caseum. In support of this, Khatun *et al.* (2019) demonstrated that eosinophils formed clusters in high numbers 30 days post-infection with *Mycobacterium avium* in the liver parenchyma (Khatun et al., 2018). Similarly, a study by Castro *et al.* (1991) found that eosinophils were attracted to mycobacteria at sites of immune inflammation in BALB/c mice and C57BL/6 mice infected with *Mycobacterium avium* or *Mycobacterium smegmatis* (Castro et al., 1991). These findings align with our study. Furthermore, IL-5Rα and IL-6 co-localized within the caseum of the granuloma, showing higher expression in this region compared to other lung areas. This suggests that these eosinophil-like cells may sustain the inflammatory response by releasing IL-6 in this region of the granuloma. The observed expression pattern of these eosinophil-like cells, alongside the abundant expression of IL-5Rα and IL-6 in the caseum, suggests that the immune response of IL-5Rα-expressing cells leads to tissue remodelling during *Mtb* infection via IL-5 signalling through the release of IL-6. In line with our findings, a study by Bohrer *et al.* (2021) reported that eosinophils were predominantly located in the outer rim of human TB granulomas, while eosinophil peroxidase, an eosinophil granular protein, was found in the necrotic core of the granuloma. This suggests eosinophil migration toward the granuloma and degranulation into its core (Bohrer et al., 2021), which aligns with

our study's findings. The migration of these eosinophil-like cells and the co-localization of IL-5Rα and IL-6 within the caseum collectively suggest that the activation of IL-5Rα-expressing cells occurs outside the granulomas, with these activated cells likely migrating toward the caseum and contributing to disease progression through inflammatory immune responses. Taken together, our results suggest that eosinophil-like cells contribute to disease pathogenesis within the TB granuloma through IL-5/IL-5Rα-mediated signalling, leading to the release of inflammatory cytokines such as IL-6.

In line with our study, Bohrer *et al*. (2021) reported that eosinophils migrate to the granulomas during *Mtb* infection. This observation was conserved across various species, including mice, zebrafish, humans, and macaques (Bohrer et al., 2021). A study investigating eosinophil granular proteins in patients with pulmonary tuberculosis (PTB) found significantly higher levels of these proteins in PTB patients compared to those with LTBI. Additionally, the levels of eosinophil granular proteins decreased following anti-tuberculosis treatment (ATT) (Moideen et al., 2018). Similarly, Essone *et al.* (2019) examined the cytokine profiles of community controls and healthcare workers highly exposed to TB, revealing elevated IL-5 levels in healthcare workers and community controls with latent *Mtb* infection compared to non-infected community controls. The expression of IL-5 observed was also higher in LTBI healthcare workers than in non-infected healthcare workers, further supporting the association of IL-5 with *Mtb* infection (Essone et al., 2019). Moreover, a study by Lee *et al.* (1996) established a transgenic mice model expressing murine IL-5 in the lung epithelium, showing that IL-5 release led to increased eosinophil accumulation in the peribronchial region, as well as increased pathology, epithelial enlargement, localised collagen deposition and eosinophil presence within the bronchi (Lee et al., 1997). Tam-X1 has been shown by Morokota et al (2002) to specifically inhibit the effects of IL-5 on the IL-5R without affecting the binding of IL-3 and GM-CSF to the IL-5R. This allows the continued activation and survival of these molecules on eosinophils (Morokata et al., 2002). These findings suggest that IL-5 expression and the subsequent recruitment of eosinophils contribute to lung tissue pathology. This aligns with our study and supports the hypothesis that Tam-X1 targets a pathway spatially associated with pathology in the TB-diseased lung, suggesting that IL-5 antagonists may have therapeutic potential. Our study demonstrates that TB-driven inflammation is mediated by immune cells expressing IL-5Rα, such as macrophages and eosinophils. However, in the case of TB-driven pathology, eosinophils are potentially the primary cells that contribute to pathology through IL-5R.

Conclusion

In conclusion, our study revealed the potential of Tam-X1, an IL-5 antagonist, as a promising HDT for TB by targeting the IL-5/IL-5R signalling pathway. This agent not only reduced the pro-inflammatory immune response during Mtb infection but also lowered the *Mtb* bacterial burden, suggesting that treatment with Tam-X1 may reduce TB-associated pathology while promoting bacterial clearance by modulating the host immune response and reducing the activation of eosinophil-like cells. Our findings

further underscore the role of eosinophil-like cells in driving inflammatory responses and disease progression during TB, mainly through the spatial association of IL-5Rα and IL-6 in the necrotic regions of the granuloma. These results provide a foundation for further investigation into Tam-X1 as a potential HDT for TB, paving the way for improved treatment strategies to alleviate the increasing emergence of drug-resistant *Mtb* strains and minimize pathology during TB.

Future work

Future studies should explore the cytotoxic effects of Tam-X1. Additionally, the mechanistic effects of Tam-X1 on inflammatory signalling during *Mtb* infection could be further investigated in a murine *in vivo* model that mimics human TB pathology. The impact of Tam-X1 on granuloma formation could also be analysed in murine models. Further research into the interactions of Tam-X1's target in the granuloma could also provide a deeper insight into their roles in immunopathogenesis. Moreover, assessing the effects of Tam-X1 in combination with current TB treatment strategies could reveal its potential as an effective adjunctive HDT. Finally, clinical trials will be necessary to evaluate the potential of Tam-X1 as an HDT for treating TB-associated lung damage.

CHAPTER 5:

PART B: RESULTS

SCREENING OF IMMUNOMODULATORY AGENTS TO EVALUATE THEIR POTENTIAL TO ENHANCE THE IMMUNE RESPONSE AGAINST *Mtb*.

5. Results: Part B

5.1 Screening immunomodulatory agents to evaluate their potential to enhance immunity through up-regulation of pro-inflammatory cytokines

To assess the effects of immunomodulatory agents targeting TLR7 and 8 on the immune response during *Mtb* infection, THP-1 monocytic cell lines were cultured and treated with 40 μM of immunomodulatory agents targeting TLRs. The supernatants were collected 3 days post-infection, and ELISA was performed to evaluate the effects of immunomodulation on inflammation.

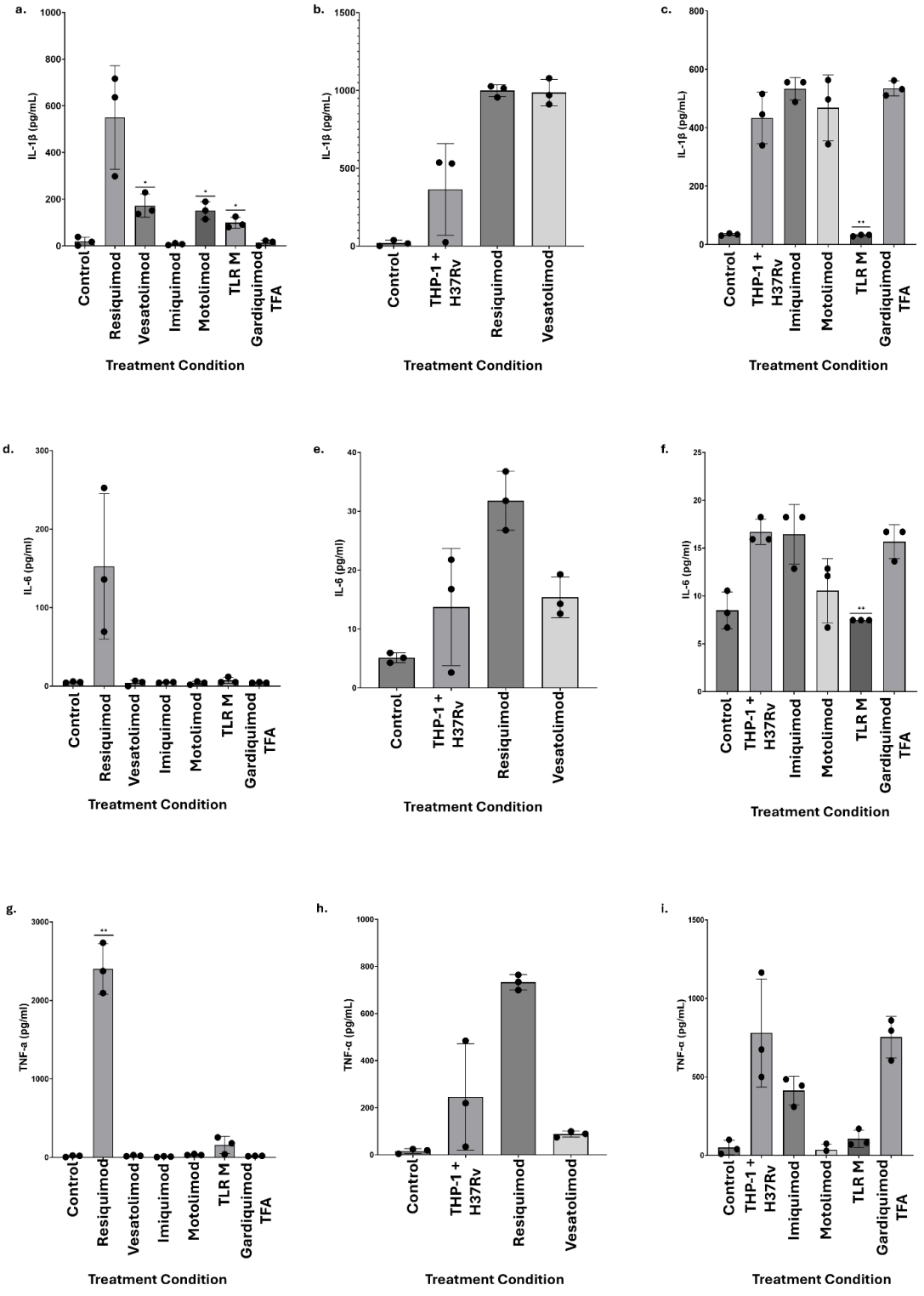

Figure 5.1: **Results of screening immunomodulatory agents targeting TLR7 and TLR8 to determine their effects on inflammatory cytokine release.** Cytokine release of IL-1β, TNF-α and IL-6

was measured using ELISA in THP-1 cells infected with H37Rv *Mtb* and treated with TLR7/8 agonists. Three replicates were performed for each group, and the mean value was plotted. Error bars represent the standard deviation of the mean. Statistical analysis was conducted using a t-test with Welch's correction to compare cytokine levels of THP-1 cells infected with H37Rv *Mtb* and treated with drugs to those of untreated THP-1 cells infected with H37Rv *Mtb* or THP-1 cells only.

Firstly, uninfected THP-1 MDMs (Fig. 5.1) treated with TLR agonists revealed that **vesatolimod**, **motolimod**, and **TLR M** significantly increased IL-1β (Fig. 5.1.a.) release compared to the control group. While not statistically significant, **Resiquimod** also showed a trend towards increased IL-1β release. Additionally, treatment with **Resiquimod** resulted in an upward trend in **IL-6** (Fig. 5.1.d.) release compared to the control. However, this did not reach statistical significance compared to the control. Treatment with **resiquimod** resulted in significantly increased release of TNF-α (Fig. 5.1.g) compared to the uninfected control group. On the other hand, treatment with **TLR M** also induced a trend towards increased TNF-α release, but this was not significant compared to the uninfected control group (Fig. 5.1.g).

In contrast, **TLR M** resulted in a significant decrease in IL-1β release compared to the untreated control during infection with H37Rv *Mtb* (Fig. 5.1.c). Furthermore, **TLR M** was associated with a significant reduction in IL-6 (Fig. 5.1.f) release compared to the untreated control. Although not significant, **resiquimod** displayed an increased trend in the release of IL-6 in infected THP-1 cells compared to the untreated control (Fig. 5.1.e). In infected THP-1 cells, treatment with **resiquimod** resulted in an increased trend in TNF-α (Fig. 5.1.h) release, although this was not significant compared to the untreated control group.

The analysis of these results showed that TLR modulation with TLR7 and 8 agonists triggered an increased immune response during *Mtb* infection by upregulating the inflammatory response, specifically treatment with TLR7 and TLR8 agonists. These outcomes thus sparked further investigation into the effects of TLR modulation with the aid of agonistic and antagonistic agents on bacterial clearance during *Mtb* infection.

5.2 Screening of TLR antagonists to determine the effects of the inhibition of TLRs on the inflammatory immune response during *Mtb* infection

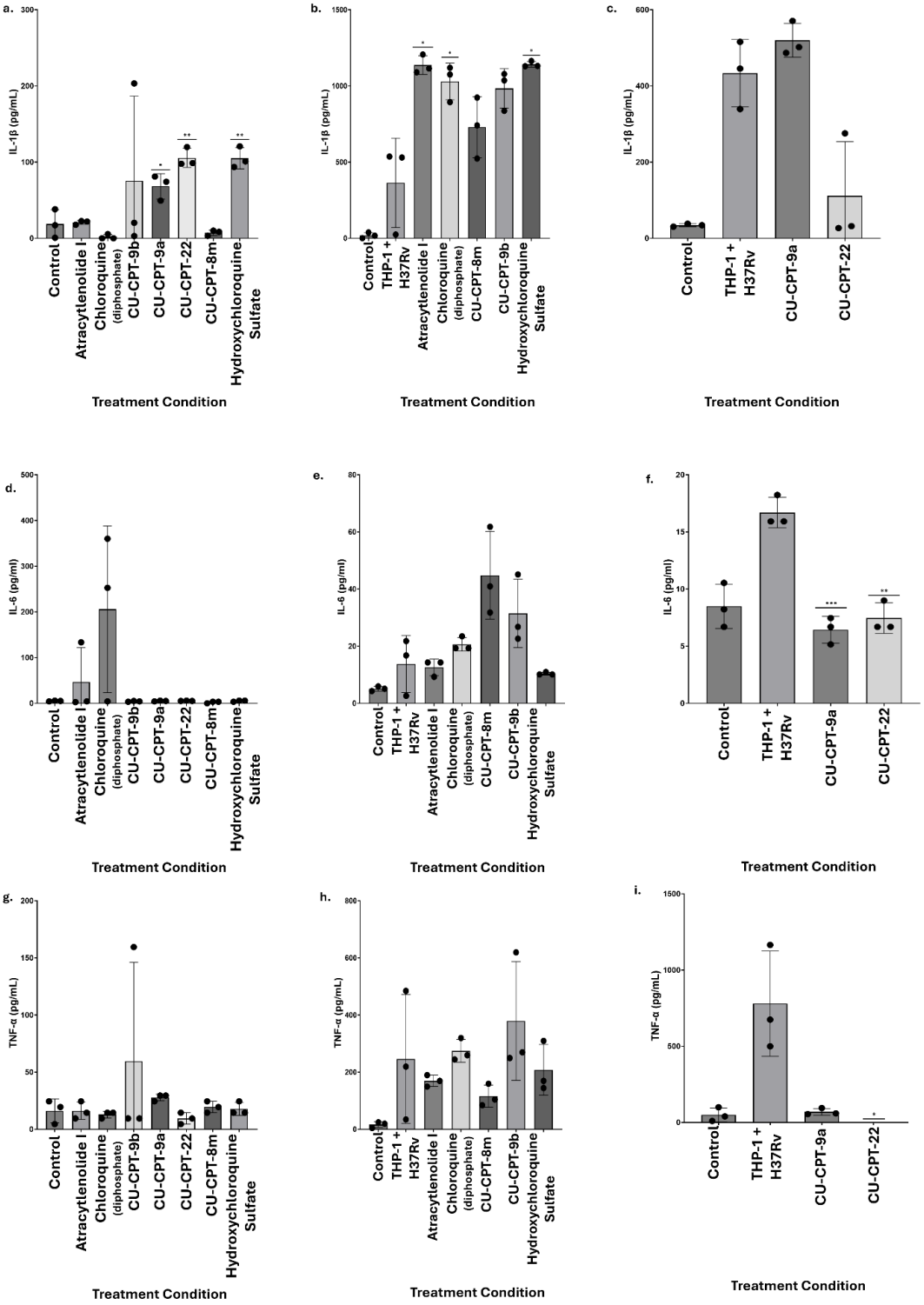

Figure 5.2: **Production of IL-1β, IL-6 and TNF-α after treatment with antagonists of TLR1, 2, 3, 4, 7, and 8.** Cytokine production of IL-1β, TNF-α and IL-6 was quantified using ELISA in THP-1 cells infected

with H37Rv *Mtb* and treated with TLR7/8 antagonists. Three replicates were performed for each group, and the mean value was plotted. Error bars represent the standard deviation of the mean. Statistical analysis was conducted using a t-test with Welch's correction to compare cytokine levels of THP-1 cells infected with H37Rv *Mtb* and treated with drugs to those of untreated THP-1 cells infected with H37Rv *Mtb* or THP-1 cells only.

In order to evaluate the effects of inhibiting TLR pathways involved in the recognition of *Mtb* on the production of key proinflammatory cytokines during *Mtb* infection, THP-1 monocytic cells were cultured and treated with 40 μM of TLR antagonists. The supernatants were collected 3 days post-infection, and ELISA was performed to measure the release of IL-1β, IL-6 and TNF-α.

In uninfected THP-1 cells treated with TLR antagonists, it was observed that treatment with **CU-CPT-9a**, which inhibits TLR8, **CU-CPT-22**, which inhibits TLR1/2, and **Hydroxychloroquine sulfate**, which inhibits TLR3, 7, 8 and 9, significantly increased the production of IL-1β compared to the control group (Fig. 5.2.a). Treatment with **Chloroquine (diphosphate)**, which inhibits TLR 3, 7, 8 and 9, and **Atractylenolide I**, which inhibits TLR 4, resulted in an upward trend in IL-6. compared to the control. However, this did not reach statistical significance compared to the control (Fig. 5.2.a).

The following immunomodulatory agents resulted in a significant increase in release of IL-1β during *Mtb* infection: **Atractylenolide I**, **Chloroquine (diphosphate)** and **Hydroxychloroquine sulfate** (Fig. 5.2.b) compared to the untreated *Mtb* control (*Mtb* H37Rv). In contrast, **CU-CPT-22** resulted in a significant decrease in the trend of IL-1β release compared to the untreated control (Fig. 5.2.c).

Furthermore, **CU-CPT-9a**, which inhibits TLR8, and **CU-CPT-22** were associated with a significant reduction in IL-6 (Fig. 5.2.f) release compared to the untreated control. Although not significant, **CU-CPT-9b** displayed an increased trend in the release of IL-6 compared to the untreated control (Fig. 5.2.e).

The analysis of these results showed that inhibition of these pathways affects the release of pro-inflammatory cytokines during Mtb infection, and this prompted further investigation on the effects of these antagonists on bacterial growth during *Mtb* infection.

5.3 Screening immunomodulatory agents to evaluate their potential to reduce bacterial burden

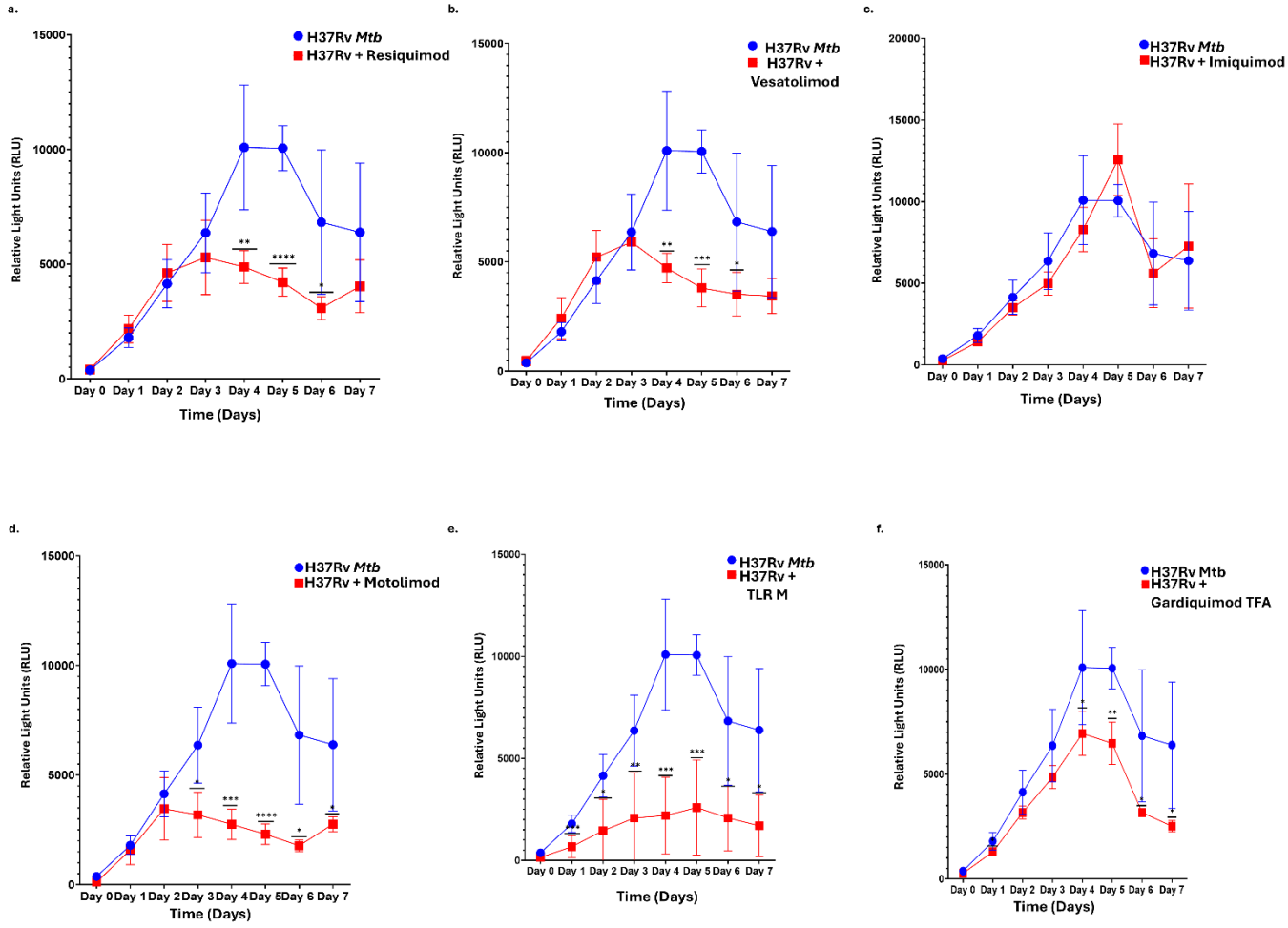

Figure 5.3: **Assessment of bacterial killing during *Mtb* infection using TLR7 and TLR8 modulators.** Luminescence was measured via luminometry to evaluate the effects of different TLR modulators on bacterial killing in THP-1 cells infected with the luminescent strain, H37Rv *Mtb* LUX. Samples were treated with TLR7/8 agonists, and luminescence was recorded over 7 days. Three replicates were performed for each group. The data plotted represents the mean values, with error bars indicating the standard deviation of the mean. Statistical analysis was performed using the t-test with Welch's correction. Significant differences between treated and control groups for each of the days are indicated by: *$p \leq 0.05$, ** $p \leq 0.01$, ***$p \leq 0.001$ and ****$p \leq 0.0001$.

To investigate the effects of TLR7/8 modulation on its ability to reduce bacterial load during *Mtb* infection, THP-1 cells were cultured and treated with TLR agonists. Subsequently, THP-1 cells were then infected with the luminescent strain H37Rv *Mtb* LUX. Luminescence was measured 4 hours after infection and then daily for 7 days, with luminescence levels correlating to *Mtb* presence.

Treatment with **Resiquimod** (Fig. 5.3.a), which activates TLR7 and TLR8, exhibited a clear downward trend in bacterial load starting on day 4 and continuing through day 6. However, a slight increase in

trend was noted on day 7 compared to the untreated control. Significant differences were observed on days 4, 5, and 6.

Moreover, treatment with **Vesatolimod** (Fig. 5.3.b), a TLR7 agonist, resulted in an overall lower trend in bacterial load compared to the untreated control. This downward trend in bacterial load was observed from day 3 up to day 7. Significant differences were recorded on day 4 through day 6.

Next, treatment with **Imiquimod** (Fig. 5.3.c), which activates TLR7, showed no significant difference between the treated group and the untreated control group. Overall, the amount of *Mtb* present in the imiquimod-treated group closely mirrored that of the control group, indicating little to no effective reduction in bacterial load following treatment.

Treatment with **Motolimod** (Fig. 5.3.d), a TLR8 agonist, resulted in a significant reduction in bacterial load on day 1 and from day 4 onward as compared to the untreated control group. A noticeable downward trend in bacterial load was maintained from day 4 to day 6. Although a slight increase in the number of bacteria was seen from day 6 to day 7, the bacterial load remained significantly lower than the number of bacteria present in the untreated control group.

Treatment with **TLR M** (Fig. 5.3.e), which activates TLR7/8, resulted in a consistently lower bacterial load than the untreated control group throughout the 7-day incubation period. Notably, this group exhibited the earliest onset of bacterial killing, beginning on day 1. The treated group displayed significantly reduced bacterial counts, as indicated by the decreased luminescence relative to the untreated control. A downward trend in the bacterial load was observed on days 6 to 7. Significant differences in bacterial load compared to the control were maintained from day 1 to day 7.

Treatment with **Gardiquimod Trifluoroacetate** (Fig. 5.3.f), which activates TLR7 and TLR8, displayed a slightly lower overall trend in bacterial load compared to the untreated control group. A significant reduction in bacterial numbers was observed from day 4 up to day 7.

Taken together, these results indicate that agonists activating TLR7 and TLR8 or both significantly reduce the bacterial load during *Mtb* infection. This suggests that modulation of TLR7 and TLR8 may assist in bacterial clearance of *Mtb* through enhancement of the innate immune response.

5.4 Analysing intracellular growth of *Mtb* upon TLR inhibition with TLR antagonists

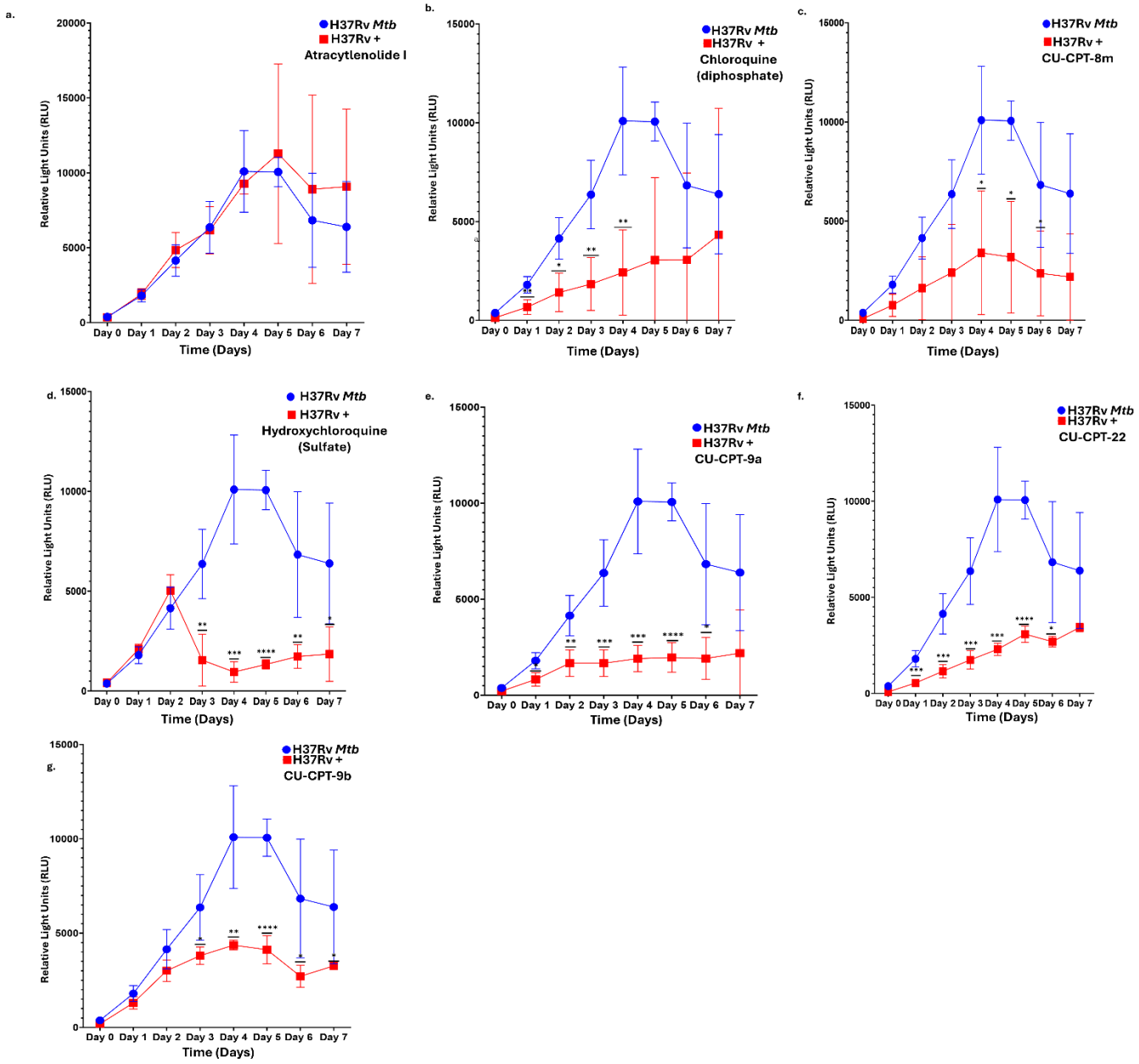

Figure 5.4: **Effects of TLR inhibition by TLR antagonists on intracellular bacterial growth in THP-1 cells infected with H37Rv *Mtb* LUX.** Luminescence was measured via luminometry to evaluate the effects of different TLR modulators on bacterial killing in THP-1 cells infected with the luminescent strain, H37Rv *Mtb* LUX. Samples were treated with TLR1, 2, 3, 4, 7, and 8 antagonists, and luminescence was recorded over 7 days. Three replicates were performed for each group. The data plotted represents the mean values, with error bars indicating the standard deviation of the mean. Statistical analysis was performed using the t-test with Welch's correction. Significant differences between treated and control groups for each of the days are indicated by: *$p \leq 0.05$, ** $p \leq 0.01$, ***$p \leq 0.001$ and ****$p \leq 0.0001$.

Next, TLR antagonists were employed to assess their effects on bacterial load during TLR modulation. THP-1 cells were cultured and treated with TLR antagonists and infected with the luminescent strain

H37Rv *Mtb* LUX. Luminescence was measured 4 hours after infection and then daily for 7 days, with luminescence levels correlating to *Mtb* presence. Treatment with **Atractylenolide I** (Fig. 5.4.a), which is a TLR4 antagonist, resulted in no overall reduction in bacterial load and no significant differences were observed compared to the untreated control. Next, treatment of *Mtb*-infected THP-1 cells with **Chloroquine (diphosphate)** (Fig. 5.4.b), showed an overall lower trend in the number of *Mtb* compared to the untreated control group. Significantly lower bacterial loads were observed from day 1 through day 4. An upward trend in bacterial load was noted, with a further increase on day 7, although the levels remained lower than those in the control group.

Significant differences were recorded on days 4 to 7. Lastly, the group treated with **CU-CPT-8m** (Fig. 5.4.c), a TLR8 antagonist, exhibited an overall lower trend in bacterial load compared to the untreated control group. Significantly lower numbers of *Mtb* were observed on days 4, 5 and 6. Treatment with **Hydroxychloroquine Sulfate** (Fig. 5.4.d), an antagonist of TLR7\8, exhibited a pronounced reduction in bacterial load in the treated group compared to the untreated control starting on day 3 and continuing through day 7. Significant differences in bacterial numbers were observed on day 3, along with a further downward trend on day 4. However, a slight upward trend in bacterial numbers was noted on days 5, 6, and 7. Despite this increase, the bacterial load remained significantly lower than that of the untreated control group for days 3 to 7.

Notably, treatment with **CU-CPT-9a** (Fig. 5.4.e), which targets TLR8, exhibited a significant reduction in bacterial numbers. This significant reduction was evident from day 1 through day 6. An overall downward trend in *Mtb* load was observed in the **CU-CPT-9a** group starting on day 2, which persisted with only minor variations compared to the untreated control group. Additionally, treatment with **CU-CPT-22** (Fig. 5.4.f), which targets TLR1 and TLR2, showed an overall lower trend in *Mtb* bacterial load compared to the untreated control from day 1 to day 6.

The group treated with **CU-CPT-9b** (Fig. 5.4.g), a TLR8 antagonist, exhibited an overall lower trend in the *Mtb* numbers as compared to the untreated control. On day 1, there was a significantly lower bacterial load in the **CU-CPT-9b**-treated group. Following this, a slight upward trend in bacterial load was observed, with significant differences noted on days 3 to 4. A downward trend in *Mtb* numbers was observed from day 4 to day 6, and a slight increase from day 6 to day 7.

The TLR antagonist, targeting TLR1, 2, 7 and 8, unexpectedly led to a decrease in bacterial load. However, this effect may have been due to antimicrobial properties or cytotoxicity associated with these antagonists, rather than inhibition of TLR activity. Consequently, the effects of lower concentrations of the selected agonists and antagonists were further investigated.

5.5 Determining the effects of treatment with reduced concentrations of TLR7/8 agonists and antagonists on the inflammatory immune response during *Mtb* infection

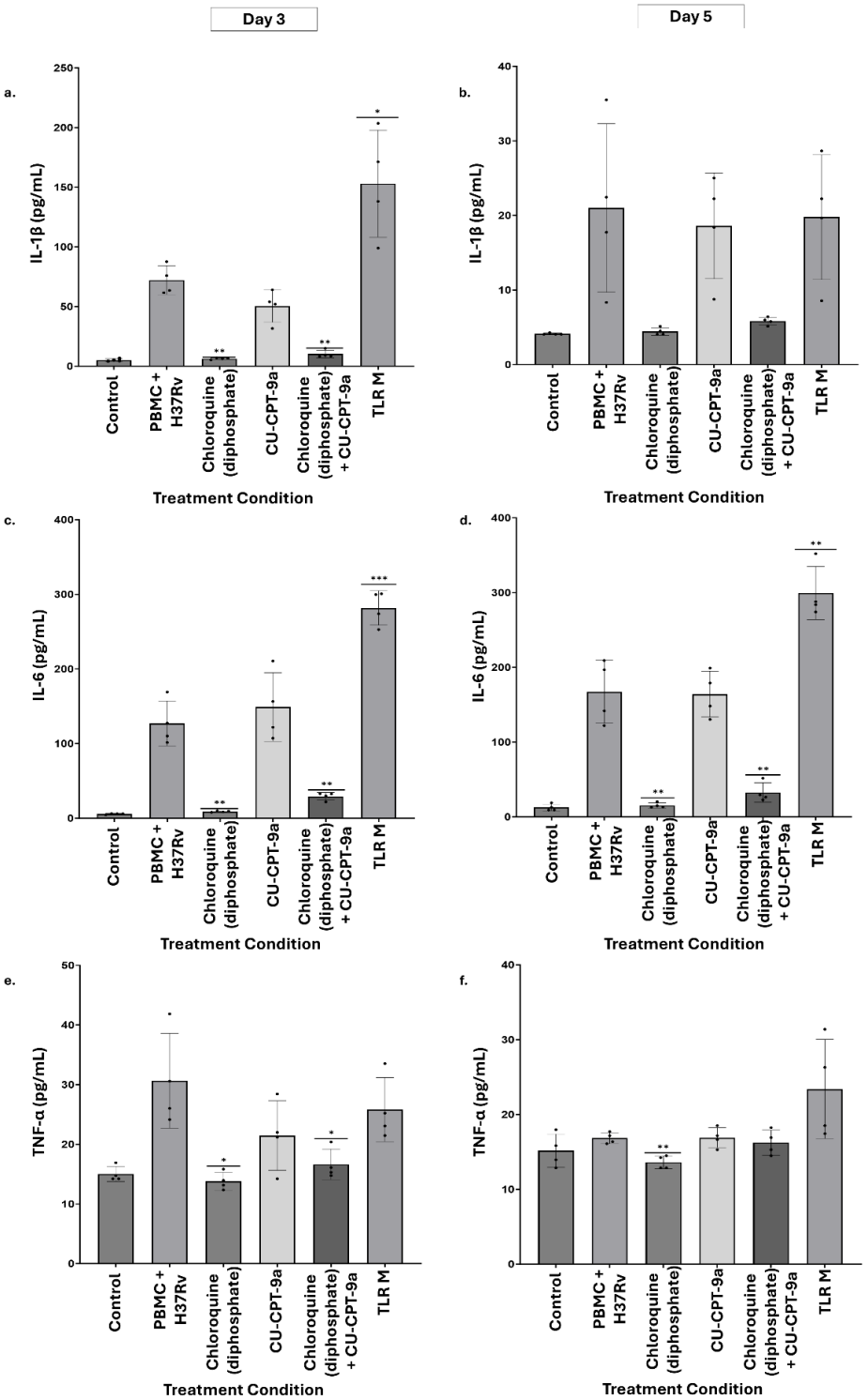

Figure 5.5: **Treatment with a lower concentration of TLR M increased the release of pro-inflammatory cytokines in PBMCs infected with H37Rv *Mtb*.** Cytokine release of IL-1β, TNF-α and

IL-6 were quantified using ELISA in PBMCs infected with H37Rv *Mtb* and treated with immunomodulatory agents. Three replicates were performed for each group, and the mean value was plotted. Error bars represent the standard deviation of the mean. Statistical analysis was conducted using a t-test with Welch's correction to compare cytokine release levels of PBMCs cells infected with H37Rv *Mtb* and treated with drugs to untreated PBMCs infected with H37Rv *Mtb*.

Upon screening immunomodulatory agents targeting TLR7 and TLR8 for their potential to enhance immune responses and bacterial clearance in *Mtb* infection, it was observed that these agents resulted in a decrease in intracellular bacterial growth in *Mtb*-infected THP-1 cells and increased inflammatory responses in both uninfected THP-1 cells and THP-1 cells infected with *Mtb*. Based on the potent bacterial clearance observed with **TLR M** treatment, this agent was selected for further analysis. Additionally, **chloroquine (diphosphate)** and **CU-CPT-9a**, which are antagonists of TLR 7/8, were included to assess the effects of TLR7/8 inhibition during *Mtb* infection. Due to the possibility that the effects observed upon **TLR M** treatment using a concentration of 40 μM might be due to cytotoxic effects, the concentration of each of the immunomodulatory agents was reduced to 20 μM for subsequent analysis.

To investigate the impact of these agents on cytokine release during *Mtb* infection, PBMCs, extracted from blood donated by healthy individuals, were treated with **TLR M**, **CU-CPT-9a**, **Chloroquine (diphosphate)**, or a combination of **CU-CPT-9a** and **Chloroquine (diphosphate)** and then infected with H37Rv *Mtb*. Supernatants were collected on day 3 and day 5 post-infection, and ELISA was performed to measure the release of IL-1β, IL-6 and TNF-α.

Treatment with **TLR M** significantly increased IL-1β and IL-6 (Fig. 5.5.a and Fig. 5.5.c) release on day 3 compared to the untreated control, with a sustained significant increase in IL-1β (Fig. 5.5.b) on day 5. Conversely, **Chloroquine (diphosphate)** significantly decreased IL-1β release on day 3 (Fig. 5.5.a) and reduced both IL-6 and TNF-α (Fig. 5.5.c-Fig. 5.5.f) on days 3 and 5.

Additionally, combined treatment with **CU-CPT-9a** and **Chloroquine (diphosphate)** resulted in a significant reduction in IL-1β (Fig. 5.5.a), IL-6 (Fig. 5.5.c) and TNF-α (Fig. 5.5.e) release on day 3. On day 5, the combination of these agents resulted in a continued significant reduction of IL-6 (Fig. 5.5.d) release on day 5.

Overall, treatment with **TLR M** induced a consistent increase in the release of inflammatory cytokines on both days 3 and 5. In contrast, **Chloroquine (diphosphate)** and the combination of **Chloroquine (diphosphate)** and **CU-CPT-9a** consistently displayed a decrease in the trend of inflammatory cytokines on days 3 and 5. These results indicated that stimulation of TLR7 and 8 by TLR M increased the immune response to *Mtb* through upregulated inflammatory responses. In contrast, the inhibition of TLR7 and 8 by antagonists decreased the immune response by downregulating inflammatory responses during *Mtb* infection.

5.6 Analysing the effects of TLR M on reducing intracellular bacterial growth in 3D collagen-alginate *Mtb*-infection model

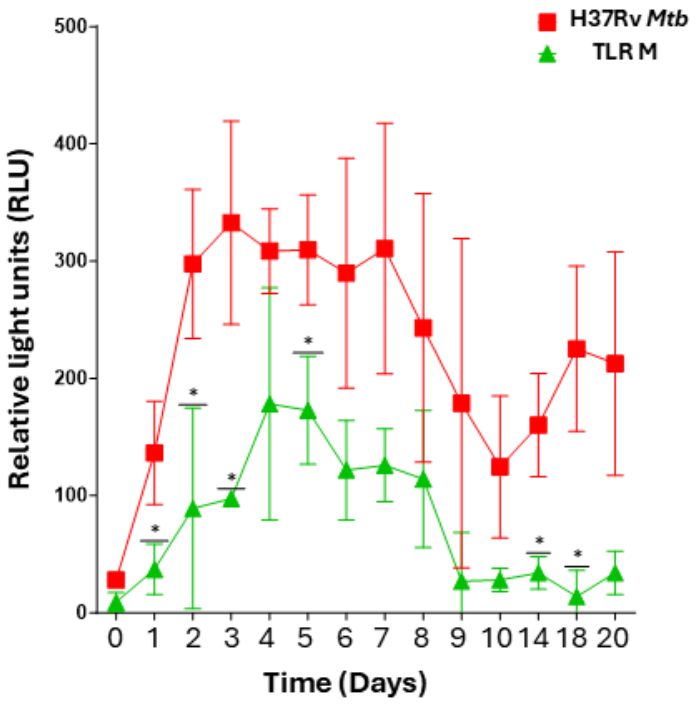

Figure 5.6. **TLR M reduces bacterial load by enhancing bacterial killing in cells infected with Mtb.** Luminescence was measured via luminometry over 20 days to assess the effects of TLR M treatment on bacterial killing in PBMCs infected with H37Rv LUX *Mtb* in a 3D collagen-alginate biomimetic model. Three replicates were performed, and the mean values were plotted. Error bars represent the standard deviation of the mean. A t-test with Welch's correction was used to determine statistical significance. Significant differences between the treated group (TLR M) and the untreated group (H37Rv *Mtb*) are indicated as follows: *p ≤ 0.05, ** p ≤ 0.01, ***p ≤ 0.001 and ****p ≤ 0.0001.

To characterise the effects of TLR7/8 modulation on antibacterial properties, a 3D biomimetic collagen-alginate matrix was established, consisting of PBMCs infected with the luminescent *Mtb* strain, H37Rv *Mtb* LUX. The spheroids were treated with 40 µM **TLR M,** and a luminometer was used to measure the emitted luminescence, which was directly proportional to the amount of *Mtb* present.

The results (Fig. 5.6) indicated a consistently lower number of *Mtb* in the group treated with **TLR M** over the 20-day incubation period compared to the untreated control group. From day 1 to day 4, an upward trend in the bacterial growth was observed, though levels remained lower than those in the untreated control group, with significant differences noted on days 1, 2, and 3.

Between days 5 and 9, there was a downward trend in the number of *Mtb* present observed in the **TLR M**-treated group, with a significant difference on day 5 compared to the untreated control group. A further decrease was noted between days 8 and 9. From days 10 to 14, there was a slight upward trend

in the number of bacteria in the **TLR M**-treated group, with a significant difference on day 14, despite a larger increase shown in the amount of *Mtb* present in the untreated control group. A slight downward trend was observed from days 14 to 18, followed by a slight upward trend from days 18 to 20, with a significant difference on day 18.

These results suggest that TLR7/8 modulation with the agonist, **TLR M**, enhances the anti-mycobacterial properties of PBMCs during *Mtb* infection. This sparked interest in characterising the effects of TLR M on inflammation in the 3D biomimetic model, which closely resembles *in vivo* interactions during *Mtb* infection.

5.7 Investigation of the effects of TLR M treatment on TLR7/8 signalling-induced inflammation during *Mtb* infection in a 3-dimensional biomimetic model

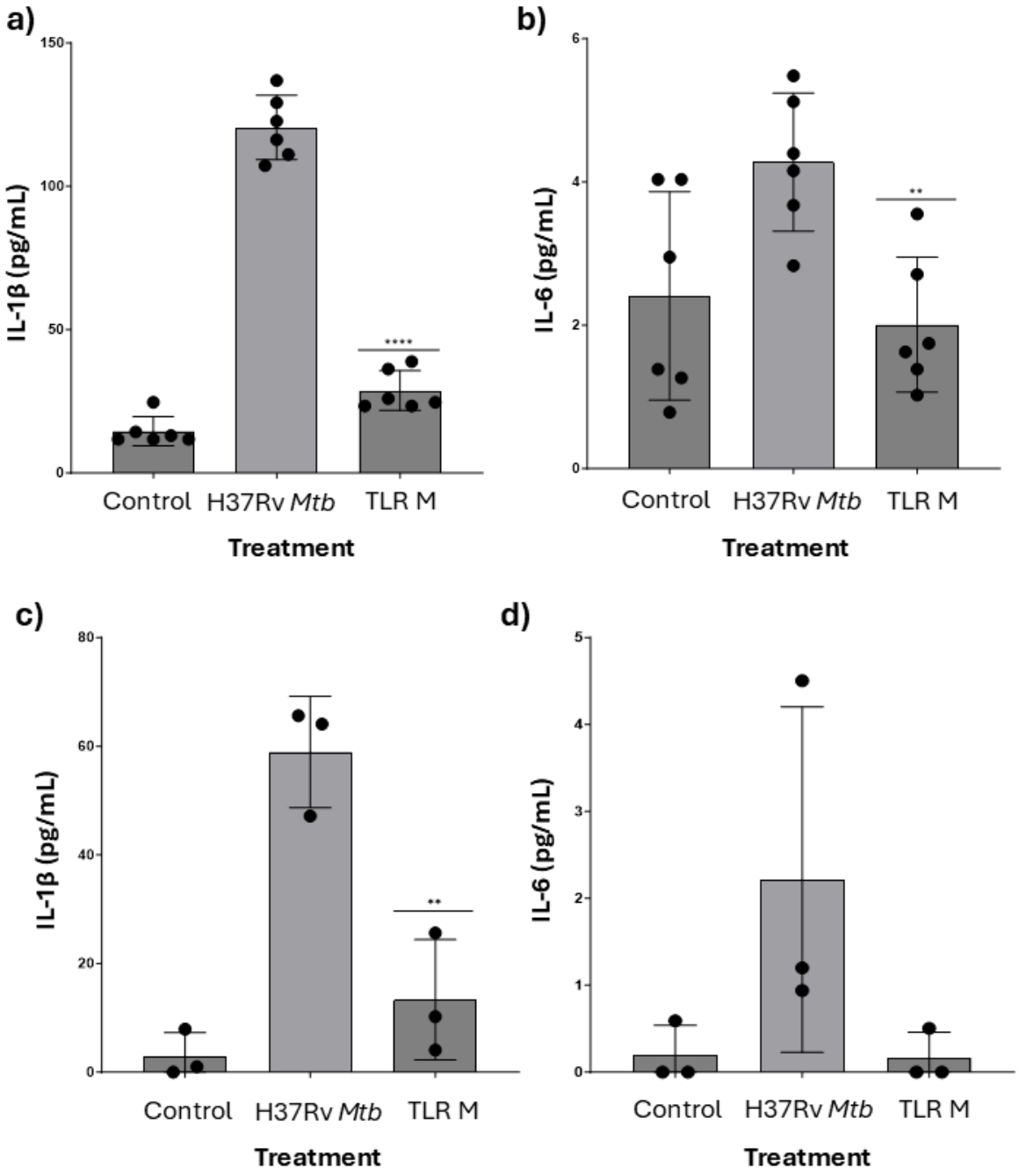

Figure 5.7. **TLR M results in reduced release of pro-inflammatory cytokines.** The pro-inflammatory cytokines IL-6 and IL-1β were measured using ELISA after treatment with TLR M in a 3D collagen-alginate biomimetic model of *Mtb*-infection. Three replicates were performed, and the mean values were plotted. The error bars represent the standard deviation of the mean. Significant differences between the treated group (TLR M) and the untreated group (H37Rv *Mtb*) were determined using the t-test with Welch's correction and are indicated as follows: *$p \leq 0.05$, ** $p \leq 0.01$, ***$p \leq 0.001$ and ****$p \leq 0.0001$. Graphs a) and b) represent data from the supernatant obtained on day 3, while graphs c) and d) represent data from the supernatant collected on day 10.

To determine the effects of TLR7/8 modulation on the inflammatory response during *Mtb* infection, a 3D biomimetic collagen-alginate model was established. This model included a control group (PBMCs only), an untreated control group (H37Rv *Mtb* + PBMCs) and a group treated with **TLR M** (PBMCs + H37Rv + **TLR M**). Supernatants were collected on days 3 and 10. ELISA was performed to measure the concentration of IL-6 and IL-1β in each of the supernatants.

As illustrated in Figure 5.7, a) and b), treatment with **TLR M** resulted in an extremely significant reduction in the release of IL-1β and a significant reduction in the release of IL-6 in the supernatant collected on day 3 compared to the untreated control group. Additionally, on day 10, **TLR M** treatment of H37Rv *Mtb*-infected PBMCs led to a significant decrease in IL-1β release (Fig. 5.7.c) compared to the untreated control group. In contrast, while there was a noticeable downward trend in IL-6 levels on day 10 (Fig. 5.7.d), this did not reach statistical significance compared to the untreated control.

These observations suggest that treatment with **TLR M** has the potential to reduce the release of pro-inflammatory cytokines during *Mtb* infection. Following this, the expression of TLR7 and TLR8 was analysed in lung tissue from patients who have undergone surgery due to severe TB-associated lung damage, aiming to further elucidate the mechanism of TLR7/8 in bacterial clearance and the inflammatory response.

5.8 Immunohistopathological characterisation of TLR7 and TLR8 in TB lung tissue

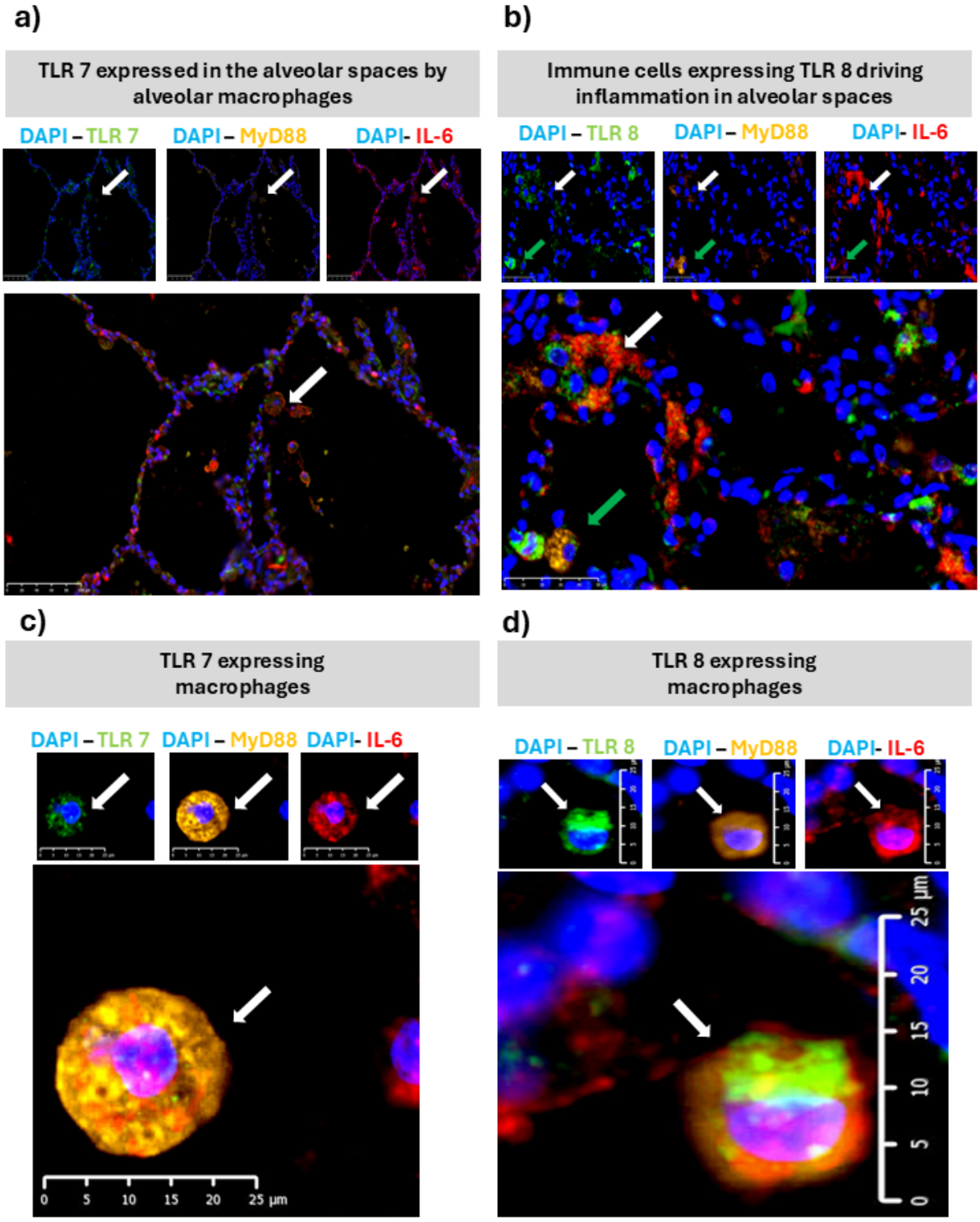

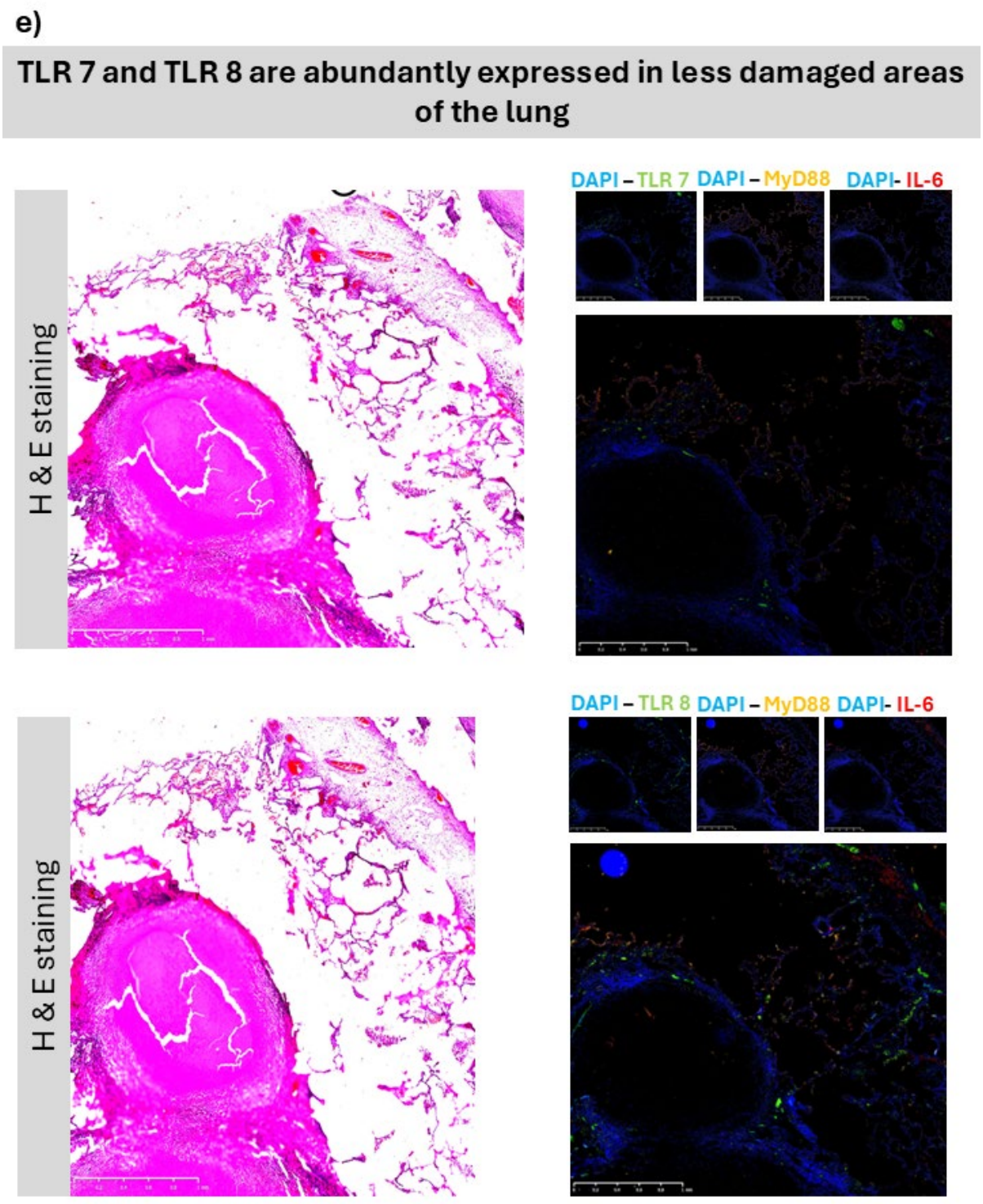

Figure 5.8. **TLR7 and TLR8 are expressed in alveolar spaces, particularly by alveolar macrophages and giant cells, and play a key role in driving inflammation.** Immunofluorescence staining was performed to visualise the localisation of TLR7 and TLR8 in resected TB lung tissue from patients who have undergone surgery due to severe TB-associated lung damage. H&E staining was performed to identify various cell types. Immunofluorescence was performed on separate tissues for both TLR7 (green) and TLR8 (green), both were co-stained with MyD88 (yellow) and IL-6 (red). Nuclei were counterstained with DAPI (blue).

Images were captured using a NanoZoomer S60 digital slide scanner at varying magnifications, with the scale bars representing appropriate lengths for each panel. Merged images illustrate the relationship between TLR7 and TLR8 release and inflammatory markers, highlighting their roles in mediating inflammation within the lung tissue during *Mtb* infection.

Immunofluorescence was performed on resected lung tissue obtained from patients with TB who underwent lung surgery due to TB-associated lung damage. The objective was to analyse the localisation of drug targets of **TLR M**, TLR7 and 8, along with the adapter protein MyD88 and IL-6, a pro-inflammatory cytokine, to analyse how the signalling pathway spatially associates with inflammation at the site of infection.

The results demonstrated that TLR7 and TLR8 were abundantly expressed in alveolar spaces (Fig. 5.8.a-b), particularly in pneumocytes and alveolar macrophages (Fig. 5.8.c-d). In contrast, these receptors were sparsely localised in cells within the lymphocytic cuff (outer cellular layer) of the granuloma (Fig. 5.8.e) and were also in giant cells and macrophages located in the cellular mass adjacent to the granuloma.

MyD88 exhibited a predominant localisation in pneumocytes, and alveolar macrophages situated near the alveolar interstitium (Fig. 5.8.a-d). Notably, MyD88 was absent in areas displaying severe pathology and within the caseum (Fig. 5.8.e). Alveolar macrophage-like cells located within alveolar spaces expressed MyD88, which co-localised with TLR7 and TLR8 (Fig. 5.6. c-d). This co-localization was also observed in giant cells located near the granuloma, while MyD88 was not detected in any regions of the granuloma itself.

IL-6 co-localised with both TLR7 and TLR8, as well as MyD88, within the alveolar spaces (Fig. 5.8.a-b), specifically in alveolar macrophages, pneumocytes and giant cells in cellular masses (Fig. 5.8.c-d). However, in cells expressing TLR7 around the caseum (Fig. 5.8.e), none co-localised with IL-6 and none expressed MyD88. Interestingly, IL-6 was sparsely expressed in the cellular ring of the granuloma and co-localised with cells expressing TLR8, despite the absence of MyD88 in that region.

Overall, TLR7 and TLR8 are more abundantly expressed in the less diseased regions of the lungs, and both TLR7 and TLR8 co-localised with My-D88 and the pro-inflammatory cytokine, IL-6. These observations may imply that TLR7 and TLR8 activation aid in immune defence against *Mtb* through the release of the pro-inflammatory cytokines via the MyD88-dependent pathway in the healthier alveolar spaces of the lung, aiding in bacterial clearance. The absence of MyD88 in the caseum regions of granulomas, as opposed to its presence in the alveolar space, suggests that this signalling pathway may play a critical role in facilitating bacterial clearance through regulated inflammatory responses.

CHAPTER 6:

PART B: DISCUSSION

6. Discussion

TB remains one of the leading causes of death worldwide, infecting 10 million people annually (Choi et al., 2023; Migliori et al., 2021). Currently, the BCG vaccine is the only available preventative method against tuberculosis. However, research has shown that the effectiveness of BCG declines over time, particularly as individuals reach adulthood. This limitation has prompted research to develop more effective vaccines against tuberculosis (Choi et al., 2023). Although treatment for TB is currently available, for some individuals, the emergence of drug-resistant strains and an insufficient immune response make it difficult to eliminate TB (Choi et al., 2023). Our study investigates the potential of modulating TLR7- and TLR8-mediated immune responses for vaccine development against tuberculosis. TLRs play a critical role in recognising *Mtb* and are described to be the link between the innate and adaptive immune system. While much of the research on TLRs in TB has focused on TLRs 2, 4, 6 and 9 during *Mtb* infection, recent studies have reported the association of TLR7/8 with *Mtb* recognition, although TLR7/8 are primarily known for their recognition of viral single stranded RNA (ssRNA) (Davila et al., 2008). Here, we observed that targeting TLR7/8 with specific agonists led to a significant decrease in bacterial load during *Mtb* infection and an increase in the inflammatory immune response. Additionally, we found that TLR7/8 spatially associates with MyD88 and the pro-inflammatory cytokine IL-6 in the less diseased regions of resected TB lung tissue.

Agonists targeting TLR7 and TLR8 enhanced the immune response during *Mtb* infection, as demonstrated by increased levels of pro-inflammatory cytokines, including IL-6, IL-1β and TNF-α. To assess the impact of TLR modulation on the immune response during *Mtb* infection, a range of immunomodulatory agents targeting TLRs were screened. This was done by measuring the inflammatory response during TLR modulation in both uninfected THP-1 cells and THP-1 cells infected with *Mtb*. Upon ligand binding to TLR7/8, downstream signalling activates the NF-κB pathway, MAPK cascade, IFN regulatory factor (IRF)-1, and IRF-5. This leads to the production of inflammatory cytokines (Petes et al., 2017; To et al., 2019). This phenomenon is illustrated in Figure 5.1. a, d, and g, where uninfected THP-1 cells treated with TLR modulators show a marked increase in cytokine production, which was sustained in THP-1 cells infected with *Mtb*. The activation of TLRs by both TLR agonists and *Mtb* ligands triggers a potent inflammatory response through activation of the MyD88-dependent pathway. This ultimately promotes the migration of the transcription factor, NF-κB to the nucleus, resulting in enhanced production of pro-inflammatory cytokines (Mabrey et al., 2021).

The increased immune response observed in uninfected THP-1 cells stimulated with TLR7/8 agonists suggests that treatment with TLR7/8 agonists can enhance the innate immune response during infection, as these agonists promote the activation of TLR7 and TLR8 (Sun et al., 2022). During *Mtb* infection, treatment with TLR7/8 agonists, resiquimod, imiquimod and gardiquimod TFA also resulted in an increased release of pro-inflammatory cytokines compared to the untreated control. This indicates that treatment with TLR7/8 agonists induces a robust immune response, surpassing that of the untreated

control. Similarly, a study performed by Bender et al. (2020) demonstrated that activating TLR8 with agonists in whole blood led to a significant upregulation of pro-inflammatory cytokines, including IL-6, IL-1β and TNF-α. TLR7 activation in this study also resulted in increased expression of these cytokines, which aligns with our findings (Bender et al., 2020). Based on these results, we further investigated the effects of TLR modulation on bacterial clearance during *Mtb* infection using both TLR7/8 agonists and antagonists.

Agonists targeting TLR7 and/or TLR8, including resiquimod, vestalimod, TLRM, and motolimod, significantly reduced bacterial load during *Mtb* infection. THP-1 cells were treated with TLR7/8 agonists and antagonists before being infected with the luminescent H37Rv *Mtb* lux strain. The luminescence measured was directly correlated with the bacterial load. The results showed that agonists targeting TLR7 and TLR8, such as resiquimod, motolimod, TLRM and vesatolimod, significantly reduced the bacterial load compared to the untreated control. As previously mentioned, these agonists can increase inflammation, which enhances innate immunity and may lead to improved antimicrobial effects through the recruitment of immune cells (Hosseini et al., 2021). Additionally, TLR7 activation has been shown to enhance phagocytosis and autophagy, processes that could further contribute to bacterial load reduction by engulfing the bacteria (Bao et al., 2017). The activation of TLRs by agonists also triggers the release of free radicals, such as reactive oxygen species (ROS) and reactive nitrogen species (RNS), which generate oxidative stress on invading microbes and directly kill them (Li et al., 2019). Similarly, Lee *et al.* (2020) demonstrated that TLR7 agonist stimulation increased the elimination of intracellular *Mtb* through increased autophagy and upregulation of nitric oxide (NO) release (Lee et al., 2020). Moreover, Maserumule *et al.* (2022) showed that pharmacological activation of TLR8 with resiquimod increased bacterial killing in *Mtb*-infected mice, including those infected with MDR and XDR strains of *Mtb* (Maserumule et al., 2022). In another study performed by Tang *et al.* (2018), TLR8 activation in C57BL/6 mice enhanced immune defence against *Mtb* and notably induced the generation of central memory $CD8^+$ T cells post-vaccination (Tang et al., 2018). However, in our study, imiquimod unexpectedly showed results similar to the untreated control group over the 7-day period. This could be due to imiquimod selectively targeting only TLR7, whereas the other agonist target both TLR7 and TLR8 or TLR8 only. This may suggest that TLR8 plays a more prominent role in the bacterial clearance of *Mtb* compared to TLR7 alone.

Next, we analysed the effects of inhibiting TLRs using TLR1, 2, 3, 4, 7 and 8 antagonists on bacterial burden during *Mtb* infection. Unexpectedly, this led to a decrease in bacterial load, which may have been due to the antimicrobial properties of the antagonists or potential cellular cytotoxicity. Interestingly, inhibition of TLR4 with Atractylenolide I, a TLR4 antagonising agent, resulted in an increased bacterial load. This outcome is likely due to TLR4's crucial role in recognising *Mtb* components, including HSP 60 and 65 and 3- and 4-acylated lipomannan. This recognition activates a range of immune responses (Park et al., 2020). In a study by Park *et al*. (2020), C3 H/HeJ TLR4-

deficient mutant mice exhibited a significant increase in disease severity, with higher bacterial burden, significant weight reduction and necrotic lung inflammation following *Mtb* infection. The absence of TLR4 also weakened the Th1 immune response in these mice (Park et al., 2020). Atractylenolide I binds to a site on TLR4 that closely resembles the binding site for LPS and thus acts as a TLR4 antagonist (Huang et al., 2024). Therefore, the observed increased bacterial load upon treatment with Atractylenolide I is consistent with these findings.

CU-CPT-9a and CU-CPT-9b, used to inhibit TLR8, unexpectedly resulted in a significantly lower bacterial burden as compared to the untreated control. These inhibitory molecules prevent TLR8 activity by stabilizing its dimer form in a resting state. Studies have shown that CU-CPT-9a and CU-CPT-9b can reduce the release of pro-inflammatory cytokines and the expression of downstream proteins associated with TLR8 signalling, such as the NF-κB pathway, IRAK-4, TRAF-3 and TNF-α (Zhang et al., 2018). In our study, treatment with 40 μM of CU-CPT-9a or CU-CPT-9b also reduced the release of TNF-α and IL-6 during *Mtb* infection in THP-1 cells. This suggests that CU-CPT-9a and CU-CPT-9b effectively inhibit TLR 8 and that observed bacterial killing may be due to the antimicrobial properties of these compounds. Interestingly, CU-CPT-9a and CU-CPT-9b contain a quinoline group in their structure, which has been proven to have direct antimicrobial effects against *Mtb*, potentially explaining the significant decrease in bacterial burden in our study (Makafe et al., 2019). Therefore, CU-CPT-9a and CU-CPT-9b were not ideal molecules for evaluating the specific role of TLR 8 inhibition in modulating anti-mycobacterial effects in this context. On the other hand, stimulation of TLRs by *Mtb* cell wall components could induce a pro-inflammatory immune response. However, if not well regulated, this can lead to excessive inflammation, potentially compromising the effector functions of host cells (Lai & Gallo, 2008). Therefore, the addition of TLR antagonists could result in the reduction of this undesired inflammation, ultimately favouring bacterial clearance.

CU-CPT-8m, a specific TLR8 agonist, resulted in an overall lower trend in bacterial burden during *Mtb* infection in THP-1 cells. In a study by Zhang *et al*. (2018), CU-CPT-8m was characterised as a potent TLR8 inhibitor with low toxicity to cells. They also observed the suppression of pro-inflammatory cytokines release following TLR8 inhibition by CU-CPT-8m. In our study, we also observed a reduction in pro-inflammatory cytokines, which is consistent with their findings (Zhang et al., 2018). However, when testing our hypothesis regarding the effects of TLR8 inhibition on the bacterial burden during *Mtb* infection, we found that CU-CPT-8m was not an ideal candidate. This is because CU-CPT-8m, a pyrazolo[1,5a]pyrimidine derivative, is known to have anti-tubercular effects due to its ability to inhibit the FAB-I enzyme involved in the fatty acid synthesis of the mycobacterium cell wall (Modi et al., 2019). For this reason, CU-CPT-8m was not an ideal candidate for evaluating the effects of TLR8 inhibition in our study.

CU-CPT-22 is a specific TLR1/2 agonist that forms a heterodimer and recognises lipoproteins found on the cell wall of *Mtb* (Mortaz et al., 2015). A study targeting TLR1/2 with CU-CPT-22 demonstrated that treatment with this agent resulted in a decrease in the release of TNF-α and IL-1β (Cheng et al., 2012). This suppression of pro-inflammatory cytokines was also observed in our study, and interestingly, this effect was also witnessed during *Mtb* infection. This suggests that CU-CPT-22 indeed dampens the inflammatory immune response, and the reduction in bacterial burden may be attributed to its antimicrobial effects. Alternatively, this effect may be due to CU-CPT-22 preserving effector functions carried out by macrophages by reducing inflammation and potential undesired cell death. To our knowledge, there is no current literature exploring the antimicrobial effects of CU-CPT-22. Thus, future work could characterise the mechanisms underlying the anti-mycobacterial effects of this compound.

Chloroquine (diphosphate) and Hydroxychloroquine (sulfate) are both TLR and autophagy inhibitors that target TLR3, 7, 8, and 9 (In 'T Veld et al., 2021). We used these agents in our study to inhibit TLRs to determine their effects on bacterial burden. Interestingly, both drugs unexpectedly decreased bacterial load despite their inhibitory effects on TLRs. Chloroquine accumulates within the lysosome, where it increases the pH and renders the enzymatic activity of lysosomes and autophagosomes inactive (Halcrow et al., 2021). As it accumulates, chloroquine binds to nucleic acids, preventing them from binding to their respective TLRs (e.g., TLR3, 7, 8, and 9), resulting in TLR activation loss. Consequently, chloroquine downregulates the expression of downstream pro-inflammatory cytokines (In 'T Veld et al., 2021). However, this effect was not observed in our study, which may be due to variability in the control group or increased inflammation due to the cytotoxicity of chloroquine. In a study conducted by Crowle *et al*. (1990), treatment with chloroquine in human macrophages infected with *Mtb* led to a decreased bacterial burden at low concentrations. This is attributed to chloroquine's interaction with the nucleic acid synthesis of certain species of bacteria, disrupting their function (Crowle and May, 1990). Chloroquine's effects in decreasing the Mtb burden may also be due to its ability to reduce iron availability and its ability to interrupt the pathogen's nucleic acid synthesis (Crowle and May, 1990; Dechow and Abramovitch, 2024). Therefore, the use of chloroquine in our study was not ideal for evaluating whether inhibiting TLRs would affect bacterial load during *Mtb* infection.

Next, we analysed the effects of TLR modulation on the production of inflammatory cytokines in PBMCs using lower concentrations of agonists and antagonists. PBMCs were chosen because they represent a more diverse population of immune cells, providing a response that more closely resembles that of human patients, in contrast to the THP-1 cells, which are used primarily to study macrophage functions (Shah et al., 2022). Our results showed that targeting TLR7/8 with a concentration of 20 µM of TLR M led to an increased inflammatory immune response to *Mtb* on both days 3 and 5, compared to the untreated control. In contrast, inhibiting TLR 7/8 using antagonists such as Chloroquine (diphosphate) and CU-CPT-9a resulted in a significant reduction of proinflammatory cytokines

production, both when used individually and in combination. This suggests that activating TLR7/8 with agonists enhances the inflammatory immune response to *Mtb*, whereas inhibiting TLR7/8 with antagonists reduces this response below that of the untreated control. These findings imply that TLR7/8 plays a crucial role in the recognition and immune response against *Mtb*. Consequently, we further investigated the potential of TLR M as an adjunctive vaccine therapy.

Treatment with TLR M significantly reduced the bacterial load during *Mtb* infection in a 3D biomimetic model over 20 days. This model, which consists of PBMCs and a collagen-alginate matrix, was used to better replicate the *in vivo* environment. Inflammatory signals and immune cells are spatially organised *in vivo*, and this model supports prolonged cell survival while closely mimicking the characteristics of human lung tissue (Marakalala et al., 2016; Tezera et al., 2017). However, this setup has limitations because it does not fully encompass the cellular complexity of the events that occur within lung tissue (Huang et al., 2021). However, this 3D biomimetic model allowed us to gather insights that better reflect the inflammatory events occurring *in vivo* during *Mtb* infection and may also provide insight into parameters such as cell death, extracellular matrix destruction and bacterial control (Tezera et al., 2017). Our results suggested that TLR7/8 activation enhanced the anti-mycobacterial properties during *Mtb* infection, further supporting our *in vitro* findings, where TLR7/8 agonists also promoted bacterial clearance during *Mtb* infection. Notably, a study by Bao *et al*. (2017) demonstrated that TLR7 activation significantly reduced *Mtb* load during infection through increased autophagy in Raw 264.7 macrophages treated with ssRNA to stimulate TLR7 (Bao et al., 2017). Additionally, research by Delgado et al. (2008) showed that imiquimod, a TLR7 agonist, and ssRNA stimulation of TLR7 downregulated BCG survival via the MyD88 pathway in mouse macrophages during *Mtb* infection (Delgado et al., 2008). The results from our 3D biomimetic model were consistent with these findings, validating our analysis obtained from PBMCs.

We further examined the effects of TLR M on the expression of pro-inflammatory cytokines in the biomimetic 3D model, which closely mimics the lung environment. Treatment with TLR M reduced the expression of the pro-inflammatory cytokines, specifically IL-6 and IL-1β, during *Mtb* infection at both days 3 and 10 post-infection. This observation is in line with a study by To *et al*. (2019), where mice treated with the TLR agonist imiquimod (via intranasal and epicutaneous routes) during infection with influenza A virus showed reduced levels of IL-1β and IL-6, suppression in the migration of pro-inflammatory cell populations (such as neutrophils), and a decrease in the viral load. This resulted in a controlled inflammatory response and a reduction of the overall severity of the disease (To et al., 2019). A similar mechanism may likely be the cause of the reduction of pro-inflammatory cytokines in our study, as we observed a significant decrease in the bacterial load following TLR M treatment. Furthermore, MyD88 has the ability to downregulate the pro-inflammatory response induced by TLR signalling by selectively inhibiting the NF-κB pathway to prevent exacerbated inflammation and maintain homeostasis (Cervantes, 2017). This effect may have contributed to the decreased expression

of pro-inflammatory cytokines and a more controlled infection in our model. These findings were also reflected in our in vitro study with 40 μM of TLR M, which similarly influenced cytokine production.

Based on our findings regarding the involvement of TLR 7/8 during *Mtb* infection, we further examined how this signalling pathway is spatially associated with inflammation at the site of infection by examining lung tissue obtained from individuals who underwent lung resection treatment. Our results revealed that TLR7 and TLR8 were abundantly expressed in the alveolar space, specifically within pneumocytes and alveolar macrophages in the less diseased regions of the lungs. Furthermore, TLR7 and TLR8 co-localised with MyD88 and the pro-inflammatory cytokine IL-6 in the less diseased areas of the lung. These findings suggest that TLR7 and TLR8 activation play a crucial role in the immune defence against *Mtb* through the release of proinflammatory cytokines via the MyD88-dependent pathway in the healthier alveolar regions of the lung, ultimately suggesting that this pathway supports bacterial clearance. The activation of MyD88 leads to the activation of NF-κB, which induces the expression of pro-inflammatory cytokines, thus enhancing a Th1 immune response (Burkert and Schumann, 2020). This localised inflammation may aid in the recruitment of additional immune cells to the site of infection, such as dendritic cells, neutrophils, and lymphocytes. In turn, the outcome is an enhanced, effective immune response against infection. This further activates the adaptive immune system, further eliminating bacteria and combating infection (Sun et al., 2022).

In contrast, cells expressing TLR7 and TLR8 around the caseum, a hallmark of pathological damage, did not co-localise with MyD88 or IL-6. The absence of MyD88 in the caseum regions of the granulomas, as opposed to its presence in the alveolar spaces, suggests that this signalling pathway is critical in facilitating bacterial clearance through regulated inflammatory responses via TLR7/8 activation. The absence of MyD88 and low expression of TLR 7/8 in this area may lead to ineffective bacterial clearance and persistent infection, potentially leading to necrosis and exacerbated inflammation and pathology (Scanga et al., 2004; Sugawara et al., 2003). Similarly, a study conducted by Scanga *et al*. (2004) found that Myd88-deficient mice exhibited a higher bacterial load, as shown by acid-fast-stained lung tissue as well as higher colony-forming units (CFUs) compared to wild-type mice infected with H37Rv *Mtb* (Scanga et al., 2004). These Myd88-deficient mice had a survival time of 42 days, compared to over 180 days in wild-type mice. Moreover, they developed more severe granulomatous inflammation, which became more pronounced by week 5 (Scanga et al., 2004). In another study by Sugawara *et al*. (2003), MyD88 knockout mice sustained granulomas with increased neutrophil infiltration compared to wild-type mice and exhibited more advanced pulmonary lesions compared to wild-type mice, along with higher CFU counts (Sugawara et al., 2003). These findings suggest that the absence of MyD88 in the more diseased regions of the lung in our study likely contributes to decreased bacterial clearance. The activity of TLR7 and TLR8 depends on MyD88, the TLR adaptor protein, and its absence within the caseum halts the downstream activity of these TLRs, resulting in increased bacterial load and potentially contributing to pathology and advanced stages of

tuberculosis (Cervantes, 2017; Scanga et al., 2004). Thus, TLR 7/8 signalling through MyD88 is not only critical for initiating the innate immune response but is also essential for maintaining granuloma integrity, preventing excessive necrosis, and controlling bacterial spread via regulated inflammatory response.

Several studies have shown that polymorphisms in the TLR8 gene are associated with increased susceptibility to pulmonary tuberculosis, particularly among males (Wang et al., 2018). This correlation has been observed in various populations, including cohorts from Russia, Indonesia, Turkey, China (Han population), Sudan, Pakistan, and South Africa (Bukhari et al., 2015; Davila et al., 2008; Salie et al., 2015; Wang et al., 2018). A PCR study also revealed significantly upregulated expression of the TLR8 gene during *Mtb* infection in THP-1 macrophages, further highlighting the importance of TLR8 in *Mtb* infection (Davila et al., 2008). These findings underscore the critical role of the innate immune system and immune sensing in modulating the host's immune response, initiating the adaptive immune system, and serving as the first line of defence in infection (Davila et al., 2008). An enhanced innate immune response, particularly in the initial stages of infection, promotes bacterial clearance and reduces the likelihood of acquiring excessive pathology (Sun et al., 2022).

Overall, our study demonstrates that TLR7 and TLR8, along with the adapter protein MyD88 and the inflammatory cytokine IL-6, are localised in the less diseased regions of the lung, specifically in pneumocytes and alveolar macrophages. This localisation contributes to TLR7/8-mediated inflammatory signalling through the Myd88 pathway. TLR7/8 signalling via TLR M resulted in increased *Mtb* clearance and enhanced inflammatory responses during *Mtb* infection. Therefore, TLR7/8 modulatory agents, specifically TLR M, may serve as adjunctive strategies, enhancing immune responses and improving vaccine efficacy. One notable characteristic during *Mtb* is a delayed Th1 response. However, agonists of TLR7/8 enhance macrophage activation, initiating a Th1 response, relaying signals to APCs, and activating the adaptive immune response. Thus, TLR M may be beneficial in overcoming the slow and inefficient immune response during *Mtb* infection.

Conclusion

In conclusion, targeting TLR7/8 signalling represents a promising therapeutic approach to modulate immune responses and improve outcomes in *Mtb* infection, particularly in cases where the immune response is insufficient. Our study highlights the potential of TLR7/8 agonists in enhancing bacterial clearance and promoting controlled inflammation during *Mtb* infection. Future research should explore the full potential of TLR7/8 agonists, both as stand-alone treatments and as adjuncts to current vaccine strategies, with the aim of developing more effective therapies and vaccines against tuberculosis. Agonists of TLR7/8 enhance macrophage activation and promote a Th1 response via NF-κB, thereby improving antigen presentation and activating the adaptive immune system (Sun et al., 2022).

Future work

Future studies could include evaluating the safety and efficacy of TLR M using cytotoxic assays and the Griess reagent assay to measure NO production. Additionally, the effects of TLR M could be evaluated in conjunction with currently approved TB drugs and in BCG-vaccinated PBMCs from human donors to assess the potential for synergistic effects. Moreover, the impact of inhibiting TLR7/8 on bacterial clearance should be examined using more clinically relevant drugs. Lastly, the efficacy of TLR M treatment should be evaluated in mouse models before progressing to *in vivo* human studies.

CHAPTER 7:

REFERENCES

References

Ahmed, A., Rakshit, S., Vyakarnam, A., 2016. HIV-TB co-infection: Mechanisms that drive reactivation of Mycobacterium tuberculosis in HIV infection. Oral Dis 22, 53–60. https://doi.org/10.1111/odi.12390

Alsayed, S.S.R., Gunosewoyo, H., 2023. Tuberculosis: Pathogenesis, Current Treatment Regimens and New Drug Targets. Int J Mol Sci. https://doi.org/10.3390/ijms24065202

Arinaminpathy Id, N., Diul, Y., Id, M., Bloom, A., Vincent, C., Ahmedovid, S., 2023. Meeting the 2030 END TB goals in the wake of COVID-19: A modelling study of countries in the USAID TB portfolio. https://doi.org/10.1371/journal.pgph.0001271

Bagnasco, D., Ferrando, M., Varricchi, G., Puggioni, F., Passalacqua, G., Canonica, G.W., 2017. Anti-Interleukin 5 (IL-5) and IL-5Ra biological drugs: Efficacy, safety, and future perspectives in severe eosinophilic asthma. Front Med (Lausanne). https://doi.org/10.3389/fmed.2017.00135

Bao, M., Yi, Z., Fu, Y., 2017. Activation of TLR7 Inhibition of Mycobacterium Tuberculosis Survival by Autophagy in RAW 264.7 Macrophages. J Cell Biochem 118, 4222–4229. https://doi.org/10.1002/jcb.26072

Baykan, A.H., Sayiner, H.S., Aydin, E., Koc, M., Inan, I., Erturk, S.M., 2022. Extrapulmonary tuberculosıs: an old but resurgent problem. Insights Imaging. https://doi.org/10.1186/s13244-022-01172-0

Behar, S.M., Martin, C.J., Booty, M.G., Nishimura, T., Zhao, X., Gan, H.X., Divangahi, M., Remold, H.G., 2011. Apoptosis is an innate defense function of macrophages against Mycobacterium tuberculosis. Mucosal Immunol. https://doi.org/10.1038/mi.2011.3

Belton, M., Brilha, S., Manavaki, R., Mauri, F., Nijran, K., Hong, Y.T., Patel, N.H., Dembek, M., Tezera, L., Green, J., Moores, R., Aigbirhio, F., Al-Nahhas, A., Fryer, T.D., Elkington, P.T., Friedland, J.S., 2016. Hypoxia and tissue destruction in pulmonary TB. Thorax 71, 1145–1153. https://doi.org/10.1136/thoraxjnl-2015-207402

Bender, A.T., Tzvetkov, E., Pereira, A., Wu, Y., Kasar, S., Przetak, M.M., Vlach, J., Niewold, T.B., Jensen, M.A., Okitsu, S.L., 2020. TLR7 and TLR8 Differentially Activate the IRF and NF-κB Pathways in Specific Cell Types to Promote Inflammation. Immunohorizons 4, 93–107. https://doi.org/10.4049/immunohorizons.2000002

Bendre, A.D., Peters, P.J., Kumar, J., 2021. Tuberculosis: Past, present and future of the treatment and drug discovery research. Current Research in Pharmacology and Drug Discovery. https://doi.org/10.1016/j.crphar.2021.100037

Blanchard, C., Rothenberg, M.E., 2009. Chapter 3 Biology of the Eosinophil. Adv Immunol. https://doi.org/10.1016/S0065-2776(08)01003-1

Bohrer, A.C., Castro, E., Hu, Z., Queiroz, A.T.L., Tocheny, C.E., Assmann, M., Sakai, S., Nelson, C., Baker, P.J., Ma, H., Wang, L., Zilu, W., du Bruyn, E., Riou, C., Kauffman, K.D., Program, T.I., Moore, I.N., Nonno, F. Del, Petrone, L., Goletti, D., Martineau, A.R., Lowe, D.M., Cronan, M.R., Wilkinson, R.J., Barry, C.E., Via, L.E., Barber, D.L., Klion, A.D., Andrade, B.B., Song, Y., Wong, K.W., Mayer-Barber, K.D., 2021. Eosinophils are part of the

granulocyte response in tuberculosis and promote host resistance in mice. Journal of Experimental Medicine 218. https://doi.org/10.1084/jem.20210469

Bohrer, A.C., Castro, E., Tocheny, C.E., Assmann, M., Schwarz, B., Bohrnsen, E., Makiya, M.A., Legrand, F., Hilligan, K.L., Baker, P.J., Torres-Juarez, F., Hu, Z., Ma, H., Wang, L., Niu, L., Wen, Z., Lee, S.H., Kamenyeva, O., Kauffman, K.D., Donato, M., Sher, A., Barber, D.L., Via, L.E., Scriba, T.J., Khatri, P., Song, Y., Wong, K.W., Bosio, C.M., Klion, A.D., Mayer-Barber, K.D., 2022. Rapid GPR183-mediated recruitment of eosinophils to the lung after Mycobacterium tuberculosis infection. Cell Rep 40, 111144. https://doi.org/10.1016/J.CELREP.2022.111144

Bruchfeld, J., Correia-Neves, M., Kallenius, G., 2015. Tuberculosis and HIV coinfection. Cold Spring Harb Perspect Med 5. https://doi.org/10.1101/cshperspect.a017871

Bukhari, M., Aslam, M.A., Khan, A., Iram, Q., Akbar, A., Naz, A.G., Ahmad, S., Ahmad, M.M., Ashfaq, U.A., Aziz, H., Ali, M., 2015. TLR8 gene polymorphism and association in bacterial load in southern Punjab of Pakistan: An association study with pulmonary tuberculosis. Int J Immunogenet 42, 46–51. https://doi.org/10.1111/iji.12170

Burkert, S., Schumann, R.R., 2020. RNA sensing of mycobacterium tuberculosis and its impact on TB vaccination strategies. Vaccines (Basel). https://doi.org/10.3390/vaccines8010067

Carranza, C., Pedraza-Sanchez, S., de Oyarzabal-Mendez, E., Torres, M., 2020. Diagnosis for Latent Tuberculosis Infection: New Alternatives. Front Immunol. https://doi.org/10.3389/fimmu.2020.02006

Castro, A., Esaguy, N., Macedo, P.M., Aguas, A.P., Silva, M.T., 1991. Live but Not Heat-Killed Mycobacteria Cause Rapid Chemotaxis of Large Numbers of Eosinophils In Vivo and Are Ingested by the Attracted Granulocytes, INFECTION AND IMMUNITY, 3009-14. https://doi:10.1128/iai.59.9.3009-3014.1991

Cervantes, J.L., 2017. MyD88 in Mycobacterium tuberculosis infection. Med Microbiol Immunol. https://doi.org/10.1007/s00430-017-0495-0

Chandra, A., Agrawal, B., Ahirwar, D.K., Yadav, L., 2024. Quinoxaline: Synthetic and pharmacological perspectives. International Journal of Pharmaceutical Research and Development 6, 25–31. https://doi.org/10.33545/26646862.2024.v6.i1a.40

Chandra, P., Grigsby, S.J., Philips, J.A., 2022. Immune evasion and provocation by Mycobacterium tuberculosis. Nat Rev Microbiol. https://doi.org/10.1038/s41579-022-00763-4

Cheng, K., Wang, X., Zhang, S., Yin, H., 2012. Discovery of small-molecule inhibitors of the TLR1/TLR2 complex. Angewandte Chemie - International Edition 51, 12246–12249. https://doi.org/10.1002/anie.201204910

Choi, G.H., Woong Kwon, K., Jae Shin, S., 2023. Importance of adjuvant selection in tuberculosis vaccine development: Exploring basic mechanisms and clinical implications. Vaccine X 15, 100400. https://doi.org/10.1016/J.JVACX.2023.100400

Cronan, M.R., 2022. In the Thick of It: Formation of the Tuberculous Granuloma and Its Effects on Host and Therapeutic Responses. Front Immunol. https://doi.org/10.3389/fimmu.2022.820134

Crowle, A.J., May, M.H., 1990. Inhibition of Tubercle Bacilli in Cultured Human Macrophages by Chloroquine Used Alone and in Combination with Streptomycin, Isoniazid, Pyrazinamide, and Two Metabolites of Vitamin D3.Antimicrob Agents Chemother. https://doi:10.1128/AAC.34.11.2217

Cubillos-Angulo, J.M., Nogueira, B.M.F., Arriaga, M.B., Barreto-Duarte, B., Araújo-Pereira, M., Fernandes, C.D., Vinhaes, C.L., Villalva-Serra, K., Nunes, V.M., Miguez-Pinto, J.P., Amaral, E.P., Andrade, B.B., 2022. Host-directed therapies in pulmonary tuberculosis: Updates on anti-inflammatory drugs. Front Med (Lausanne). https://doi.org/10.3389/fmed.2022.970408

Davila, S., Hibberd, M.L., Dass, R.H., Wong, H.E.E., Sahiratmadja, E., Bonnard, C., Alisjahbana, B., Szeszko, J.S., Balabanova, Y., Drobniewski, F., Van Crevel, R., Van De Vosse, E., Nejentsev, S., Ottenhoff, T.H.M., Seielstad, M., 2008. Genetic association and expression studies indicate a role of Toll-like receptor 8 in pulmonary tuberculosis. PLoS Genet 4. https://doi.org/10.1371/journal.pgen.1000218

De Francesco Daher, E., Da Silva, G.B., Guardão Barros, E.J., 2013. Review: Renal tuberculosis in the modern era. American Journal of Tropical Medicine and Hygiene. https://doi.org/10.4269/ajtmh.2013.12-0413

Dechow, S.J., Abramovitch, R.B., 2024. Targeting Mycobacterium tuberculosis pH-driven adaptation. Microbiology (N Y) 170, 001458. https://doi.org/10.1099/MIC.0.001458

Delgado, M.A., Elmaoued, R.A., Davis, A.S., Kyei, G., Deretic, V., 2008. Toll-like receptors control autophagy. EMBO Journal 27, 1110–1121. https://doi.org/10.1038/emboj.2008.31

Divangahi, M., Khan, N., Kaufmann, E., 2018. Beyond Killing Mycobacterium tuberculosis: Disease Tolerance. Front Immunol. https://doi.org/10.3389/fimmu.2018.02976

Drain, P.K., Bajema, K.L., Dowdy, D., Dheda, K., Naidoo, K., Schumacher, S.G., Ma, S., Meermeier, E., Lewinsohn, D.M., Sherman, D.R., 2018. Incipient and Subclinical Tuberculosis: a Clinical Review of Early Stages and Progression of Infection. https://doi:10.1128/CMR.00021-18

Dulberger, C.L., Rubin, E.J., Boutte, C.C., 2020. The mycobacterial cell envelope — a moving target. Nat Rev Microbiol. https://doi.org/10.1038/s41579-019-0273-7

Elena-Pérez, S., Heredero-Jung, D.H., García-Sánchez, A., Estravís, M., Martin, M.J., Ramos-González, J., Triviño, J.C., Isidoro-García, M., Sanz, C., Dávila, I., 2021. Molecular Analysis of IL-5 Receptor Subunit Alpha as a Possible Pharmacogenetic Biomarker in Asthma. Front Med (Lausanne) 7. https://doi.org/10.3389/fmed.2020.624576

Essone, P.N., Leboueny, M., Maloupazoa Siawaya, A.C., Alame-Emane, A.K., Aboumegone Biyogo, O.C., Dapnet Tadatsin, P.H., Mveang Nzoghe, A., Essamazokou, D.U., Mvoundza Ndjindji, O., Padzys, G.S., Agnandji, S.T., Takiff, H., Gicquel, B., Djoba Siawaya, J.F., 2019. M. tuberculosis infection and antigen specific cytokine response in healthcare workers frequently exposed to tuberculosis. Sci Rep 9. https://doi.org/10.1038/s41598-019-44294-0

Gaur, P., Zaffran, I., George, T., Rahimli Alekberli, F., Ben-Zimra, M., Levi-Schaffer, F., 2022. The regulatory role of eosinophils in viral, bacterial, and fungal infections. Clin Exp Immunol. https://doi.org/10.1093/cei/uxac038

Ghazaei, C., 2018. Mycobacterium tuberculosis and lipids: Insights into molecular mechanisms from persistence to virulence. Journal of Research in Medical Sciences. https://doi.org/10.4103/jrms.JRMS_904_17

Glick, D., Barth, S., Macleod, K.F., 2010. Autophagy: Cellular and molecular mechanisms. Journal of Pathology. https://doi.org/10.1002/path.2697

Goletti, D., Al-Abri, S., Battista Migliori, G., Lindestam Arlehamn, C., Haldar, P., Sundling, C., da Costa, C., Wang To, K., Martineau, A.R., Petersen, E., Zumla, A., Shan Lee, S., 2024. World Tuberculosis Day 2024 theme “Yes! We can end TB” can be made a reality through concerted global efforts that advance detection, diagnosis, and treatment of tuberculosis infection and disease. https://doi.org/10.1016/j.ijid.2024.106993

Gupta, M., Lobo, F.D., Adiga, D.S.A., Gupta, A., 2016. A histomorphological pattern analysis of pulmonary tuberculosis in lung autopsy and surgically resected specimens. Patholog Res Int 2016. https://doi.org/10.1155/2016/8132741

Gygli, S.M., Borrell, S., Trauner, A., Gagneux, S., 2017. Antimicrobial resistance in Mycobacterium tuberculosis: Mechanistic and evolutionary perspectives. FEMS Microbiol Rev. https://doi.org/10.1093/femsre/fux011

Halcrow, P.W., Geiger, J.D., Chen, X., 2021. Overcoming Chemoresistance: Altering pH of Cellular Compartments by Chloroquine and Hydroxychloroquine. Front Cell Dev Biol. https://doi.org/10.3389/fcell.2021.627639

Hamid, Q., Barkans, J., Meng, Q., Ying, S., Abrams, J.S., Kay, A.B., Moqbel, R., 1992. Human Eosinophils Synthesize and Secrete Interleukin-6, In Vitro, Blood. 80(6), 1496–1501. https://doi.org/10.1182/blood.V80.6.1496.1496

Hawn, T.R., Matheson, A.I., Maley, S.N., Vandal, O., 2013. Host-Directed Therapeutics for Tuberculosis: Can We Harness the Host? Microbiology and Molecular Biology Reviews 77, 608–627. https://doi.org/10.1128/mmbr.00032-13

Hayford, F.E.A., Dolman, R.C., Blaauw, R., Nienaber, A., Smuts, C.M., Malan, L., Ricci, C., 2020. The effects of anti-inflammatory agents as host-directed adjunct treatment of tuberculosis in humans: a systematic review and meta-analysis. Respir Res. https://doi.org/10.1186/s12931-020-01488-9

Hosseini, R., Lamers, G.E.M., Bos, E., Pancras, &, Hogendoorn, C.W., Koster, A.J., Meijer, A.H., Spaink, H.P., Schaaf, M.J.M., 2021. The adapter protein Myd88 plays an important role in limiting mycobacterial growth in a zebrafish model for tuberculosis. https://doi:10.1007/s00428-021-03043-3

Hsu, D., Irfan, M., Jabeen, K., Iqbal, N., Hasan, R., Migliori, G.B., Zumla, A., Visca, D., Centis, R., Tiberi, S., 2020. Post tuberculosis treatment infectious complications. International Journal of Infectious Diseases 92, S41–S45. https://doi.org/10.1016/j.ijid.2020.02.032

Huang, X., Lowrie, D.B., Fan, X.Y., Hu, Z., 2024. Natural products in anti-tuberculosis host-directed therapy. Biomedicine and Pharmacotherapy. https://doi.org/10.1016/j.biopha.2023.116087

Huang, Y., Huang, Z., Tang, Z., Chen, Y., Huang, M., Liu, H., Huang, W., Ye, Q., Jia, B., 2021. Research Progress, Challenges, and Breakthroughs of Organoids as Disease Models. Front Cell Dev Biol. https://doi.org/10.3389/fcell.2021.740574

Hunter, R.L., 2011. Pathology of post primary tuberculosis of the lung: An illustrated critical review. Tuberculosis. https://doi.org/10.1016/j.tube.2011.03.007

Im, K., Mareninov, S., Diaz, M.F.P., Yong, W.H., 2019. An introduction to performing immunofluorescence staining, in: Methods in Molecular Biology. Humana Press Inc., pp. 299–311. https://doi.org/10.1007/978-1-4939-8935-5_26

In 'T Veld, A.E., Jansen, M.A.A., Ciere, L.C.A., Moerland, M., 2021. Hydroxychloroquine Effects on TLR Signalling: Underexposed but Unneglectable in COVID-19. J Immunol Res. https://doi.org/10.1155/2021/6659410

Jacobo-Delgado, Y.M., Rodríguez-Carlos, A., Serrano, C.J., Rivas-Santiago, B., 2023. Mycobacterium tuberculosis cell-wall and antimicrobial peptides: a mission impossible? Front Immunol. https://doi.org/10.3389/fimmu.2023.1194923

Jeong, E.K., Lee, H.J., Jung, Y.J., 2022. Host-Directed Therapies for Tuberculosis. Pathogens. https://doi.org/10.3390/pathogens11111291

Kasprowicz, V.O., Achkar, J.M., Wilson, D., 2011. The tuberculosis and HIV epidemic in South Africa and the kwazulu-natal research institute for tuberculosis and HIV. Journal of Infectious Diseases. https://doi.org/10.1093/infdis/jir414

Kayongo, A., Nyiro, B., Siddharthan, T., Kirenga, B., Checkley, W., Lutaakome Joloba, M., Ellner, J., Salgame, P., 2023. Mechanisms of lung damage in tuberculosis: implications for chronic obstructive pulmonary disease. Front Cell Infect Microbiol. https://doi.org/10.3389/fcimb.2023.1146571

Khandelia, P., Yadav, S., Singh, P., 2023. An overview of the BCG vaccine and its future scope. Indian Journal of Tuberculosis. https://doi.org/10.1016/j.ijtb.2023.05.012

Khatun, A., Sakurai, M., Sakai, Y., Tachibana, M., Ohara, N., Morimoto, M., 2018. Mycobacterial infection induces eosinophilia and production of α-defensin by eosinophils in mice. J Vet Med Sci 81, 138. https://doi.org/10.1292/JVMS.18-0619

Kilinç, G., Saris, A., Ottenhoff, T.H.M., Haks, M.C., 2021. Host-directed therapy to combat mycobacterial infections*. Immunol Rev. https://doi.org/10.1111/imr.12951

Kim, H.Y., Cho, J.G., Akkerman, O.W., Padanilam, X., Seaworth, B., Alffenaar, J.W.C., 2021. Anti-Tuberculosis Drugs and Adverse Events, in: Essential Tuberculosis. Springer International Publishing, pp. 121–129. https://doi.org/10.1007/978-3-030-66703-0_13

Krug, S., Parveen, S., Bishai, W.R., 2021. Host-Directed Therapies: Modulating Inflammation to Treat Tuberculosis. Front Immunol 12, 660916–660916. https://doi.org/10.3389/FIMMU.2021.660916/PDF

Lai, Y., Gallo, R.L., n.d. Toll-like receptors in skin infectious and inflammatory diseases.Infectious disorders drug targets, 8(3), 144–155. https://doi.org/10.2174/1871526510808030144

Lanzafame, M., Vento, S., 2016. Tuberculosis-immune reconstitution inflammatory syndrome. J Clin Tuberc Other Mycobact Dis. https://doi.org/10.1016/j.jctube.2016.03.002

Lee, H.J., Kang, S.J., Woo, Y., Hahn, T.W., Ko, H.J., Jung, Y.J., 2020. TLR7 Stimulation With Imiquimod Induces Selective Autophagy and Controls Mycobacterium tuberculosis Growth in Mouse Macrophages. Front Microbiol 11. https://doi.org/10.3389/fmicb.2020.01684

Lee, J.J., Mcgarry, M.P., Farmer, S.C., Denzler, K.L., Larson, K.A., Carrigan, P.E., Brenneise, I.E., Horton, M.A., Haczku, A., Gelfand, E.W., Leikauf, G.D., Lee, N.A., 1997. Interleukin-5 Expression in the Lung Epithelium of Transgenic Mice Leads to Pulmonary Changes Pathognomonic of Asthma. The Journal of experimental medicine, 185(12), 2143–2156. https://doi.org/10.1084/jem.185.12.2143

Leonard, J.M., 2017. Central Nervous System Tuberculosis. Microbiol Spectr 5. https://doi.org/10.1128/microbiolspec.TNMI7-0044-2017

Levine, B., Mizushima, N., Virgin, H.W., 2011. Autophagy in immunity and inflammation. Nature. https://doi.org/10.1038/nature09782

Li, W., Zhou, Z., Zhou, X., Khoo, B.L., Gunawan, R., Chin, Y.R., Zhang, L., Yi, C., Guan, X., Yang, M., 2023. 3D Biomimetic Models to Reconstitute Tumor Microenvironment In Vitro: Spheroids, Organoids, and Tumor-on-a-Chip. Adv Healthc Mater 12, 2202609. https://doi.org/10.1002/ADHM.202202609

Li, Y., Deng, S.L., Lian, Z.X., Yu, K., 2019. Roles of toll-like receptors in nitroxidative stress in mammals. Cells 8. https://doi.org/10.3390/cells8060576

Liu, T., Huang, T., Li, J., Li, A., Li, C., Huang, X., Li, D., Wang, S., Liang, M., 2023. Optimization of differentiation and transcriptomic profile of THP-1 cells into macrophage by PMA. PLoS One 18. https://doi.org/10.1371/journal.pone.0286056

Loddenkemper, R., Lipman, M., Zumla, A., 2016. Clinical aspects of adult tuberculosis. Cold Spring Harb Perspect Med 6. https://doi.org/10.1101/cshperspect.a017848

Mabrey, F.L., Morrell, E.D., Wurfel, M.M., 2021. TLRs in COVID-19: How they drive immunopathology and the rationale for modulation. Innate Immun. https://doi.org/10.1177/17534259211051364

Maitra, A., Bates, S.D.S., Shaik, M., Evangelopoulos, Di., Abubakar, I., McHugh, T.D., Lipman, M., Bhakta, S., 2016. Repurposing drugs for treatment of tuberculosis: A role for non-steroidal anti-inflammatory drugs. Br Med Bull 118, 138–148. https://doi.org/10.1093/bmb/ldw019

Makafe, G.G., Hussain, M., Surineni, G., Tan, Y., Wong, N.K., Julius, M., Liu, L., Gift, C., Jiang, H., Tang, Y., Liu, Jianxiong, Tan, S., Yu, Z., Liu, Z., Lu, Z., Fang, C., Zhou, Y., Zhang, J., Zhu, Q., Liu, Jinsong, Zhang, T., 2019. Quinoline Derivatives Kill Mycobacterium tuberculosis by Activating Glutamate Kinase. Cell Chem Biol 26, 1187-1194.e5. https://doi.org/10.1016/J.CHEMBIOL.2019.05.003

Marakalala, M.J., Raju, R.M., Sharma, K., Zhang, Y.J., Eugenin, E.A., Prideaux, B., Daudelin, I.B., Chen, P.Y., Booty, M.G., Kim, J.H., Eum, S.Y., Via, L.E., Behar, S.M., Barry, C.E., Mann, M., Dartois, V., Rubin, E.J., 2016. Inflammatory signaling in human tuberculosis granulomas is spatially organized. Nat Med 22, 531–538. https://doi.org/10.1038/nm.4073

Maranatha, D., Bahri, S., 2020. Tuberculous pyopneumothorax as a complication of inadequate treatment in active pulmonary tuberculosis: A case report. J Pure Appl Microbiol 14, 1115–1120. https://doi.org/10.22207/JPAM.14.2.05

Martin, C.J., Booty, M.G., Rosebrock, T.R., Nunes-Alves, C., Desjardins, D.M., Keren, I., Fortune, S.M., Remold, H.G., Behar, S.M., 2012. Efferocytosis is an innate antibacterial mechanism. Cell Host Microbe 12, 289–300. https://doi.org/10.1016/j.chom.2012.06.010

Maserumule, C., Passemar, C., Oh, O.S.H., Hegyi, K., Brown, K., Weimann, A., Dinan, A., Davila, S., Klapholz, C., Bryant, J., Verma, D., Gadwa, J., Krishnananthasivam, S., Vongtongsalee, K., Kendall, E., Trelles, A., Hibberd, M.L., Prados-Rosales, R., Andi, K., Kumar, S.S., Ordway, D., MacAry, P.A., Floto, R.A., 2022. Phagosomal RNA sensing through TLR8 controls susceptibility to tuberculosis. https://doi.org/10.1101/2022.06.14.496072

Matteucci, K.C., Correa, A.A.S., Costa, D.L., 2022. Recent Advances in Host-Directed Therapies for Tuberculosis and Malaria. Front Cell Infect Microbiol. https://doi.org/10.3389/fcimb.2022.905278

Migliori, G.B., Ong, C.W.M., Petrone, L., D'ambrosio, L., Centis, R., Goletti, D., 2021. The definition of tuberculosis infection based on the spectrum of tuberculosis disease. Breathe. https://doi.org/10.1183/20734735.0079-2021

Modi, P., Patel, S., Chhabria, M., 2019. Structure-based design, synthesis and biological evaluation of a newer series of pyrazolo[1,5-a]pyrimidine analogues as potential anti-tubercular agents. Bioorg Chem 87, 240–251. https://doi.org/10.1016/j.bioorg.2019.02.044

Moideen, K., Kumar, N.P., Nair, D., Banurekha, V. V, Bethunaickan, R., Babu, S., 2018. Heightened Systemic Levels of Neutrophil and Eosinophil Granular Proteins in Pulmonary Tuberculosis and Reversal following Treatment. Infection and immunity, 86(6), e00008-18. https://doi.org/10.1128/IAI.00008-18

Morokata, T., Ida, K., Yamada, T., 2002. Characterization of YM-90709 as a novel antagonist which inhibits the binding of interleukin-5 to interleukin-5 receptor. International immunopharmacology, 2(12), 1693–1702. https://doi.org/10.1016/s1567-5769(02)00191-1

Mortaz, E., Adcock, I.M., Tabarsi, P., Masjedi, M.R., Mansouri, D., Velayati, A.A., Casanova, J.L., Barnes, P.J., 2015. Interaction of Pattern Recognition Receptors with Mycobacterium Tuberculosis. J Clin Immunol 35, 1–10. https://doi.org/10.1007/s10875-014-0103-7

Moule, M.G., Cirillo, J.D., 2020. Mycobacterium tuberculosis Dissemination Plays a Critical Role in Pathogenesis. Front Cell Infect Microbiol. https://doi.org/10.3389/fcimb.2020.00065

Ndlovu, H., Marakalala, M.J., 2016. Granulomas and inflammation: Host-directed therapies for tuberculosis. Front Immunol. https://doi.org/10.3389/fimmu.2016.00434

Nigam, A., Mukherjee, U., Verma, M., 2022. Global Impact of Tuberculosis and HIV coinfection. Microsphere 1, 82–88. https://doi.org/10.59118/jsst1347

Nuwagira, E., Baluku, J.B., Meya, D.B., Philpotts, L.L., Siedner, M.J., Bajunirwe, F., Mpagama, S.G., Lai, P.S., 2022. Burden, clinical features and outcomes of post-tuberculosis lung disease in sub-Saharan Africa: A protocol for a systematic review and meta-analysis. BMJ Open. https://doi.org/10.1136/bmjopen-2022-062260

Olive, A.J., Sassetti, C.M., 2018. Tolerating the unwelcome guest; How the host withstands persistent Mycobacterium tuberculosis. Front Immunol. https://doi.org/10.3389/fimmu.2018.02094

Ou, Y., Yang, Z., Zhou, Y., Yue, H., Hua, L., Liu, Z., Lin, G., Cai, H., Chen, Y., Hu, W., Sun, P., 2024. Antagonizing interleukin-5 receptor ameliorates dextran sulfate sodium-induced experimental colitis in mice through reducing NLRP3 inflammasome activation. Eur J Pharmacol 965. https://doi.org/10.1016/j.ejphar.2024.176331

Palos, I., Luna-Herrera, J., Lara-Ramírez, E.E., Loera-Piedra, A., Fernández-Ramírez, E., Guadalupe Aguilera-Arreola, M., Paz-González, A.D., Monge, A., Wan, B., Franzblau, S., Rivera, G., 2018. Anti-mycobacterium tuberculosis activity of esters of quinoxaline 1,4-Di-N-oxide. Molecules 23. https://doi.org/10.3390/molecules23061453

Park, J., Kim, H., Kwon, K.W., Choi, H.H., Kang, S.M., Hong, J.J., Shin, S.J., 2020. Toll-like receptor 4 signaling-mediated responses are critically engaged in optimal host protection against highly virulent Mycobacterium tuberculosis K infection. Virulence 11, 430–445. https://doi.org/10.1080/21505594.2020.1766401

Pelaia, C., Paoletti, G., Puggioni, F., Racca, F., Pelaia, G., Canonica, G.W., Heffler, E., 2019. Interleukin-5 in the Pathophysiology of Severe Asthma. Front Physiol. https://doi.org/10.3389/fphys.2019.01514

Petes, C., Odoardi, N., Gee, K., 2017. The Toll for trafficking: Toll-like receptor 7 delivery to the endosome. Front Immunol. https://doi.org/10.3389/fimmu.2017.01075

Pooranagangadevi, N., Padmapriyadarsini, C., 2022. Treatment of Tuberculosis and the Drug Interactions Associated With HIV-TB Co-Infection Treatment. Frontiers in Tropical Diseases. https://doi.org/10.3389/fitd.2022.834013

Prakash Babu, S., Narasimhan, P.B., Babu, S., 2019. Eosinophil Polymorphonuclear Leukocytes in TB: What We Know so Far. Front Immunol. https://doi.org/10.3389/fimmu.2019.02639

Rahlwes, K.C., Dias, B.R.S., Campos, P.C., Alvarez-Arguedas, S., Shiloh, M.U., 2023. Pathogenicity and virulence of Mycobacterium tuberculosis. Virulence. https://doi.org/10.1080/21505594.2022.2150449

Ramalingam, P., Ganapaty, S., Rao, C.B., 2010. In vitro antitubercular and antimicrobial activities of 1-substituted quinoxaline-2,3(1H,4H)-diones. Bioorg Med Chem Lett 20, 406–408. https://doi.org/10.1016/j.bmcl.2009.10.026

Raphoko, L.A., Lekgau, K., Lebepe, C.M., Leboho, T.C., Matsebatlela, T.M., Nxumalo, W., 2021. Synthesis of novel quinoxaline-alkynyl derivatives and their anti-Mycobacterium tuberculosis activity. Bioorg Med Chem Lett 35. https://doi.org/10.1016/j.bmcl.2021.127784

Ravimohan, S., Kornfeld, H., Weissman, D., Bisson, G.P., 2018. Tuberculosis and lung damage: from epidemiology to pathophysiology. European respiratory review : an official journal of the European Respiratory Society. https://doi.org/10.1183/16000617.0077

Riedl, A., Schlederer, M., Pudelko, K., Stadler, M., Walter, S., Unterleuthner, D., Unger, C., Kramer, N., Hengstschläger, M., Kenner, L., Pfeiffer, D., Krupitza, G., Dolznig, H., 2017. Comparison of cancer cells in 2D vs 3D culture reveals differences in AKT-mTOR-S6K signaling and drug responses. J Cell Sci 130, 203–218.

https://doi.org/10.1242/JCS.188102/259005/AM/COMPARISON-OF-CANCER-CELLS-CULTURED-IN-2D-VS-3D

Romagnoli, A., Etna, M.P., Giacomini, E., Pardini, M., Remoli, M.E., Corazzari, M., Falasca, L., Goletti, D., Gafa, V., Simeone, R., Delogu, G., Piacentini, M., Brosch, R., Fimia, G.M., Coccia, E.M., 2012. ESX-1 dependent impairment of autophagic flux by Mycobacterium tuberculosis in human dendritic cells. Autophagy 8, 1357–1370. https://doi.org/10.4161/auto.20881

Roufosse, F., 2018. Targeting the interleukin-5 pathway for treatment of eosinophilic conditions other than asthma. Front Med (Lausanne). https://doi.org/10.3389/fmed.2018.00049

Rustad, T.R., Sherrid, A.M., Minch, K.J., Sherman, D.R., 2009. Hypoxia: A window into Mycobacterium tuberculosis latency. Cell Microbiol. https://doi.org/10.1111/j.1462-5822.2009.01325.x

Sabir, N., Hussain, T., Mangi, M.H., Zhao, D., Zhou, X., 2019. Matrix metalloproteinases: Expression, regulation and role in the immunopathology of tuberculosis. Cell Prolif. https://doi.org/10.1111/cpr.12649

Salie, M., Daya, M., Lucas, L.A., Warren, R.M., van der Spuy, G.D., van Helden, P.D., Hoal, E.G., Möller, M., 2015. Association of toll-like receptors with susceptibility to tuberculosis suggests sex-specific effects of TLR8 polymorphisms. Infection, Genetics and Evolution 34, 221–229. https://doi.org/10.1016/j.meegid.2015.07.004

Santoso, A., Rasiha, R., Zainal, A.T.F., Khairunnisa, I.N., Fais, M.K., Gunawan, A.M.A.K., 2023. Transforming growth factor-β and matrix metalloproteinases as potential biomarkers of fibrotic lesions induced by tuberculosis: a systematic review and meta-analysis. BMJ Open 13. https://doi.org/10.1136/bmjopen-2022-070377

Sasindran, S.J., Torrelles, J.B., 2011. Mycobacterium tuberculosis infection and inflammation: What is beneficial for the host and for the bacterium? Front Microbiol 2. https://doi.org/10.3389/fmicb.2011.00002

Sastre, B., Rodrigo-Muñoz, J.M., Garcia-Sanchez, D.A., Cañas, J.A., Del Pozo, V., 2018. Eosinophils: Old players in a new game. J Investig Allergol Clin Immunol. https://doi.org/10.18176/jiaci.0295

Scanga, C.A., Bafica, A., Feng, C.G., Cheever, A.W., Hieny, S., Sher, A., 2004. MyD88-Deficient Mice Display A Profound Loss in Resistance to Mycobacterium tuberculosis Associated with Partially Impaired Th1 Cytokine and Nitric Oxide Synthase 2 Expression. Infect Immun 72, 2400–2404. https://doi.org/10.1128/IAI.72.4.2400-2404.2004

Schönbeck, U., Mach, F., Libby, P., 1998. Generation of Biologically Active IL-1 by Matrix Metalloproteinases: A Novel Caspase-1-Independent Pathway of IL-1 Processing 1, The Journal of Immunology. 61(7), 3340–3346. https://doi.org/10.4049/jimmunol.161.7.3340

Seung, K.J., Keshavjee, S., Rich, M.L., 2015. Multidrug-resistant tuberculosis and extensively drug-resistant tuberculosis. Cold Spring Harb Perspect Med 5. https://doi.org/10.1101/cshperspect.a017863

Shah, P.T., Tufail, M., Wu, C., Xing, L., 2022. THP-1 cell line model for tuberculosis: A platform for in vitro macrophage manipulation. Tuberculosis (Edinb) 136. https://doi.org/10.1016/J.TUBE.2022.102243

Shukla, S., Richardson, E.T., Athman, J.J., Shi, L., Wearsch, P.A., McDonald, D., Banaei, N., Boom, W.H., Jackson, M., Harding, C. V., 2014. Mycobacterium tuberculosis Lipoprotein LprG Binds Lipoarabinomannan and Determines Its Cell Envelope Localization to Control Phagolysosomal Fusion. PLoS Pathog 10. https://doi.org/10.1371/journal.ppat.1004471

Spencer, L.A., Szela, C.T., Perez, S.A.C., Kirchhoffer, C.L., Neves, J.S., Radke, A.L., Weller, P.F., 2009. Human eosinophils constitutively express multiple Th1, Th2, and immunoregulatory cytokines that are secreted rapidly and differentially. J Leukoc Biol 85, 117–123. https://doi.org/10.1189/jlb.0108058

Srivastava, S., Dey, S., Mukhopadhyay, S., 2023. Vaccines against Tuberculosis: Where Are We Now? Vaccines (Basel). https://doi.org/10.3390/vaccines11051013

Stek, C., Allwood, B., Walker, N.F., Wilkinson, R.J., Lynen, L., Meintjes, G., 2018. The Immune Mechanisms of Lung Parenchymal Damage in Tuberculosis and the Role of Host-Directed Therapy. Front Microbiol. https://doi.org/10.3389/fmicb.2018.02603

Sugawara, I., Yamada, H., Mizuno, S., Takeda, K., Akira, S., 2003. Mycobacterial Infection in MyD88-Deficient Mice. Microbiol Immunol 47, 841–847. https://doi.org/10.1111/j.1348-0421.2003.tb03450.x

Sun, H., Li, Y., Zhang, P., Xing, H., Zhao, S., Song, Y., Wan, D., Yu, J., 2022. Targeting toll-like receptor 7/8 for immunotherapy: recent advances and prospectives. Biomark Res. https://doi.org/10.1186/s40364-022-00436-7

Takatsu, K., 2011. Interleukin-5 and IL-5 receptor in health and diseases. Proc Jpn Acad Ser B Phys Biol Sci. https://doi.org/10.2183/pjab.87.463

Tang, J., Sun, M., Shi, G., Xu, Y., Han, Y., Li, X., Dong, W., Zhan, L., Qin, C., 2018. Toll-like receptor 8 agonist strengthens the protective efficacy of ESAT-6 immunization to Mycobacterium tuberculosis infection. Front Immunol 8. https://doi.org/10.3389/fimmu.2017.01972

Tezera, L., Bielecka, M., Elkington, P., 2017. Bioelectrospray Methodology for Dissection of the Host-pathogen Interaction in Human Tuberculosis. Bio Protoc 7. https://doi.org/10.21769/bioprotoc.2418

Tiwari, D., Martineau, A.R., 2023. Inflammation-mediated tissue damage in pulmonary tuberculosis and host-directed therapeutic strategies. Semin Immunol 65, 101672. https://doi.org/10.1016/j.smim.2022.101672

To, E.E., Erlich, J., Liong, F., Luong, R., Liong, S., Bozinovski, S., Seow, H.J., O'Leary, J.J., Brooks, D.A., Vlahos, R., Selemidis, S., 2019. Intranasal and epicutaneous administration of Toll-like receptor 7 (TLR7) agonists provides protection against influenza A virus-induced morbidity in mice. Sci Rep 9. https://doi.org/10.1038/s41598-019-38864-5

Tobin, D.M., 2015. Host-directed therapies for tuberculosis. Cold Spring Harb Perspect Med 5. https://doi.org/10.1101/cshperspect.a021196

Tsuchiya, S., Yamabe, M., Yamaguchi, Y., Kobayashi, Y., Konno, T., Tada, K., 1980. ESTABLISHMENT AND CHARACTERIZATION OF A HUMAN ACUTE MONOCYTIC LEUKEMIA CELL LINE (THP-1), J. Cancer. 26(2), 171–176. https://doi.org/10.1002/ijc.2910260208

Tyagi, P., Dharmaraja, A.T., Bhaskar, A., Chakrapani, H., Singh, A., 2015. Mycobacterium tuberculosis has diminished capacity to counteract redox stress induced by elevated levels of endogenous superoxide. Free Radic Biol Med 84, 344–354. https://doi.org/10.1016/j.freeradbiomed.2015.03.008

Urbanowski, M.E., Ordonez, A.A., Ruiz-Bedoya, C.A., Jain, S.K., Bishai, W.R., 2020. Cavitary tuberculosis: the gateway of disease transmission. Lancet Infect Dis. https://doi.org/10.1016/S1473-3099(20)30148-1

Van Crevel, R., Kleinnijenhuis, J., Oosting, M., Joosten, L.A.B., Netea, M.G., 2011. Innate immune recognition of mycobacterium tuberculosis. Clin Dev Immunol. https://doi.org/10.1155/2011/405310

Varricchi, G., Bagnasco, D., Borriello, F., Heffler, E., Canonica, G.W., 2016. Interleukin-5 pathway inhibition in the treatment of eosinophilic respiratory disorders: evidence and unmet needs. Curr Opin Allergy Clin Immunol 16, 186. https://doi.org/10.1097/ACI.0000000000000251

Verma, A., Ghoshal, A., Dwivedi, V.P., Bhaskar, A., 2022. Tuberculosis: The success tale of less explored dormant Mycobacterium tuberculosis. Front Cell Infect Microbiol. https://doi.org/10.3389/fcimb.2022.1079569

Wang, M.G., Zhang, M.M., Wang, Y., Wu, S.Q., Zhang, M., He, J.Q., 2018. Association of TLR8 and TLR9 polymorphisms with tuberculosis in a Chinese Han population: A case-control study. BMC Infect Dis 18. https://doi.org/10.1186/s12879-018-3485-y

Wang, S., Gao, D., Chen, Y., 2017. The potential of organoids in urological cancer research. Nat Rev Urol 14, 401. https://doi.org/10.1038/NRUROL.2017.65

World Health Organization. 2024. World Health Organization tuberculosis factsheet No. 104. WHO. Geneva. https://https://www.who.int/news-room/fact-sheets/detail/tuberculosis#:~:text=In%202023%2C%20an%20estimated%2010.8,and%20a%20health%20security%20threat

World Health Organization. 2022. Global Tuberculosis Report. WHO. Geneva. 2023. https://https://www.who.int/teams/global-programme-on-tuberculosis-and-lung-health/tb-reports/global-tuberculosis-report-2023

Young, C., Walzl, G., Du Plessis, N., 2020. Therapeutic host-directed strategies to improve outcome in tuberculosis. Mucosal Immunol. https://doi.org/10.1038/s41385-019-0226-5

Zhang, S., Hu, Z., Tanji, H., Jiang, S., Das, N., Li, J., Sakaniwa, K., Jin, J., Bian, Y., Ohto, U., Shimizu, T., Yin, H., 2018. Small-molecule inhibition of TLR8 through stabilization of its resting state. Nat Chem Biol 14, 58–64. https://doi.org/10.1038/nchembio.2518

Zhao, L., Fan, K., Sun, X., Li, W., Qin, F., Shi, L., Gao, F., Zheng, C., Babu, S., Kolloli, A., Nair, D., 2023. Host-directed therapy against mycobacterium tuberculosis infections with diabetes

mellitus OPEN ACCESS EDITED BY REVIEWED BY. Front. Immunol 14, 1305325. https://doi.org/10.3389/fimmu.2023.1305325

Zhuang, L., Yang, L., Li, L., Ye, Z., Gong, W., 2024. Mycobacterium tuberculosis: immune response, biomarkers, and therapeutic intervention. MedComm (Beijing). https://doi.org/10.1002/mco2.419

Zumla, A., Rao, M., Wallis, R.S., Kaufmann, S.H.E., Rustomjee, R., Mwaba, P., Vilaplana, C., Yeboah-Manu, D., Chakaya, J., Ippolito, G., Azhar, E., Hoelscher, M., Maeurer, M., 2016. Host-directed therapies for infectious diseases: Current status, recent progress, and future prospects. Lancet Infect Dis. https://doi.org/10.1016/S1473-3099(16)00078-5